Structural and Functional Analysis of Prokaryotic Pentameric Ligand-Gated Ion Channels

Dissertation

zur

Erlangung der naturwissenschaftlichen Doktorwürde

(Dr. sc. nat.)

vorgelegt der

Mathematisch-naturwissenschaftlichen Fakultät

der

Universität Zürich

von

Sibylle Engeler

von Aadorf (TG)

Promotionskomitee

Prof. Dr. Raimund Dutzler (Leitung und Vorsitz)

Prof. Dr. Markus Grütter

Prof. Dr. Martin Jinek

Zürich, 2016

to my exceptional family

Acknowlegdements

First, I would like to thank Prof. Dr. Raimund Dutzler for giving me the opportunity to work with the pentameric ligand gated ion channels and to learn a lot about many different biochemical techniques. Especially in the last months of my PhD he supported me and gave me the freedom to work according to my own time schedule. I would like to thank my thesis committee, Prof. Dr. Markus Grütter and Prof. Dr. Martin Jinek for their interest and time.

I wish to express my gratitude to the former and primarily the current members of the Dutzler lab (the "Daimunds") for the nice atmosphere, the valued chats, the supporting during long working days, the funny lunch and tea breaks, the running… making the lab a very nice place! A special thank goes also to Ricarda who started with the pLGICs project and to Iwan and Carlo.

Particularly I am very grateful to (alphabetically listed):

Alessia, the Cristinas, Eric, Ines, Janine, Justin, Nita, Novandy, René, Sinem, Stephan, Valeria. Especially to Yvonne, who keeps the lab running and always had an open ear for all and everyone.

I wish to thank to the members of the former lab of Prof. Dr. Markus Grütter where I worked for my master thesis. A special thank goes to Prof. Dr. Markus Seeger who introduced me into the art of Ribosome Display and taught me how to work with membrane proteins.

I would like to thank also the group of Prof. Dr. Martin Jinek, to Heidi, to Reto, to Magda, to Nadine, to Michi, to Anshu, to Barbara and to Frank and to the "high-throughput" team.

I wish to say thanks to the infrastructure team of the department of Biochemistry, the crystallization facility, the IT team, the secretaries, the institute of Physiology and the FGCZ.

A big thank goes to my family and friends for their continuous support and encouragement.

Table Of Content

List of Figures

List of Tables

Abstract

Pentameric ligand gated ion channels (pLGICs) form a large family of integral membrane proteins involved in fast signal transduction at synapses. They are located at the postsynaptic side where they convert a chemical signal triggered by release of neurotransmitters from the presynaptic cell into the synaptic cleft to an electrical signal, in the postsynaptic cell. Dysfunction of these receptors can cause severe diseases such as Alzheimer's disease, epilepsy or schizophrenia. Since their discovery in the 1970ies they have been intensively studied with biochemical and electrophysiological methods, investigating both structure and function.

Forty years after their discovery, the structure of the acetylcholine binding protein (AChBP) was solved which is a homologue of the N-terminal extracellular domain of a pLGIC. Recently, structures of the procaryotic homologues GLIC (from *Gloebacter violaceus*) with bound ligand and ELIC (from *Erwinia chrysanthemi*) without ligand were determined.Pentameric ligand gated ion channels are composed of an extracellular, ligand-binding domain, predominantely consisting of β-strands and a transmembrane pore domain consisting of α-helices. Upon binding to a specific agonist in a conserved part of the extracellular domain, a conformational change occurs which is transduced to the transmembrane part and leading to the opening of the ion channel. This rearrangement is transferred via a conserved interface between the two domains. To gain more insight into this important gating mechanism, two different strategies involving both - structural and functional investigations, were performed in this work.

Towards this goal, specific protein binders were selected by Ribosome and Phage Display for the above mentioned prokaryotic homologues GLIC and ELIC. Such binders have the potential to act as crystallization chaperones. Additionally they could stabilize the channel in a specific conformation or influence its functional properties. For GLIC, single chain variable fragments (scFvs) and designed ankyrin repeat proteins (DARPins) were successfully selected from synthetic Phage and Ribosome Display libraries. These binders were further analyzed to characterize their binding specificity, their affinity and assess their potential impact on structure. Twelve binders are highly specific and show high affinity to GLIC. Attempts to co-crystallize the binders with GLIC have not been successful. *In vivo* experiments to evaluate the effect of these binders on the function of the channel revealed no significant binding. In the case of ELIC, 33 DARPins were selected by Ribosome Display and 12 nanobodies, were selected from a Phage Display library originating from immunized alpacas. The majority of these binders, have adverse biochemical properties such as aggregation and unspecific binding.

In a second approach to examine the gating mechanism of these channels, mutations of residues located in the conserved interface between the extracellular and transmembrane domain were characterized by two-electrode voltage clamp experiments. Several amino acids in the β1-β2 loop, β6-β7 loop, the β10-α1 linker and the α2- α3 loop of both homologues were mutated to alanine and expressed in *Xenopus laevis* oocytes. The oocytes were subjected to two-electrode voltage clamp electrophysiology and the evoked currents were compared to oocytes expressing the corresponding wild type protein. To ensure that the proteins are properly folded and correctly located at the plasma membrane a surface assay was performed, using an antibody targeting a tag fused to the expressed protein. Based on the electrophysiological data and the subsequent oocyte surface assays, several residues, relevant for the gating mechanism, were identified.

Our results show that in both homologues the corresponding mutations have a similar effect, which emphasizes the high conservation of this mechanism. Similar studies with eukaryotic nAChR revealed

a comparable behavior, underlining the conservation of the gating mechanism among the family. Therefore our results underline the relevance of the prokaryotic homologues GLIC and ELIC as model system.

Zusammenfassung

Pentamere liganden-gesteuerte Ionenkanäle (pLGICs) bilden eine grosse Familie von integralen Membranproteinen die in der schnellen Signalübertragung an Synapsen involviert sind. Sie befinden sich in der postsynaptischen Membran der Nervenzellen wo sie ein chemisches Signal, das durch die Ausschüttung von Neurotransmittern aus der präsynaptischen Zelle in den synaptischen Spalt ausgelöst wird, in ein elektrisches Signal umwandeln. Fehlfunktionen dieser Rezeptoren können schwerwiegende Krankheiten wie Alzheimer, Epilepsie oder Schizophrenie auslösen. Seit ihrer Entdeckung in den 1970er Jahren wurden sie daher intensiv mit Hilfe biochemischer und elektrophysiologischer Methoden erforscht um ihre Funktion und Struktur zu untersuchen.

Vierzig Jahre nach ihrer Entdeckung wurde die Struktur des acetlycholin-bindenden Proteins (AChBP) aufgeklärt, welches ein Homolog der N-terminalen extrazellulären Domäne eines pLGICs ist. Kürzlich wurden die ersten Strukturen der prokaryotischen Homologe GLIC (aus *Gloebacter violaceus*) mit gebundenem Liganden und jene von ELIC (aus *Erwinia chrysanthemi*) ohne den Liganden, gelöst.

Pentamere liganden-gesteuerte Ionenkanäle bestehen aus einer extrazellulären Domäne, welche mehrheitlich aus β-Strängen besteht an die die Liganden binden, sowie aus einer transmembranen Porendomäne die von α-Helixen dominiert wird. Durch das Binden spezifischer Agonisten an eine hochkonservierte Region der extrazellulären Domäne wird eine konformationelle Änderung ausgelöst, welche an die Transmembrandomäne übertragen wird und so die Öffnung des Ionenkanals bewirkt. Diese Reorganisation wird durch eine konservierte Schnittstelle übertragen, die sich zwischen den zwei Domänen befindet. Um mehr über diesen wichtigen Mechanismus zu erfahren, wurden zwei unterschiedliche Strategien, unter Einbezug von strukturellen und funktionellen Untersuchungen, verfolgt.

In einem ersten Schritt wurden spezifische Proteinbinder für die obengenannten prokaryotischen Homologe GLIC und ELIC mit Ribosomen und Phagen Display selektioniert. Solche Binder können als Kristallisationshelfer agieren, die Kanäle in einer definierten Konformation stabilisieren oder einen Einfluss auf die Funktion haben. Es wurden erfolgreich scFv-Fragmente und DARPins für GLIC mit Phagen Display beziehungsweise Ribosomen Display selektioniert und ihre Spezifität, Affinität und Einfluss auf Struktur und Funktion analysiert. Obwohl 12 dieser Binder sehr spezifisch und mit hoher Affinität an GLIC binden, veränderten sie weder die Kristallisationseigenschaften des Kanals noch konnte einen Einfluss auf die Funktion gemessen werden. Für ELIC zeigten die meisten der 33 DARPins, die mit Hilfe des Ribosomen Displays selektioniert wurden und der 12 Nanobodies, die durch die Immunisierung von Alpakas gewonnen und mit Hilfe des Phagen Displays identifiziert wurden, unerwartete biochemische Eigenschaften wie Aggregation und Unspezifität.

Eine andere Möglichkeit den Aktivierungsmechanismus dieser Kanäle zu untersuchen, ist die Mutation von Aminosäuren die sich in der konservierten Schnittstelle zwischen der extrazellulären und der Transmembrandomäne befinden. Mehrere Aminosäuren im β1-β2 Loop, im β6-β7 Loop, im β10-α1 Linker und im α2- α3 Loop beider Homologe wurden zu Alanin mutiert und in Oozyten des Krallenfrosches (*Xenopus laevis*) exprimiert. Die Oozyten wurden einem elektrophysiologischen Experiment unterzogen um die entstehenden Ströme nach Ligandenapplikation zu messen, welche dann mit denjenigen des Wildtyps verglichen wurden. Um Sicherzustellen, dass die Kanäle trotz Mutation korrekt gefaltet sind und an der Oozytenmembran lokalisiert sind, wurde ein Oberflächentest durchgeführt, wobei ein Antikörper einen mit den exprimierten Homologen fusionierten Tag bindet.

Durch obengenannte Experimente konnten mehrere Aminosäuren identifiziert werden, welche für die Aktivierung wichtig sind. Es wurde gezeigt, dass die Mutationen in beiden Homologen einen ähnlichen Effekt haben was die Konservierung dieses Prozesses unterstreicht. Ähnliche Studien mit eukaryotischen nAChR zeigen ein vergleichbares Verhalten, was die Konservierung des Aktivierungsmechanismus innerhalb der Familie unterstreicht und die Verwendung von GLIC und ELIC als gutes Modellsystem aufzeigt.

1. Introduction

1.1 Electrical and chemical synapses

The brain is the primary organ of our and other animal's nervous system. Communication between the neurons is mandatory for function and mediated by cell-cell interactions, called synapses (greek, *syn*: together and *haptein*: grasp, touch). In general there are 2 different types of synapses (Figure 1), chemical synapses and electrical synapses [1].

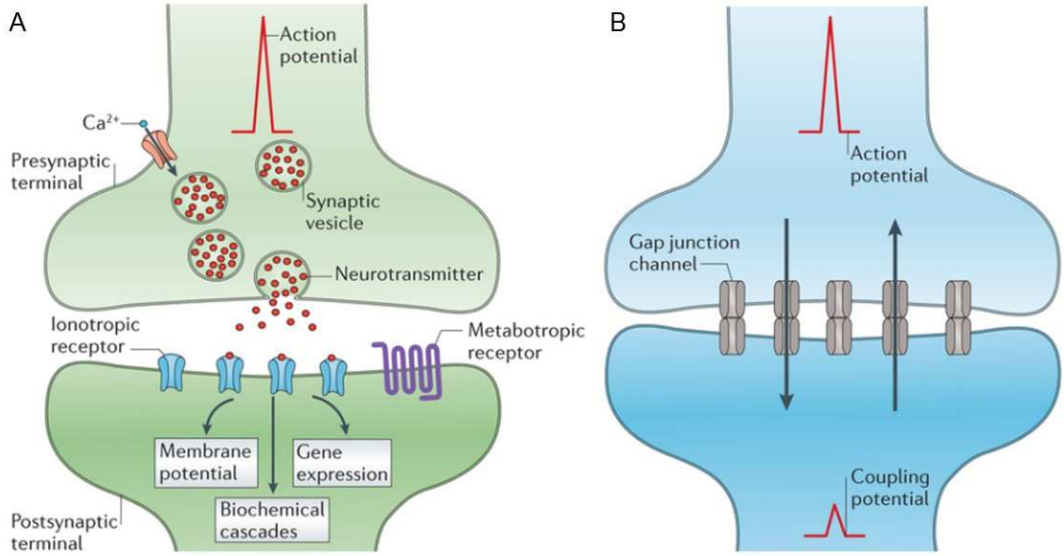

Figure 1 Signal transmission at chemical and electrical synapses.

A) Chemical synapse. An action potential in the presynaptic cell causes the depolarization of the membrane which leads to the influx of calcium ions through voltage-gated calcium channels (VGCCs). Vesicles filled with neurotransmitter fuse with the presynaptic membrane and release their content into the synaptic cleft. The binding of neurotransmitters to different receptors in the postsynaptic membrane, can have various effects (as a change of the membrane potential, initiation or termination of gene expression and the initiation of biochemical signaling cascades). Subsequently the neurotransmitter has to be removed from the synaptic cleft by re-uptake or enzymatic degradation etc. B) Electrical synapse. The interior of the two cells are connected by gap junctions, which are clusters of intercellular channels. An action potential in the presynaptic cell causes the depolarization of the membrane of the postsynaptic cell, but with a certain attenuation depending on the membrane resistance. Compared to the chemical transmission, the electrical transmission is faster and bidirectional. Figure adapted from [1].

Whereas at chemical synapses, the cells approach each other at a distance of 20-40 nm, the cells in electrical synapses are separated by only about 3.5 nm. In electrical synapses, the cytoplasms of two adjacent cells are connected via gap junctions, which are clusters of intercellular channels [2, 3]. These channels are formed by 2 hexameric hemichannels and establish a bidirectional passage for the flow of ions such as calcium [4]. An action potential in the presynaptic cell causes the depolarization of the adjacent cell, but with a certain attenuation depending on the membrane resistance. The electrical synapses are mostly located in part of the nervous system that is involved in fast responses.

The chemical synapses arose earlier in evolution and they are also important in the communication of unicellular organisms and play a role in quorum sensing in bacteria, the detection of bacterial density [5]. In the nervous system an action potential in the presynaptic cell leads to the depolarization of the membrane and subsequent influx of calcium ions into the cell through voltage-gated calcium channels

(VGCCs). Vesicles, filled with neurotransmitter, deplete into the synaptic cleft by exocytosis. Different receptors, located in the membrane of the postsynaptic cell, bind these molecules and cause a change in membrane potential, initiation or termination of gene expression or the initiation of biochemical signaling cascades. Afterwards, the neurotransmitter has to be removed from the synaptic cleft, by re-uptake or enzymatic cleavage [3, 6, 7]. Many of the receptors, involved in signal transduction in synapses, are ligand-gated ion channels that are part of three subfamilies: nucleotide-gated ion channels, ionotropic glutamate receptors and pentameric ligand-gated ion channels.

1.2 Pentameric ligand-gated ion channels

1.2.1 Structure of pentameric ligand-gated ion channels

Pentameric ligand-gated ion channels (pLGICs) or Cys-loop receptors constitute a large family of integral membrane proteins, which transduce signals in the form of ions across cell membranes after binding to a specific neurotransmitter released by the adjacent pre-synaptic cell into the synaptic cleft. They therefore translate a chemical signal into an electrical one. pLGICs consist of an extracellular ligand binding domain (ECD) and a transmembrane ion channel. Cys-loop receptors are pentameric proteins and have a conserved loop between the β6- and β7-sheet which is bracketed of two cysteines. This receptor superfamily can be divided into excitatory (activated by acetylcholine or serotonin) and inhibitory receptors (activated by glycine, glutamate or GABA), which are cation- or anion-selective, respectively [8-10].

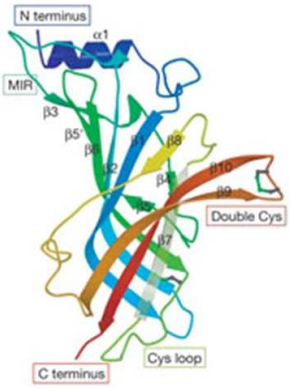

Figure 2 Ribbon representation of an acetylcholine binding protein.

The N-terminal α-helix (blue) is followed by a β-sandwich, consisting of 10 β-strands. Disulfide bonds are colored in green. In a complete ion channel the C-terminus would be connected to the transmembrane α-helices. Figure adapted from [11].

The subfamily of nicotinic acetylcholine receptors (nAChRs) are present at the neuromuscular junction and in neuronal tissues [12, 13]. Despite investing large efforts, to date no crystal structure of a nicotinic acetylcholine receptor could be determined [14-17]. In 2001 however, Brejc and colleagues [11] determined the structure of the acetylcholine-binding protein (AChBP) from *Lymnaea stagnalis,* originally discovered by Smit and colleagues [18], which is a homologue of the N-terminal extracellular domain of a Cys-loop receptor. In the following years, several structures of acetylcholine-binding proteins, with and without agonist were solved [19-22]. These structures have revealed the fold of the protein, containing an N-terminal α-helix and a β-sandwich, consisting of an inner β-sheet with 6 and an

outer β-sheet with 4 strands. In general the AChBP shows an immunoglobulin like fold and the structures gave insight into the agonist binding site (Figure 2).

In 2005, the structure of the membrane-associated acetylcholine receptor (AChR) from the Torpedo electric ray was solved by electron microscopy and, despite the low resolution, it allowed for the comprehension of general structural features and provided initial insight into potential gating mechanisms [23]. Surprisingly, in the same year, benefiting from the increased knowledge of genomic data, prokaryotic homologues of Cys-loop receptors were identified [24]. Regardless of less than 30% sequence identity compared to eukaryotic family members, they show conservation in their overall structure and in functional characteristics such as desensitization, ion selectivity and the sensitivity to several chemical compounds [25-31]. However, in contrast to eukaryotic receptors, they all lack the cysteines in the β6-β7 loop, and form homopentamers. Only few years after the discovery of prokaryotic homologues, X-ray structures of the cation-selective homologue ELIC, from the phytopathogenic bacterium *Erwinia chrysanthemi*, and GLIC, from the cyanobacterium *Gloebacter violaceus*, were solved with a resolution of 3.3 Å and 2.9 Å, respectively (Figure 3). Both bacterial homologues show conserved tertiary and quaternary structures. The proteins are homopentamers, the extracellular domain consists of 10 β-strands and it forms a tube that is 60 Å high and 90 Å wide. The transmembrane part of the protein consists of 4 α-helices per subunit, with α-helix 2 of each subunit lining the pore, whereas the α-helices 1, 3 and 4 shield the channel. Along the pore axis from the extracellular side three consecutive rings of hydrophobic amino acids form the channel gate, followed by 2 rings of polar and 1 ring of charged residues that interact with ions and influence the selectivity. Additionally charged residues in the extracellular part of the pore also contribute to ion selectivity by making the electrostatic potential negative. The selectivity of pLGICs is not for a specific ion but it is based on the charge of permeating ions. Both GLIC and ELIC are known to be cation-selective.[26, 27, 32].

The prokaryotic homologues GLIC and ELIC lack disulfide bridges and do not contain a cytoplasmic domain between the α-helices 3 and 4 that is present in eukaryotic proteins. A eukaryotic homologue GluCl from *Caenorhabtitis elegans,* whose structure was solved at a resolution of 3.3 Å, contains the C-loop and the Cys-loop disulphides, conserved in eukaryotic family members [10]. Further high resolution X-ray structures of eukaryotic Cys-loop receptors were solved in the following years [33, 34]. The prokaryotic homologue ELIC was crystallized in a presumably non-conductive conformation, since the pore is blocked by hydrophobic side chains [32], whereas GLIC and GluCl were crystallized with bound ligands (protons in case of GLIC and glutamate plus ivermectin in case of GluCl) and show a potential conductive conformation of the channel as underlined by the larger pore diameter and the tilt of the C-terminus of the α2-helices from the channel axis [10, 26, 27].

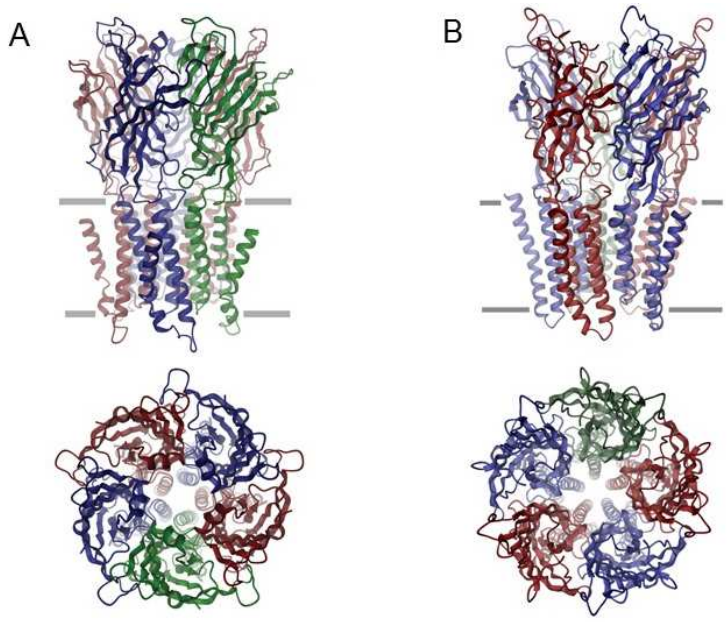

Figure 3 Ribbon representation of ELIC and GLIC.

A) ELIC. View from within the membrane with the extracellular domain above. The cell membrane is indicated by grey bars. Below, the top view from the extracellular side is shown. B) GLIC. View from the side with the extracellular domain above, the cell membrane is indicated by grey bars. Below, the top view from the extracellular side is shown. Whereas ELIC was crystallized in a potential non-conductive conformation, GLIC is supposed to be in a conductive state. Adapted from [26, 32].

Another crystal structure of GluCl, cocrystallized with ivermectin and the open channel blocker picrotoxin, reinforced the open channel hypothesis, since picrotoxin was found to occlude the pore. A cysteine mutant of GLIC, where residues in the loop between the α-helices 2 and 3 were crosslinked to residues located in the β6- β6 loop, shows a so-called “locally closed” conformation with a smaller pore diameter, which partly resembles the non-conductive pore of ELIC [35]. Recently the structure of GLIC was determined at neutral pH. In this structure, which resembles the locally closed conformation, the C-terminal part of the α2-helix is tilted thereby blocking the pore whereas the α2- α3 loop has changed its conformation [35, 36]. Furthermore, a structure of GluCl in absence of ivermectin in a supposedly non-conductive conformation was published, which resembles the structure of ELIC [37]. Recently the structure of the glycine receptor GlyR in different states (agonist-bound, antagonist-bound and desensitized or partially open) was determined by electron cryo-microscopy [38]. Although several structures of pLGICs are now available, a definitive assignment to the different states of the receptor remains uncertain. Although the above mentioned nAChR structure represents a presumably closed conformation since no agonist was added [23], the conformation of its α2-helices appears to be similar to GLIC and GluCl. Further investigations of the ligand bound nAChR revealed only slight changes in the pore and it was thus questioned how the available structures can be assigned to functional conformations [39]. Despite these discrepancies, all family members show similar overall structures and it is likely that they might share a comparable activation mechanism.

Pentameric ligand-gated ion channels are activated by different agents, called ligands or agonists. ELIC is activated by primary amines [40] whereas GLIC responds to protons [41]. The anion-selective GluCl from *Caenorhabtitis elegans* is activated by glutamate and ivermectin [10]. The ligand binding pocket of pLGICs lies at the interface between two subunits in the extracellular domain and the structural rearrangement upon binding a ligand was studied in the acetylcholine binding protein (AChBP). The C-

loop, capping the binding site, showed the biggest structural rearrangements. Upon binding of agonist, the loop closes the binding site via a 7 Å movement, whereas the binding to an antagonist appears to push the loop outwards [19]. After agonist binding, structural rearrangements cause the opening of the pore in the transmembrane part of the protein. It is supposed, that this conformational change is transduced via a conserved interface composed of loops of the extracellular as well as of the transmembrane domain. The "*principal pathway of gating*" postulated by Lee and colleagues, involves conserved residues (arginines and glutamates) at the extracellular domain, which interact with conserved positions at the top of the pore domain. The β10- α1 linker (or pre-M1 linker) is supposed to be coupled to the α2-α3 loop (or M2-M3 loop) via the β1-β2 loop [42]. The acetylcholine receptor shows interactions of residues from the β1-β2 loop and the β6-β7 loop (or Cys-loop) as well with residues located at the β10-α1 linker and the α2-α3 loop indicating another signal transduction pathway via the Cys-loop, the "*Cys-loop pathway*" [43]. In Figure 4 the corresponding loops of the domain interfaces of GLIC and ELIC are shown (see attached publication "*Signal transduction at the domain interface of prokaryotic pentameric ligand-gated ion channels*").

Chimeras of the acetylcholine binding protein and the pore domain of the serotonin receptor only showed activation, when the β1-β2 loop, the β6-β7 loop and the β8-β9 loop, located in the extracellular part, were exchanged with the corresponding loops of the homologue forming the pore, which underlines the significance of the coupling of these loops with the aside placed α2-α3 loop from the transmembrane part for function [44].

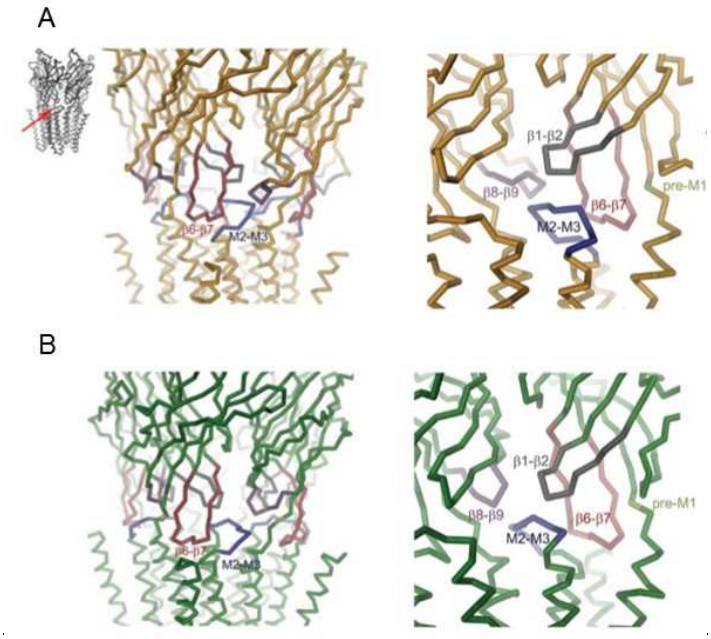

Figure 4 Domain interface of GLIC and ELIC.

A) Domain interface of ELIC, shown as Cα-trace. The β1-β2 loop, β6-β7 loop, β8-β9 loop and the β10-α1 linker from the extracellular domain as well the α2-α3 loop from the transmembrane part are colored. B) Domain interface of GLIC, shown as Cα-trace. The β1-β2 loop, β6-β7 loop, β8-β9 loop and the β10-α1 linker from the extracellular domain as well the α2-α3 loop from the transmembrane part are colored. Image adapted from the publication "*Signal transduction at the domain interface of prokaryotic pentameric ligand-gated ion channels*".

1.2.2 Activation of pentameric ligand-gated ion channels

The activation of pentameric ligand-gated ion channels upon binding to a specific agonist has been investigated for a long time and models, based on enzyme kinetics were established. A two-state model describing the processes of receptor activation has been established in the late fifties by Del Castillo and Katz and includes a closed agonist-receptor complex (Figure 5). The binding of the agonist (A) to its receptor (R) present in a closed conformation, is fast and only depends on the binding affinity of the agonist to the resting state. Subsequently the closed agonist-bound receptor (AR) undergoes a transition resulting in an open channel conformation (AR*). This transition is described by an equilibrium constant, called efficacy, which is the capability of the ligand to open the channel [45]. Diverse agonists differ in their efficacy, the ability to promote channel opening.

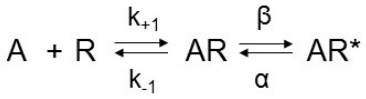

Figure 5 Model to explain activation of a receptor.

The closed receptor (R) binds its agonist (A) with an association rate constant k_{+1}.and subsequently undergoes a transition leading to channel opening (AR*). k_{-1} is the agonist dissociation constant, β the channel opening and α the channel closing rate constant. Adapted from [46].

Preliminary experiments with frog endplates displayed a cooperative binding behavior of the receptors to the agonist, which has led to the assumption that these proteins possess numerous binding sites, which are allosterically linked. Because the agonist binding to an AChBP does not show any cooperativity, the above shown model of the AChBP is only partly useful to describe the changes underlying the highly cooperative channel activation. Another model for activation, proposed by Monod and colleagues suggests, that even in the absence of a ligand the receptor can be present in an active conformation and it considers the possibility of more than one agonist bound to the receptor describing cooperativity (Figure 6) [47].

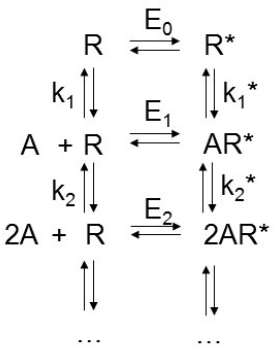

Figure 6 Model according to Monod, Wyman and Changeux.

The receptor (R) can exist in the inactive and active (R*) form even in absence of an agonist (A). This model also takes into account that more than one agonist can be bound to the receptor. Adapted from [47].

Upon prolonged exposure to the agonist, pLGICs become refractory to activation, called desensitization. Although a ligand remains bound, the channels enter a non-conductive conformation. In Figure 7, a patch clamp recording of ELIC expressed in *Xenopus laevis* oocytes shows desensitization upon long exposure of the agonist cysteamine. Even though the agonist is applied for more than 30 seconds, after only 1 second the evoked current decreases rapidly. Eventually only small bursts of single channels can be observed [40]. In synapses, neurotransmitters are removed from the synaptic cleft by reabsorption or enzymatic digestion [3, 6, 7] within milliseconds, whereas the desensitization of ELIC, for example, happens within seconds and it's therefore much slower. It was also observed that certain eukaryotic pLGICs such as the α7-nAChR desensitize much faster. Thus desensitization may have a biological relevance and can play a role in memory and learning processes [48].

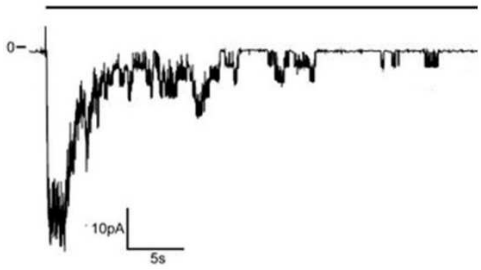

Figure 7 Patch clamp recording of ELIC expressed in *X. laevis* oocytes.

Upon long exposure to the agonist cysteamine at a concentration of 5 mM (black bar) ELIC desensitizes, which is manifested in the current decay. The vertical black bar corresponds to 10 pA and the horizontal bar to 5 seconds. Adapted from [40].

Considering the allosteric, cooperative mechanism and the desensitization of pLGICs, a general reaction model describing a ligand-gated ion channel binding 2 ligand molecules was established (Figure 8). The different conformations of the receptor with and without agonist are shown and it was postulated, that even in absence of the agonist, the receptors can adopt a desensitized conformation [49].

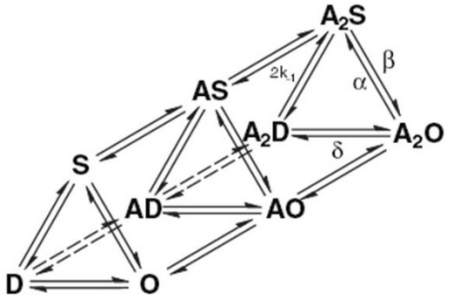

Figure 8 Reaction mechanism of a receptor binding two agonist molecules.

Different states of the receptor with or without ligand are depicted. S: closed, non-conductive state. O: open, conductive state. D: desensitized state. β: channel opening rate constant. α: channel closing rate constant. δ: entry into desensitized state. k_{-1}: ligand dissociation rate constant. Figure adapted from [49].

In fact, Corringer and colleagues showed, that up to 1 % of the nicotinic acetylcholine receptors without ligand are present in the desensitized state [50]. Furthermore, a recent study suggested the existence of multiple conformations for a given state and proposed asymmetric conformational changes in homopentamers. For ELIC it is was also proposed that, during the transition between states, the conformational changes are not evenly distributed among the different regions of the protein [51].

To understand the allosteric gating mechanisms of these receptors at the molecular level, structural knowledge of the diverse states are required. Distinct conformations of the channels are observed in the ELIC and GLIC structures. Agonist binding to the extracellular domain causes a conformational change, which leads to the opening of the channel (gating) in the transmembrane part in less than a millisecond. The comparison of the structures of GLIC and ELIC proposes an anticlockwise twist of each extracellular subdomain and a tilt of the α2-helices which line the pore [26, 27, 52]. A very recent study of the glycine receptor (GlyR) in different conformations proposes an iris-like expansion and an anticlockwise rotation of the transmembrane α-helices as well [38]. Upon long exposure to the specific agonist, the channels get into an unresponsive, desensitized state. It is debated whether the crystal structure of GLIC corresponds to a desensitized state and the structure of ELIC to a nonfunctional conformation [25, 30, 39]. To learn more about the gating of pLGICs, it is necessary to identify residues that are important for conformational changes between different channel conformations. At the same time it is crucial to assign the different structures to the different states, and to determine structures of the same homologue in different conformations. With the help of specific protein binders which detect certain states of the channels, different conformations could be stabilized and ideally crystallized.

1.3 Specific protein binders

Specific protein binders can be used as chaperones for crystallization or as modulators of the function of the targeted protein. Several specific protein binders, selected *in vivo* or *in vitro*, have already been successfully used for other membrane transport proteins, to influence the protein function *in vivo* or to prevent ligand binding to the protein [53-55]. Protein binders that are used as crystallization chaperones are of great interest in the field of structural biology as reviewed in [56]. These protein ligands enlarge the hydrophilic part of membrane proteins and thus generate a larger surface for possible crystal contacts. Furthermore a binder can reduce the flexibility of certain regions or loops, which may prevent efficient crystallization or stabilize the target protein in a defined conformation [57].

So far, the most successful binding proteins are antibodies and their fragments (Fab fragments, scFvs and nanobodies, Figure 9). Antibodies are produced by B-lymphocytes that are differentiated into an effector B-cell, upon exposure to an immunogenic intruder (bacterium, virus, foreign proteins) and upon activation by a T helper cell. For structural and functional studies, purified monoclonal antibodies are needed at high concentrations. Since B-lymphocytes, isolated from the blood of the animal which was immunized with the target protein (the immunogenic substance), eventually die in culture, they need to be immortalized. The fusion with a lymphocyte tumor cell, forming a hybridoma cell-line, results in cells, which produce the desired monoclonal antibody and which are able to propagate infinitely.

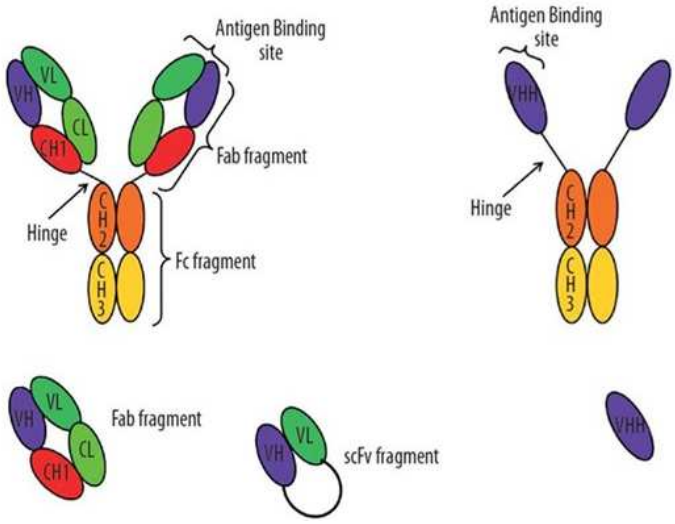

Figure 9 Schematic representation of antibodies.

Left: schematic representation of a conventional antibody (ca. 150 kD), a Fab fragment (ca. 50 kD) and a scFv fragment (ca. 25 kD). Right: schematic representation of a heavy chain antibody and a nanobody (ca. 15 kD). Figure adapted from *creative biolabs*.

The complementary determining regions (CDRs) in the variable part of the antibodies form the antigen binding site. In Figure 10, a Fv fragment with highlighted CDRs is shown. Both variable domains from the heavy and the light chain (V_H and V_L, respectively) have 3 CDRs which interact non-covalently. The remainders of the variable part provide structural support and also affect the CDR conformation and orientation and therefore increase the binding diversity [58, 59] [60].

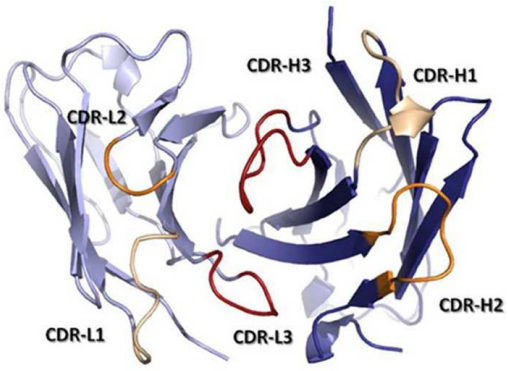

Figure 10 Ribbon representation of a Fv fragment

Ribbon representation of a Fv fragment seen from the antigen perspective. Dark blue) variable part of the heavy chain (V_H), light blue) variable part of the light chain (V_L). Yellow) CDR1, orange) CDR2, red) CDR3. Figure adapted from [58].

Antibody fragments only consisting of its variable parts, show better biochemical characteristics in terms of expression yields and stability. They can be obtained from mature antibodies by digestion with certain proteases (pepsin, papain) or they are recombinantly expressed in bacteria or yeast [61]. For identifying the fragments for the recombinant production, the DNA coding for the desired antibody fragment has to

be known. For that purpose, B-lymphocytes, expressing the corresponding antibody, are collected and the DNA encoding for the antibody fragment is PCR-amplified with specific primers and cloned into a Phage Display library. This library is subjected to 1-2 rounds of Phage Display and the specific binders for the target protein are subsequently selected [62, 63].

Twenty years ago, the structure of the cytochrome c oxidase, co-crystallized with an antibody fragment was solved [64]. Further membrane protein structures bound to specific antibody fragments (Fab or Fv fragments), could be determined in the following years [10, 65-68]. In the late 80's of the last century, a group of students during a practical course in Brussels, by chance discovered antibodies that were smaller than the known immunoglobulins. This phenomena was investigated more thoroughly by Hamers and Casterman who discovered that these newly detected antibodies only consist of a heavy chain and that these chains lacking the constant domain of the antigen binding part of the molecule and thus only have a single antigen binding domain per chain (Figure 9). These heavy chain only nanobodies appear in many camelids, ratfishs and in nurse sharks [69, 70], but investigations revealed an independent evolutionary background of different heavy chain antibodies [71]. The binding epitopes of these heavy chain antibodies, also named nanobodies or VHH, corresponds to the variable part of the heavy chain of antibodies. Because of the small size (about 15 kD) and the long CDR3 loop (16-18 amino acids versus 12 amino acids in human antibodies) they are supposed to be able to recognize cavities as binding epitopes [62, 72, 73]. Several membrane protein structures determined with the help of these heavy chain antibody fragments (nanobodies) have been published recently [34, 74-77].

Synthetic repeat proteins such as DARPins [78] that are selected *in vitro* by Ribosome Display, have become promising alternatives to antibodies in structural biology and for functional investigations. They are based on naturally appearing ankyrin proteins, which mediate protein-protein interactions in all 3 kingdoms of life [79, 80]. DARPins consist of several internal repeats, capped by an N- and a C-terminal domain (Figure 11). They have successfully been selected for various membrane proteins such as the bacterial multidrug exporter AcrB [53], the Na^+ citrate exporter CitS [81], the neurotensin receptor 1 [82] and the multidrug ABC-transporters MsbA and LmrCD [54, 57].

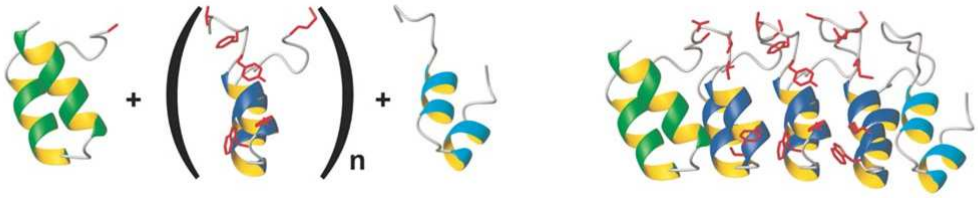

Figure 11 Cartoon representation of a DARPin.

Left: The N-terminal (green) and C-terminal (cyan) domains can cap a variable amount of internal repeats (blue). Right: cartoon representation of a MPB binding DARPin molecule (off7) consisting of 3 internal repeats (N3C DARPin). Randomized positions of this DARPin library are shown as red sticks. Figure adapted from [78].

1.4 Aim of thesis

Although, ligand gated ion channels have been studied for more than 40 years, the detailed mechanism of channel gating remains unclear. Upon binding to an agonist in the extracellular domain, the C-loop caps the binding site, followed by structural rearrangement of the transmembrane part leading to pore opening. To understand the allosteric mechanism, a comparison of the structures of the receptors in different conformations is required. Several structures of family members were solved in the last years, including the high resolution X-ray structures of the prokaryotic homologues GLIC and ELIC, and the eukaryotic GluCl. However in all cases only the structure in a single conformation was available. Whereas GLIC and GluCl were crystallized with bound agonist in a presumably open conformation, the structure of ELIC supposedly shows a closed state of the pore. To gain deeper insight into the function of these channels, it was tried to determine the structure of GLIC and ELIC in a different conformation. Since previous approaches to crystallize GLIC at low proton concentration in a closed state and ELIC with a bound agonist were unsuccessful, it was attempted to select specific protein binders, which may act as crystallization chaperones and may stabilize the protein in a different conformation. In a second set of experiments, this work contributed to a larger study in the group that aimed at a thorough investigation of the gating mechanism by characterizing the role of residues located at the interface between the extracellular and the transmembrane domain of the channels. This region is known to play an important role in the transduction of structural changes between the two domains following agonist binding. The function of the channel mutants was characterized by two-electrode voltage clamp electrophysiology and the structure of certain mutants were determined by X-ray crystallography to investigate the impact of the mutation on the structure.

2. Results

2.1 Selecting specific protein binders

Specific protein binders can be used as auxiliary proteins for the crystallization of their target protein. They can bind to loops or other flexible regions of their target, thereby reducing its flexibility and enlarging the soluble part available for crystal contacts. Binders can stabilize trap the target protein in a certain conformation or have an impact on protein function [53, 55-57]. To generate specific binding proteins for GLIC or ELIC three different classes of binding proteins were used. i) scFvs (single chain variable fragments) which were selected *in vitro* by Phage Display. ii) DARPins, which were selected *in vitro* by Ribosome Display and iii) nanobodies which were selected *in vivo* by immunization of alpacas followed by Phage Display. After the selection procedure the binders were characterized by ELISA, size exclusion chromatography (SEC) and surface plasmon resonance (SPR). For a better understanding of the gating mechanism of pentameric ligand gated ion channels, the structure of the targeted proteins has to be determined in different conformations. GLIC was crystallized at high proton concentrations and the structure solved in a presumably conductive state [26]. Since all the selection experiments with GLIC were conducted at neutral or slightly basic pH, we expected the channel to be in a nonconductive state and the binders to specifically recognize this conformation and potentially stabilize it for crystallization. The Ribosome Display selection with ELIC was performed with the target protein bound to its agonist and antagonist, propylamine and acetylcholine, respectively, and therefore it was assumed that ELIC may be in a desensitized or closed state depending on the bound ligand. This attempt has led to the identification of only a few unspecific binders. Therefore an additional selection procedure without any ligand was performed. In a second strategy, alpacas were immunized with ELIC, followed by Phage Display with ligand free ELIC, which allowed the identification of several nanobodies targeting ELIC.

2.1.1 Construct preparation

To select for specific binders with various display techniques and for structural analysis, high concentrations of detergent purified target protein are needed. The pentameric ligand gated ion channels GLIC and ELIC can be recombinantly produced in *E.coli*, extracted from the bacterial membranes with detergent and purified by metal chelate affinity chromatography (IMAC), via a fused a His_{10} tag. The DNA coding for ELIC was cloned in a pET26 vector, and the protein was expressed upon induction of transformed bacteria grown in minimal media with Isopropyl-β-D-thiogalactopyranosid (IPTG). Initially GLIC, cloned in the same vector, was expressed in cells grown in Terrific Broth (TB) medium in shaker flasks. Since the obtained yields were low in comparison to ELIC (0.05-0.3 mg/L versus 0.5-1 mg/L), a different expression strategy for GLIC has been established. The DNA coding for GLIC was cloned in a pBAD vector, where expression of the gene of interest is under the control of the arabinose promoter. Like in the original construct, the protein is preceded by an N-terminal PelB signal sequence, a His_{10}-tag, the fusion protein MBP and a 3C cleavage site (Figure 12).

Figure 12 Construct of GLIC and ELIC.

The construct of GLIC and ELIC (red) contains an N-terminal PelB signal sequence (blue), followed by a His_{10}-tag (light blue), MBP as fusion protein (green) and a HRV 3C cleavage site (light green).

Compared to the arabinose-induced overexpression, the disadvantage of the IPTG induced T7 expression system lies in residual expression of the target protein even in the absence of inducer. This can result in reduced cell growth and lower protein yields. Using a pBAD expression system, this problem could be circumvented [83]. The new expression system was tested in 5 ml TB culture with MC1061 cells containing a vector coding for GLIC. Cells were supplied with different arabinose concentrations for induction. After the overnight expression, the cells were lysed and the protein extracted with DDM. A western blot analysis revealed that the induction with 0.04 % arabinose gives the highest protein yields after extraction (Figure 13).

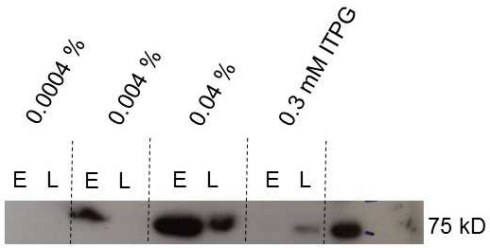

Figure 13 Western blot with expression test of GLIC in a pBAD vector.

Expression of GLIC in 5 ml cultures in an arabinose inducible system compared to the previously used IPTG inducible T7 system. After induction with different arabinose concentrations, the cells were harvested, lysed (L). Subsequently the MBP-GLIC fusion protein was extracted with DDM and insoluble parts were removed by centrifugation (E). The expression yields were compared with the expression levels of the pET-vector. The fusion protein was detected with an anti His_{10}-antibody.

Although the scale-up of the expression of GLIC with the pBAD system from the 5 ml culture to a 9 l fermenter culture was not not linear and the protein yields per cell are slightly lower than expected, for subsequent experiments the expression in fermenter was preferred over the shaker flasks. This is because in the fermenter the cells can grow to higher maximal cell density due to better aeration (OD 2-4 in flasks versus OD 15-20 in the fermenter) and thus more protein per liter of culture can be produced in that way. After expression of the protein over night at 18 °C, the cells were harvested, lysed and the protein extracted with 1 % DDM. After centrifugation of the sample to separate the extracted protein from non-lysed cells and cell debris, GLIC was affinity purified by a Ni-NTA- chromatography. Afterwards, the His-MBP fusion was cleaved with the HRV 3C protease during dialysis to lower the imidazole concentration, removed by binding to Ni-NTA resin and the membrane protein was subjected to size exclusion chromatography. ELIC, expressed in minimal medium, was purified similar to GLIC but instead using the detergent UDM. In Figure 14 a size exclusion chromatogram of a Superdex S200 column of both GLIC and ELIC is shown. The peaks at the retention volume of the column of 8.36 ml and 7.97 contained aggregated protein and DNA. ELIC and GLIC elute at 11.91 ml and at 11.75 ml,

respectively, which corresponds to the expected elution volume of membrane proteins with similar size and in the same detergent.

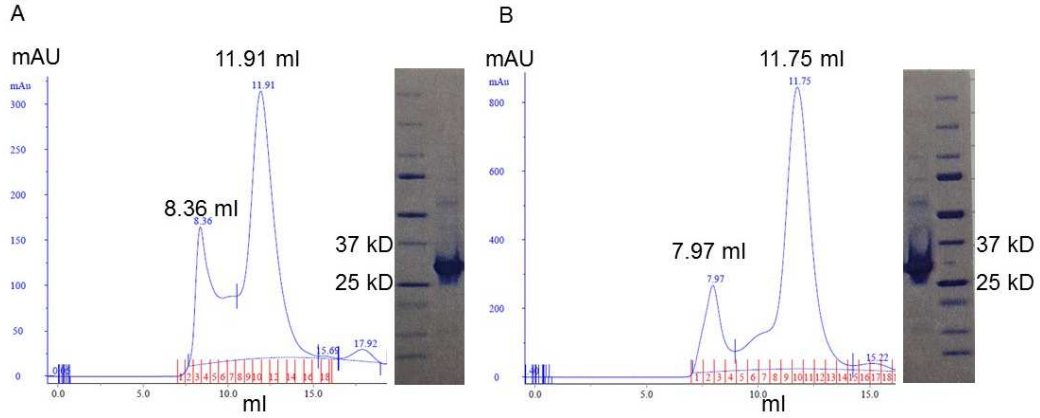

Figure 14 Size exclusion profile of GLIC and ELIC.

A) Size exclusion chromatogram of GLIC. Absorbance was measured at 280 nm. The peak at the retention volume of 11.91 ml corresponds to GLIC as confirmed by SDS-PAGE. The peak at 8.36 ml is at the void volume of the column. B) Size exclusion chromatogram of ELIC. Absorbance was measured at 280 nm. The peak at the retention volume of 11.75 ml corresponds to ELIC as confirmed by SDS PAGE. The peak at 7.97 ml elutes at the void volume of the column.

For the selection of specific binders from libraries containing either single chain variable fragments (scFvs), DARPins or nanobodies, and for analysis by ELISA and surface plasmon resonance (SPR) GLIC and ELIC were expressed with an N-terminal biotinylation tag (Avi-tag). The lysine located within this 15 amino acids long tag can be biotinylated *in vitro* with the BirA enzyme. Biotin binds with high specificity and affinity to chicken avidin, the commercially available neutravidin or the fungal streptavidin. With this tag, the biotinylated protein can be specifically immobilized on a surface as required for various binding experiments. Since in this study, a N-terminal tag was used (Figure 15), in that way only the top of the extracellular domain of GLIC and ELIC was covered, whereas the rest of the extracellular domain and the membrane and the intracellular part were still accessible for binding experiments.

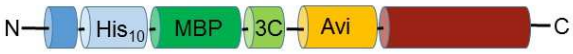

Figure 15 Construct of GLIC and ELIC with an N-terminal Avi-tag.

The construct of GLIC and ELIC (red) incorporate an N-terminal PelB signal sequence (blue), followed by a His_{10}-tag (light blue), MBP as fusion protein (green) and a HRV 3C cleavage site (light green). GLIC and ELIC are preceded by an Avi-tag (yellow) which acts as substrate for the BirA enzyme for in vitro biotinylation.

As alternative to the biochemical biotinylation, a chemical modification strategy can be employed where a chemical reagent (EZ-Link Sulfo-NHS-LC-LC) linked to biotin, reacts with the amino group of a lysine on the protein surface. In this work, the biochemical biotinylation was used, because in this case the biotinylation site is defined and by this strategy the largest part of the protein remains accessible for binders. The *in vitro* biotinylation had no influence on the protein expression yields or function. To show its functionality, *X.laevis* oocytes were injected with mRNA coding for N-terminal Avi-tagged GLIC and

currents were recorded the next day by two-electrode voltage-clamp (TEVC) electrophysiology. In these experiments, the expression levels and functional properties of the channels can be assessed. Upon exposure to the agonist, protons in case of GLIC, the channel changes its conformation and ions can flow along their electrochemical gradient. The resulting currents can be measured and used for an evaluation of expression levels and functional properties. In Figure 16, the currents evoked from *X.laevis* oocytes expressing the wild type channel after exposure to high proton concentration is compared to those of oocytes expressing Avi-tagged GLIC. No significant difference could be observed, which ensures, that the addition of the tag did not alter the functional properties of the protein.

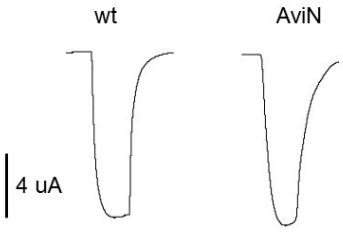

Figure 16 Two-electrode voltage clamp (TEVC) of GLIC wildtype and avi-tagged GLIC

TEVC of GLIC wild type and avi-tagged GLIC expressed on X.laevis oocytes. Currents were recorded at pH 4 and the voltage was clamped at -40 mV. The N-terminal Avi-tag has no influence on the protein function. The black bar shows currents of 4 µA.

To analyze the efficiency of enzymatic biotinylation, the purified and biotinylated GLIC was mixed with magnetic streptavidin coated beads and, after a short incubation time, the beads binding the biotinylated protein were pulled down with a magnet and washed twice. The supernatant was then loaded on a SDS gel to evaluate the biotinylation efficiency. By that procedure it was shown that virtually all proteins bind to the streptavidin coated magnetic beads, thus suggesting that at least one avi-tag per pentamer is biotinylated (Figure 17).

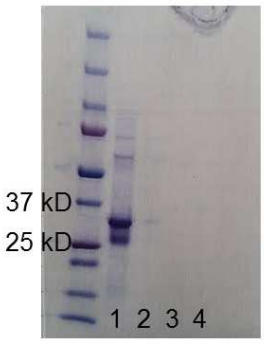

Figure 17 SDS-PAGE of the biotinylation test.

Coomassie blue stained gel showing the efficiency of biotinylation. 1: Input (purified and biotinylated protein). 2: Supernatant after 15 min incubation with the streptavidin coated beads. 3 + 4 supernatant after 2 and 3 washing steps, respectively. The band between 37 kD and 25 kD correspond to the biotinylated protein.

After successful purification and biotinylation of GLIC and ELIC both proteins were used for selecting specific protein binders with various selection methods such as Phage and Ribosome Display.

2.1.2 Phage Display with a single chain variable fragment (scFv) library

Phage Display, first described in 1985 [84], is a potent method to select a specific binder for a desired target protein. Phages, carrying a phagemid, which is a vector containing both a phage and a bacterial origin of replication, *display* the binders as fusions to their coat proteins. Coat proteins of filamentous bacteriophages (e.g. M13) are genetically engineered and linked to the variable chain of an antibody (Figure 18). Although the genetic fusion to either the major coat protein pVIII or to the minor coat protein pIII is possible, the fusion to the pIII is common.

Figure 18 Construct of a scFv linked to a phage protein.

The genetic fusion of the heavy and the light chain to the pIII coat protein results in a phage expressing the scFv thereby physically connecting phenotye and genotype. For ELISA experiments a myc-tag is fused to the scFv. The stop codon TAG is over read by the TG1 cells, producing a scFv-protein III fusion. The coat proteins and necessary replication enzymes are provided by the helper phage which has a mutated origin of replication.

The phages, expressing the binders as fusion proteins and thus connecting the genotype and phenotype of the binder in the same particle, are screened against the immobilized target protein (Figure 19). After incubation, unbound phages are washed away, whereas phages displaying a protein that binds specifically to the target are eluted and used for infecting bacteria for amplification. After superinfection of the bacteria with the helper phage, which supplies the viral components for ss-DNA replication and packaging of the phagemids into phages in the periplasms, the produced phage particles present in the medium are harvested and used for the next selection cycle [85].

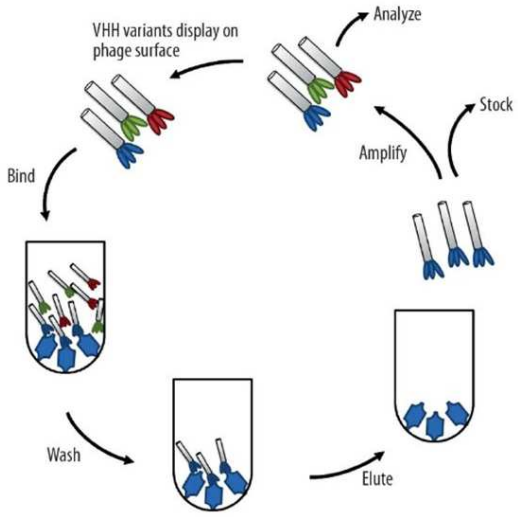

Figure 19 Phage Display cycle

A library, consisting of single chain variable fragments, displayed on the surface of phage particles is incubated with the immobilized target protein for binding selection. After several washing steps the specifically bound phages are eluted and used for infecting E.coli cells for amplification for the next selection cycle. After 3 to 4 cycles the selected binders are analysed by ELISA. Adapted from [86].

The commonly used helper phage M13K07 has a slightly malfunctioning origin of replication and therefore is packaged less frequently into the phage particles. The produced phage particles incorporate either the scFv-pIII fusion or the pIII from the helper phage. Since most of the pIII proteins are derived from the helper phage and only a small fraction from the phagemid, the phages contain maximal one antibody fragment which is necessary for monovalent display [87, 88]. The ratios of pIII fused to a binder to wild type pIII can vary between 1:9 and 1:10000 [89, 90]. After 2 or 3 selection rounds the phages are subjected to an ELISA experiment where their binding affinity and specificity is tested. The DNA of those binders is sequenced and the binders are characterized by various experiments.

Single chain variable fragments (scFv) are heterodimeric antibody fragments, which consist of the variable part of the heavy (V_H) and the light chain (V_L) of an antibody connected with a flexible polylinker of 15-20 amino acids (Figure 9, [91, 92]). They maintain the binding specificity and affinity of the conventional full length antibody [93, 94].

For selection of specific scFv binders for GLIC by Phage Display, the ETH-2 Gold library was used, which contains about $3x10^9$ different scFv clones [95]. The library consists of the human germline heavy chain segment DP47 and the light chain segments DPL16 or DPK22, which represent 12%, 25% and 16%, respectively of the antibody repertoire in humans [96]. The usage of the DP47 segment provides advantages as the higher thermodynamic stability [97] and the option for the purification with Protein A [98]. The sequence of a scFv is shown in Figure 20.

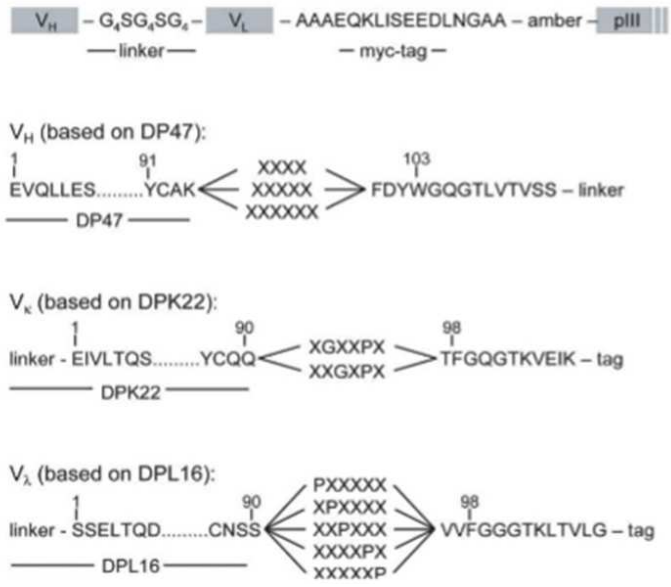

Figure 20 ScFv sequence.

The heavy and the light chains of the scFv are connected with a GS-linker, followed by a myc-tag, an amber stop-codon (TAG) and the minor coat protein pIII of filamentous phage. The variable residues, depicted as X, are located in the complementary determining region (CDR) 3. Figure adapted from [95].

The variable residues are located in the complementary determining region (CDR) 3 which is the most diverse loop. The heavy and the light chain are connected with a glycine-serine linker and fused to the DNA of the pIII protein of the phage. This connection to the minor coat protein of filamentous phage ensures the physical connection of pheno- and genotype during the Phage Display selection

After three selection rounds a phage ELISA was performed where the total output of phages was used to analyze the enrichment of binders from round 1 to 3. In Figure 21 the increasing enrichment of phages pulled down during the selection from round 1 to 3 is visible, whereas neither cross-reactions with a control membrane protein nor with neutravidin or the plastic of the plate was detected. After round 3 the enrichment compared to background is 19-20 fold.

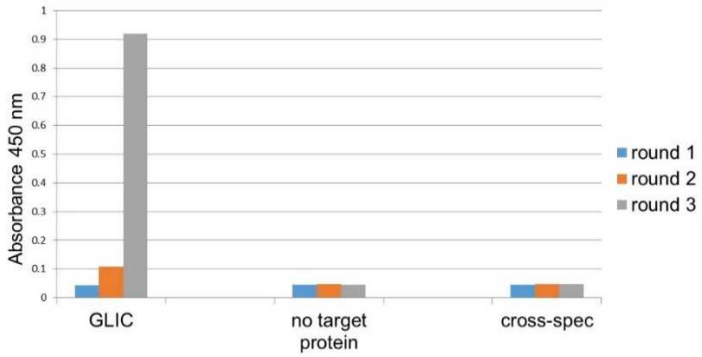

Figure 21 Total phage ELISA.

The colored bars correspond to the signals of binders of round 1 to 3. GLIC was used as target protein, as controls only neutravidin and a SLC11 homologue (cross-spec) were taken to determine the background of non-specifically bound phages. Enrichment of scFv binders for GLIC from Phage Display round 1 to 3 is clearly visible. No signals could be observed for wells containing either neutravidin or a different membrane protein.

Subsequently, TG1 E. *coli* cells were infected with phages from round 2 and 3. Single colonies were picked and grown in 96-deep-well plates. After inoculation, a single clone ELISA of binders from round 2 and 3 was performed to show how many specific binders were selected by Phage Display. For each well, a control well not containing any target protein was tested to see if the scFvs unspecifically bind to plastic or the coated neutravidin. These controls were used to determine the background. In Figure 22 the ELISA signals from binders from round 2 (A) and round 3 (B) are shown. Whereas ELISA signal from round 2 binders are low, the signals of the round 3 ELISA are significantly over background (estimated as 0.05). Since either no or very low signals were observed in the control wells, were no membrane protein was immobilized, these scFv binders from round 3 were considered to bind specifically to the target protein.

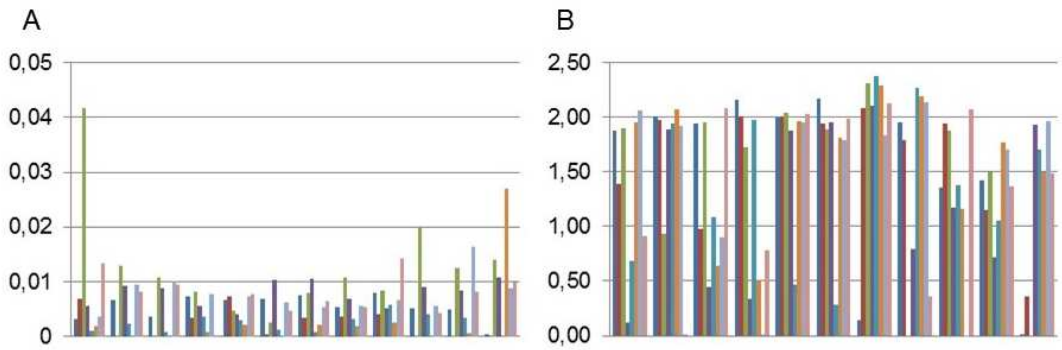

Figure 22 Single clone ELISA with scFv binders from round 2 and 3.

On the Y-axis the ELISA signal is shown.Single clones are displayed in different colors. A) Single clone ELISA with scFv binders from round 2. All signals, except one, were low within the the background signal from wells without

target protein. B: Single clone ELISA with scFv binders from round 3. Many wells with signals 10 to 30 fold over background are observed.

The scFv binders that show high and specific signals in ELISA, were sequenced. Ten different scFv sequences were obtained and some of them appeared more than once. The scFvs of the ETH-2 Gold library are composed of a heavy and a light chain (DPL16 or DPK22) and were randomized in the complementary determining region (CDR) 3, meaning that the differences between the individual scFvs consist of different light chains and different amino acids in CDR 3 [95]. In Table 1 the selected scFvs with their respective sequences in the CDR 3 and their frequency of appearance are listed.

Name	#	Heavy chain	DPL16	DPK22
A	33x	QTLH	KPPWMP	
B	17x	NSSR	YDYRWP	
D	6x	RSLS	RPPWLP	
E	4x	QTLI	LPYFMP	
F	2x	APWRR	PVPLSS	
G	1x	QSLH	LPFWLP	
H	1x	GTSR	RWTEPP	
I	1x	FTKSL	HGRTPF	
K	1x	NSSR	KYSDLP	
C	1x	SSGLS		HGLTPL

Table 1 List of scFvs.

In the first column the labels of the selected scFvs are shown. # lists the frequency of appearance of clones with the same sequence. E.g. scFv A was found 33 times whereas scFv K only once. The third column shows the sequence in the randomized CDR 3 of the heavy chain, the fourth and fifth column, the sequences of the CDR* of the corresponding light chains.

Competent HB2151 E. *coli* cells were transformed with the DNA of the 10 scFvs selected by Phage Display and single clone ELISA. After inoculation, the cells were harvested, lysed and the scFvs were purified over a Protein A column, followed by a size exclusion chromatography (SEC) (Figure 23). Nine out of the 10 different scFvs could be successfully expressed and purified. The purity of the scFvs after the Protein A column purification and the size exclusion was confirmed by a SDS-Page. The two peaks observed after SEC (Figure 23, B) both correspond to the scFv, with the first peak potentially corresponding to an oligomeric state. The protein yields after SEC range between 2-10 mg/l.

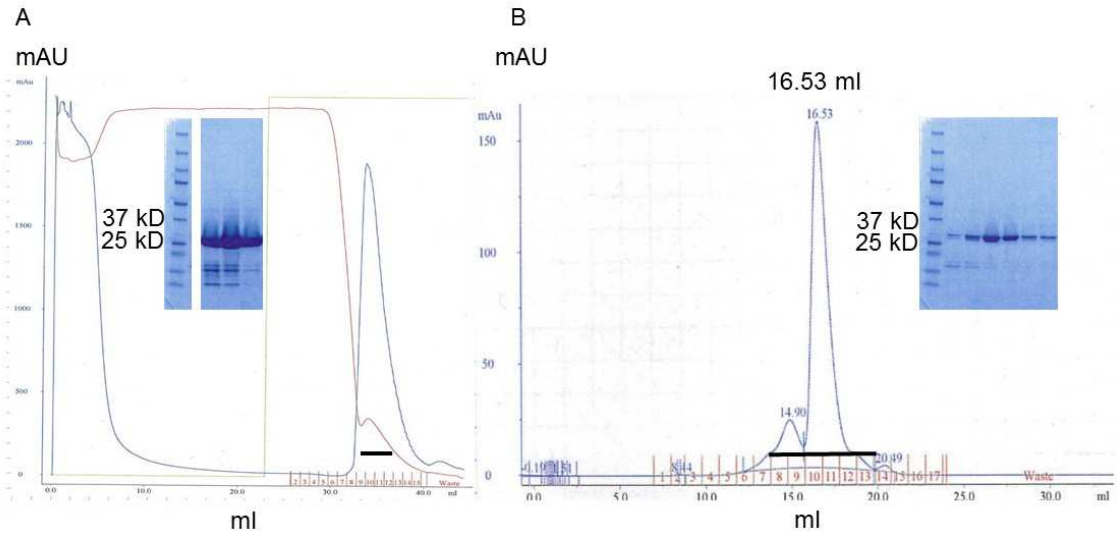

Figure 23 Protein A column and size exclusion profile of a scFv

A) Protein A column profile of a scFv. The blue curve shows the absorption at 280 nm. The red and the gray curve correspond to the conductivity and the concentration of the elution buffer, respectively. B) Size exclusion chromatogram of a scFv. The blue curve depicts the absorbance at 280 nm and shows a monodisperse peak. The retention volume of 16.52 ml corresponds to the expected molecular weight of the scFv of about 27 kDa. No aggregation peaks are observed. The purity of the scFvs after the Protein A column and the size exclusion was confirmed by SDS-PAGE and the black bar indicates the fractions that were loaded on the gel. The bands between 25 and 37 kDa correspond to the scFv.

To test if the scFv and the target protein GLIC form a stable complex, the purified scFv was mixed with GLIC in a 1.5 molar excess and co-migration was monitored by SEC with a Superdex S200 column. Co-elution of both proteins means that the binders have a K_D lower than 1 µM. In Figure 24 a chromatogram of a scFv that co-migrates with GLIC is shown. A SDS-gel of the fractions of the first peak with a retention volume of 10.4 ml shows both proteins, which suggests a co-migration. A peak shift towards higher molecular weight (from 11. 9 ml of GLIC to 10.4 ml of the complex) could be observed on SEC, which is due to the increased size of the complex. Due to a not strictly 1:1 binding of one scFv to one GLIC subunit or due to dissociation of the complex on the column, the peak is not monodisperse. The peak at the elution volume of 16.46 ml corresponds to unbound scFv, loaded in excess, which is confirmed by the SDS-gel. The small peak at 14.7 ml retention volume might contain an oligomeric species of the scFv. Four scFvs, named A, E, G and H co-elute with GLIC.

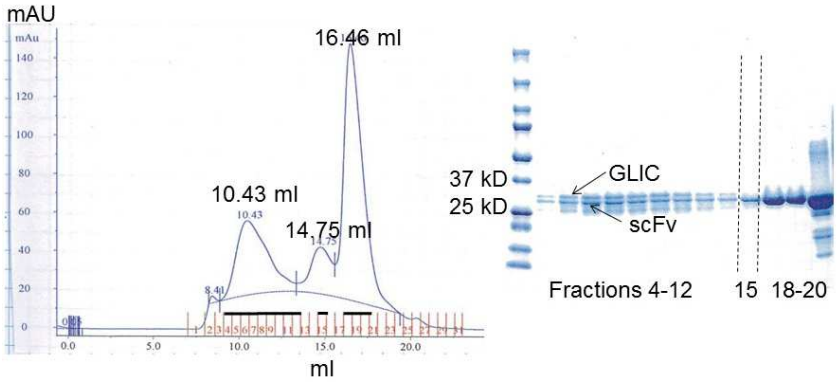

Figure 24 Size exclusion chromatogram of scFv co-eluting with GLIC

Size exclusion chromatogram of a scFv co-eluting with GLIC. The retention volume of the first peak at 10.43 ml is shifted towards higher molecular weight, for about 1 ml compared to the retention volume of GLIC, indicating co-migration of GLIC and the scFv. The peak at 16.46 ml corresponds to the unbound scFv loaded in excess. The SDS-PAGE confirms the co-elution of both proteins, since GLIC and the scFv are present in the first peak. The black bar shows the fractions selected for SDS-PAGE.

To probe whether the scFvs recognize GLIC in a membrane environment and impact channel function, a *X. laevis* oocyte binding assay was performed to investigate whether scFvs would bind to GLIC expressed at the plasma membrane of an oocyte. The oocytes were injected with mRNA coding for GLIC and the protein was expressed for 2 days. Afterwards the oocytes expressing the protein and non-injected oocytes as control, were incubated with purified myc-tagged scFvs. After 3 washing steps, bound scFv would be detected by an antibody binding to the fused myc-tag. No signals after adding the enzyme substrate could be observed, which means that the scFvs did not bind to the target protein. This means that the binding epitope of scFvs is not accessible to the outside either because it lies close to the membrane interface or on the intracellular part of GLIC. Alternatively, the vitelline layer surrounding the oocytes maybe impermeable for the binders.

To obtain a general estimate of the binding affinities of selected scFvs to GLIC, the interaction was characterized by Surface Plasmon Resonance (SPR) spectroscopy. SPR is a useful optical method, which measures changes in the refractive index after binding of analytes to immobilized ligands on a polymer layer. This technique provides data on specificity, affinity and kinetic parameters of protein-protein interactions [99-101]. For these investigations, purified and enzymatically biotinylated GLIC was coated on a ProteOn™ NLC Sensor Chip and the measurements were performed with a ProteOn XPR36 device. In Figure 25, SPR sensorgrams of the scFv A, E and G, applied with different concentrations, are shown. The data was globally fitted, using a 1:1 Langmuir kinetic model expecting a single scFv binding site on each subunit of the pentamer. The quality of the data and therefore its fitting depends on several factors such as buffer composition, purity and concentration of analyte and ligand, the density of immobilized membrane protein and the flow rate [102, 103]. A possible effect of the solvent was decreased by using the same buffer for purification of scFv and GLIC and for the measurement. Both proteins were subjected to size exclusion chromatography to reduce the amount of contaminant proteins and GLIC was biotinylated enzymatically which leads to an additional purification step during immobilization on the neutravidin coated chip. The immobilization density as well as the flow rates were adjusted according to the recommendations. The fits showed large errors potentially due to a possible rebinding of the analyte to the immobilized protein or due to a non-homogenous analyte. Despite these errors it was still possible to estimate the affinities of the present binders. Whereas the binding affinities of the scFv A and scFv E are in the low single-digit nano molar range, that one of the

scFv G is of around 50 nM. Described binding affinities of scFvs range between 10 nM up to 1 pM [104, 105]. To determine the binding affinities with higher accuracy, additional experiments with lower analyte concentrations in the range of 0.1-10 times the expected K_D would have to be performed [103].

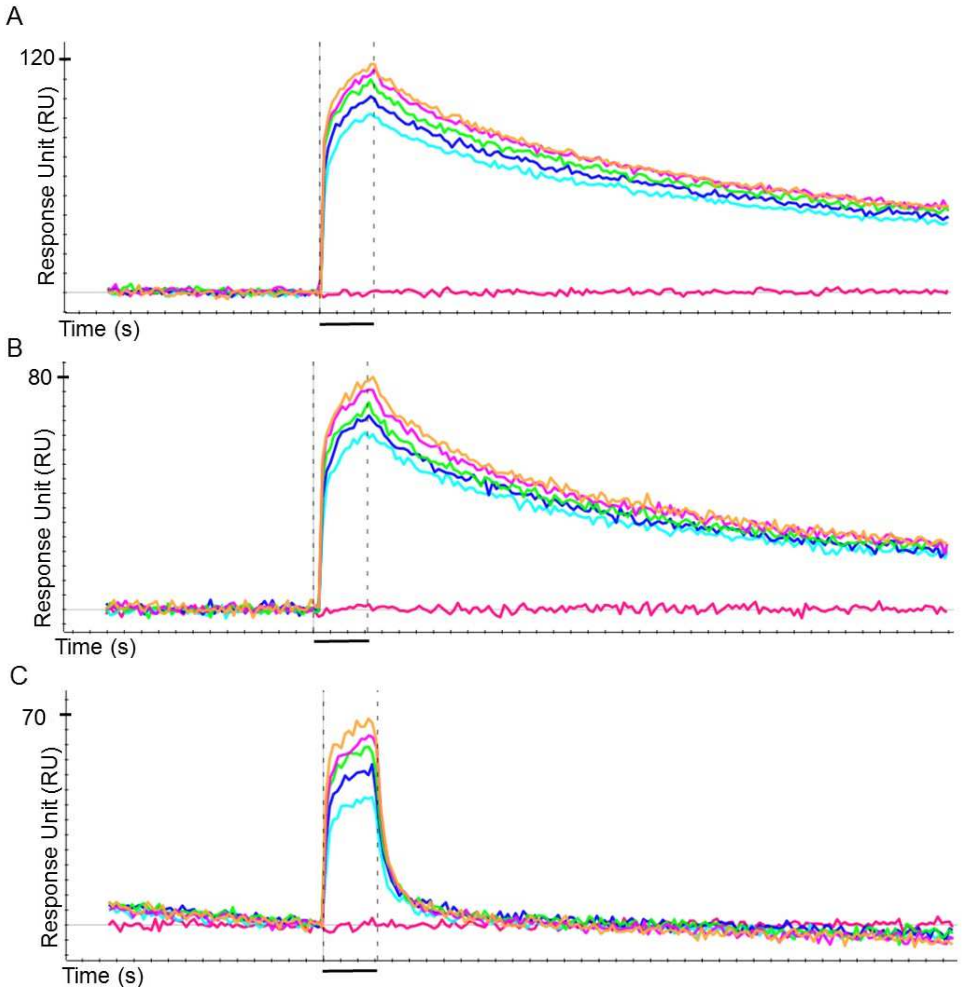

Figure 25 Surface Plasmon Resonance (SPR) sensorgrams of scFvs

Binding affinities of the scFv A (A), scFv E (B) and scFv G (C) to GLIC were analyzed with surface plasmon resonance (SPR). The X-axis corresponds to the time measured in seconds and the Y-axis to the response unit (RU). Different concentrations of analyte are used, depicted in unique colors (yellow: 600 nM, purple: 300 nM, green: 150 nM, dark blue) 75 nM, light blue) 37 nM, pink) 0 nM). The first dotted line shows the association signal of the scFvs whereas the second dotted line indicates the beginning of the dissociation. The black bar corresponds to 60 seconds.

For co-crystallization, GLIC and the 4 single chain variable fragments that co-elute on SEC, were expressed and purified separately, mixed in a 1:1.5 molar ratio of membrane protein to binder. Despite screening in a broad range of conditions no crystals could be observed, even in conditions at low pH were GLIC crystallizes, indicating, that the binding of scFvs might prevent crystal formation. The co-crystallization of the single-chain variable fragments (scFvs) together with GLIC was possibly impaired because the flexible GS-linker connecting the heavy and the light segment of the binding protein may have interfered with the formation of crystal contacts. To overcome potential problems with the flexible linker, the 4 scFvs A, E, G and H that co-elute with GLIC on a size exclusion chromatography were

converted to Fab fragments that contain the variable and one of the constant regions of the light and heavy chain of an antibody (see Figure 9). For that purpose, the DNA of the highly affine scFvs was fused to the human constant heavy and light chain on two separate vectors, which were obtained from CH1 of IgG1 and Cκ, respectively. After cloning of the scFvs into the corresponding vector containing the constant parts, the heavy and light chains were combined by vector-backbone exchange cloning (VBEx-cloning). The heavy and the light chain of the Fab are preceded by the signal sequences phoA (from alkaline phosphatase) and ompA (from outer membrane protein), respectively, which ensures the periplasmic expression [106]. There, the oxidizing conditions allowed the disulphide-bond formation and the assembly to a full-length and functional Fab.

A Fab fragment is supposed to be less flexible than a scFv and, due to its larger size, it offers a larger hydrophilic surface to form new crystal contacts. Because of their larger size, Fabs could also be used as tools for electron microscopy to increase the size of the particle and thus facilitate its identification. The smallest protein thus far determined by single particle electron microscopy is the 170 kD big γ-secretase [107], it is thus likely that a complex of Fabs binding to GLIC, with a combined size of more than 400 kD (assuming one Fab per subunit) should be visible in cryo EM.

The Fab fragments, derived from the scFvs, were overexpressed in MC1061 cells and the lysate was purified with a Protein A column. Subsequently the Fabs were subjected to size exclusion chromatography. Three different Fabs (originating from scFvs E, H and G) could be expressed and purified. In Figure 26 an elution profile of the Protein A column purification and a size exclusion chromatogram is shown. On SEC, the Fab fragments elute at a volume of 16.7 ml as a monodisperse peak and the protein yields after purification range between 0.5-2 mg/l of expression culture.

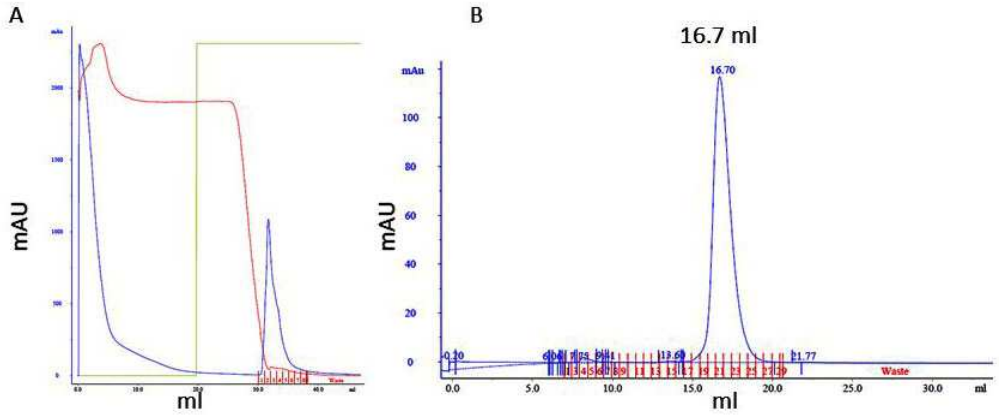

Figure 26 Protein A column and size exclusion chromatogram of Fab fragment.

A) Protein A column chromatogram: the blue curve corresponds to the absorbance at 280 nm, the red and the green curve depict the conductivity and the concentration of the elution buffer respectively. B) Size exclusion chromatogram of a Superdex S200 column: the blue curve corresponds to the absorbance at 280 nm and shows a monodisperse peak of the Fab eluting at 16.7 ml.

To investigate if these 3 Fab fragments still form stable complexes with GLIC, their co-migration in a binary complex was investigated by SEC on a preparative Superdex S200 column. In Figure 27 a Superdex S200 profile of GLIC co-eluting with a Fab fragment is shown. A shift in the elution volume towards higher molecular weight, from 11.9 ml for GLIC to 10.92 ml for GLIC in complex with the Fab fragment and the presence of 3 bands on SDS-PAGE (for GLIC and for the heavy and the light chain of the Fab) with appropriate molecular weight confirm the co-elution of the two proteins. The peak at 16.27 ml corresponds to the unbound Fab fragments, which were loaded in excess.

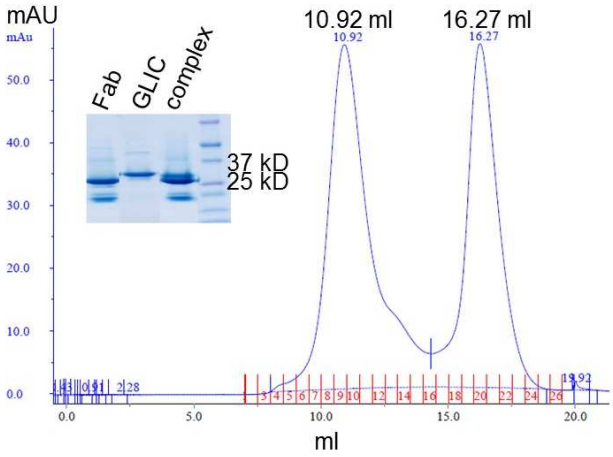

Figure 27 Size exclusion chromatogram of a GLIC Fab complex.

The blue curve depicts the absorption at 280 nm. The retention volume of the first peak of 10.92 ml indicates co-migration of GLIC and the Fab fragment, since it is shifted towards higher molecular weight. The peak at 16.27 ml corresponds to excess unbound Fab fragments. The SDS-PAGE confirms to co-elution of both proteins, since GLIC and the heavy and the light chain of the Fab fragment at about 25 kD and 20 kD, respectively, are present in the first peak.

To evaluate whether the binding affinities of the Fabs are similar to those of the corresponding scFv, the Fabs were subjected to SPR (Figure 28). The 1:1 Langmuir kinetic model, describing a single Fab binding on each subunit of GLIC, was used for fitting. As for the scFvs, the data only allows for an approximate estimate of binding affinities. It was not possible to determine the binding affinity of Fab A by SPR, but co-elution experiments with GLIC on SEC suggest an affinity of lower than 1µM. Fab E shows an estimated binding affinity in the single-digit nanomolar range which is in the same order of magnitude as the corresponding scFv. Fab G has a reduced binding affinity compared to the scFv G of about 100 nM. Fab fragment H shows similar affinities as Fab G.

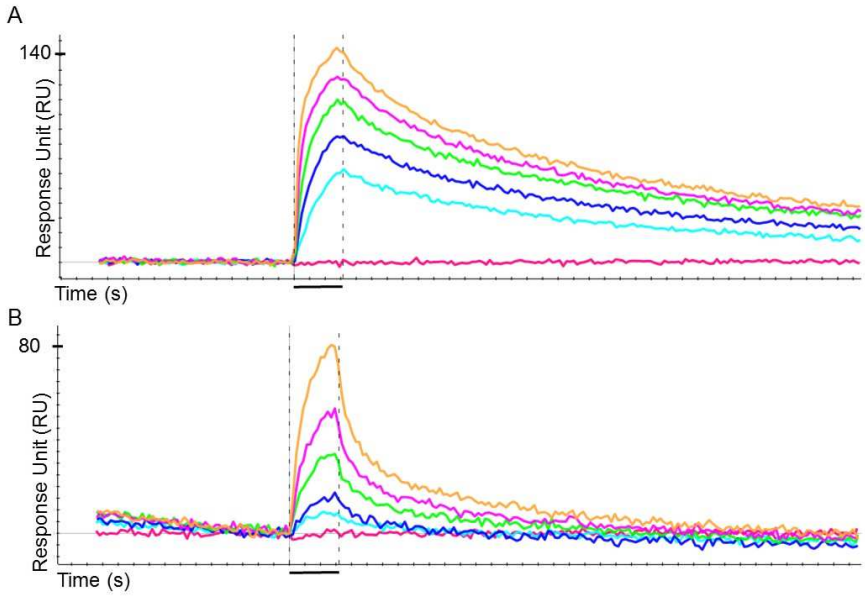

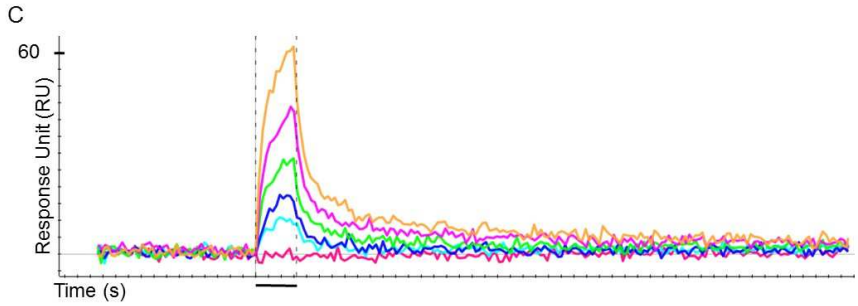

Figure 28 SPR sensorgrams of Fab E, Fab G and Fab H

Binding affinity of a Fab generated from scFvs binding to GLIC as measured by SPR. Runs with different Fab concentrations are depicted in unique colors (yellow: 600 nM, purple: 300 nM, green: 150 nM, dark blue) 75 nM, light blue) 37 nM, pink) 0 nM). The first dotted line shows the application of Fab and the second dotted line indicates the beginning of the dissociation. The black bar corresponds to 60 seconds. A) Fab E. B) Fab G. C) Fab H

For co-crystallization, GLIC and the Fab fragments were expressed and purified separately, mixed in a 1:1.5 molar ratio of membrane protein to binder and screened in a broad range of conditions. Crystals grew in 1 M ammonium formate, at pH 4.5, with addition of 0.05 M Na-Acetate, 10% PEG 4000, at a condition were GLIC crystallizes on its own. After data collection and crystallographic analysis it was confirmed that crystals are of the same space group as the native protein and that they only contain GLIC in the known conformation.

In summary, 10 different scFvs specifically binding GLIC have been selected. Four of the selected binders had promising biochemical characteristics and high binding affinities and therefore could be purified as complex on a size exclusion column. Despite the tight binding, the co-crystallization of the scFv-GLIC complex was not successful. Since the GS-linker, connecting the heavy and the light chain of the scFvs might have prevented crystal formation, the 4 high-affinity scFv binders were converted to Fab fragments, which lack the flexible linker and thanks to their bigger size potentially provide additional surface for crystal contacts. Although the Fabs bind with similar properties as their corresponding scFv, no crystals of the complex were obtained. Still, the Fabs may become useful tools for single particle electron microscopy. As the selection of antibody-based binders from a scFv library did not allow the identification of novel crystal forms for GLIC, another strategy was used to obtain specific binding proteins with a different molecular scaffold.

2.1.3 Ribosome Display with DARPins

Designed ankyrin repeat proteins (DARPins) are synthetic proteins that were originally developed in the group of Prof. Dr. Andreas Plueckthun and that are based on naturally occurring ankyrins, which mediate protein-protein interactions in all 3 kingdoms of life [79, 80]. DARPINs are composed of multiple structural repeats, form elongated and slightly curved structures and therefore contain a concave binding surface [108]. Each repeat consists of 33 amino acids and is folded in a β-turn followed by 2 α-helices and a loop region. Based on their design, DARPins are composed of 2-3 internal repeats, framed by two capping repeats and are thus named N2C and N3C respectively. These binders have been well characterized. They are generally very stable due to conserved hydrogen bonds and a tight packing [78, 109, 110]. In this study a second generation N3C-DARPin library designed by Prof. Dr. Markus Seeger [111] was used. In Figure 29, the general construction of such an N3C DARPin is shown with the N- and the C-terminal capping repeats, flanking the 3 internal repeats.

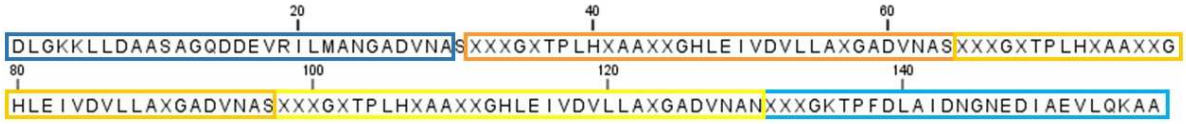

Figure 29 Sequence of an N3C DARPin from the new library.

The 3 internal repeats (orange, dark and bright yellow) are flanked by an N-terminal (dark blue) and a C-terminal (light blue) capping repeat. Randomized positions are indicated by X.

This second generation library is supposed to be more suitable for membrane proteins. It contains an extended randomized surface with a reduced share of hydrophobic residues and an increased fraction of tyrosines in the variable positions. Thanks to this design, the problems of non-specific binding of hydrophobic DARPins is expected to be reduced. Figure 30 compares the randomized positions in the internal repeat of a DARPin of the original and of the new library.

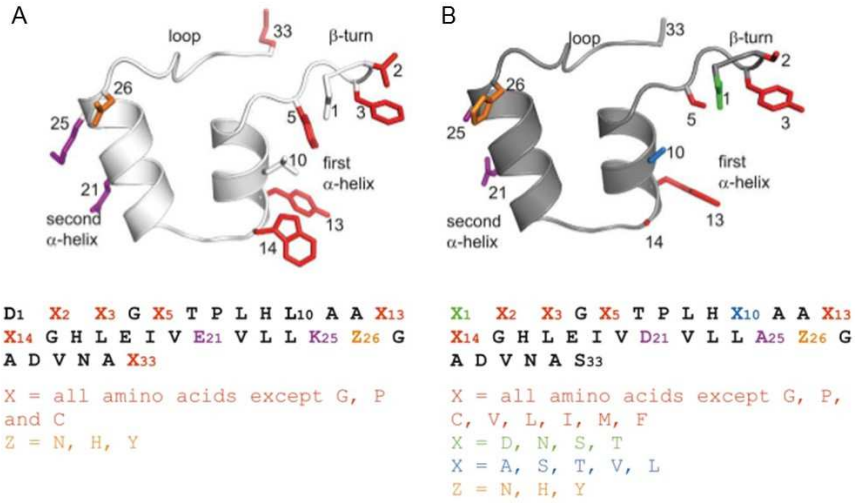

Figure 30 Randomization of internal repeats of a DARPin of the first and second generation.

A) Randomization of a DARPin of the original library (off7, PDP 1SVX). Seven amino acids are randomized in each internal repeat. B) Randomization of a DARPin of the second generation (C7_16, PDB 4JB8). The sequence and the color code of the diversified residues of a new library DARPin are shown at the bottom. The residues colored in violet D, A and S of a new library DARPin were an E, K and X in the original DARPin library. Figure adapted from [111].

The calculated diversity of this new library is 1.9×10^{24} [111], which is somewhat higher than the original library containing 3.8×10^{23} unique proteins [109]. Due to the limitations in DNA assembly, the actual diversity is in the range of 10^{11}.

Ribosome Display is a powerful *in vitro* selection method for specific protein binders from large libraries. In this method, mRNA, coding for the DARPin binder, a T7 promoter, the ribosome binding site (RBS) and stem loops, is translated *in vitro*. A spacer sequence, lacking the stop-codon, prevents the nascent binder to dissociate from the ribosome and thus ensures the coupling of genotype and phenotype by formation of a ternary complex. The ribosomal complexes are selected from the translation mix by binding to the immobilized target protein. After washing away unbound complexes, the DNA encoding

for specifically bound proteins can be recovered and used for the next selection cycle (Figure 31). After 3 to 4 rounds of selection, the DNA of retained binders is transformed into bacterial cells and the purified DARPins are analyzed by ELISA and size exclusion chromatography. The advantage of the Ribosome Display technique, compared to Phage Display is, that the diversity of the library is not limited by the transformation efficiency of bacterial cells and since with the PCR amplifications in each round, additional random mutations may be introduced, which could improve the binding properties further [112-114].

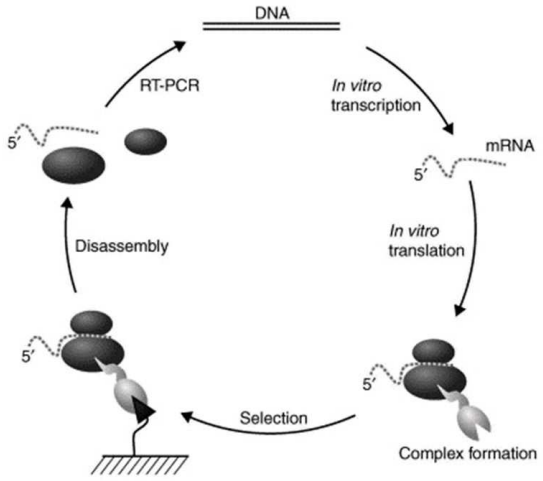

Figure 31 Ribosome Display selection cycle.

A library consisting of mRNAs of potential binders is translated *in vitro*. The ternary complex, consisting of mRNA, the ribosome and the nascent binder is subsequently selected by binding to an immobilized target protein. After washing away of unbound complexes, the DNA encoding for specific binders is generated by reverse transcription, and amplified by PCR. Amplified DNA is subsequently *in vitro* transcribed and used for the next selection round. Figure adapted from [114].

During Ribosome Display, a critical step is the ligation of the PCR-amplified DNA segments of the affinity selected DARPins with the vector containing the ribosomal binding site (RBS), the T7 promoter and the stem loops. For that purpose, the original vector pRDV, carrying the DNA of the β-lactamase, has to be digested and gel-purified before it is ligated with the DNA coding for the DARPins. Despite the thorough digestion and purification, there was always a small fraction of non-digested vector present in the sample. This doesn't cause problems as long as sufficient DARPin DNA is available and the diversity of the library is maintained after ligation, but in some cases this residual β-lactamase DNA can prevent efficient ligation and the thus reduce the diversity of the DARPin DNA pool for the next selection cycle. To avoid this possible problem, the selected DARPin DNA was ligated with short terminal fragments, containing the respective sequences required for transcription and translation of the binding proteins (Figure 32). Following this strategy, the ligation had to be carried out with 3 instead of 2 ligation partners and to make sure that the ligation efficiency was not reduced, the double amount of DNA compared to the original protocol, was ligated and used as template for the PCR on ligation.

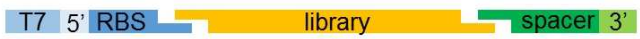

Figure 32 Ligation step during a Ribosome Display cycle.

Before transcription of the DARPin library DNA (yellow) into mRNA, a ligation step adds the T7 promoter and the ribosome binding site (blue) at the 5' end, and the spacer sequence and the 3' stabilizing stem loops (green) at the 3' site. Instead of ligation into the full-length pRDV vector containing these sites, ligation of only the fragments coding for the important sequences was carried out.

2.1.3.1 DARPins selected for GLIC

A total of four rounds of Ribosome Display with the target protein GLIC were performed with a gradual increase of the stringency of washing steps and a decreasing number of PCR cycles after each step. Since the selection was carried out at slightly basic pH, the proton-activated GLIC should be present in a closed, non-conducting conformation. After the fourth selection round, the DARPins were cloned into the arabinose-inducible pBAD expression vector, containing an N-terminal His-tag and a HRV 3C cleavage site. After transformation into competent E. coli MC1061 cells, a single clone ELISA with immobilized GLIC, detecting the His-tag of the DARPin, was performed to select for specific GLIC binders. Wells, only coated with neutravidin were used as control. Out of 192 tested single clones, 64 gave a signal which was significantly higher than the background in the control wells. These clones were sequenced and 27 different DARPINS were found. In Figure 33 an alignment of identified binders is shown.

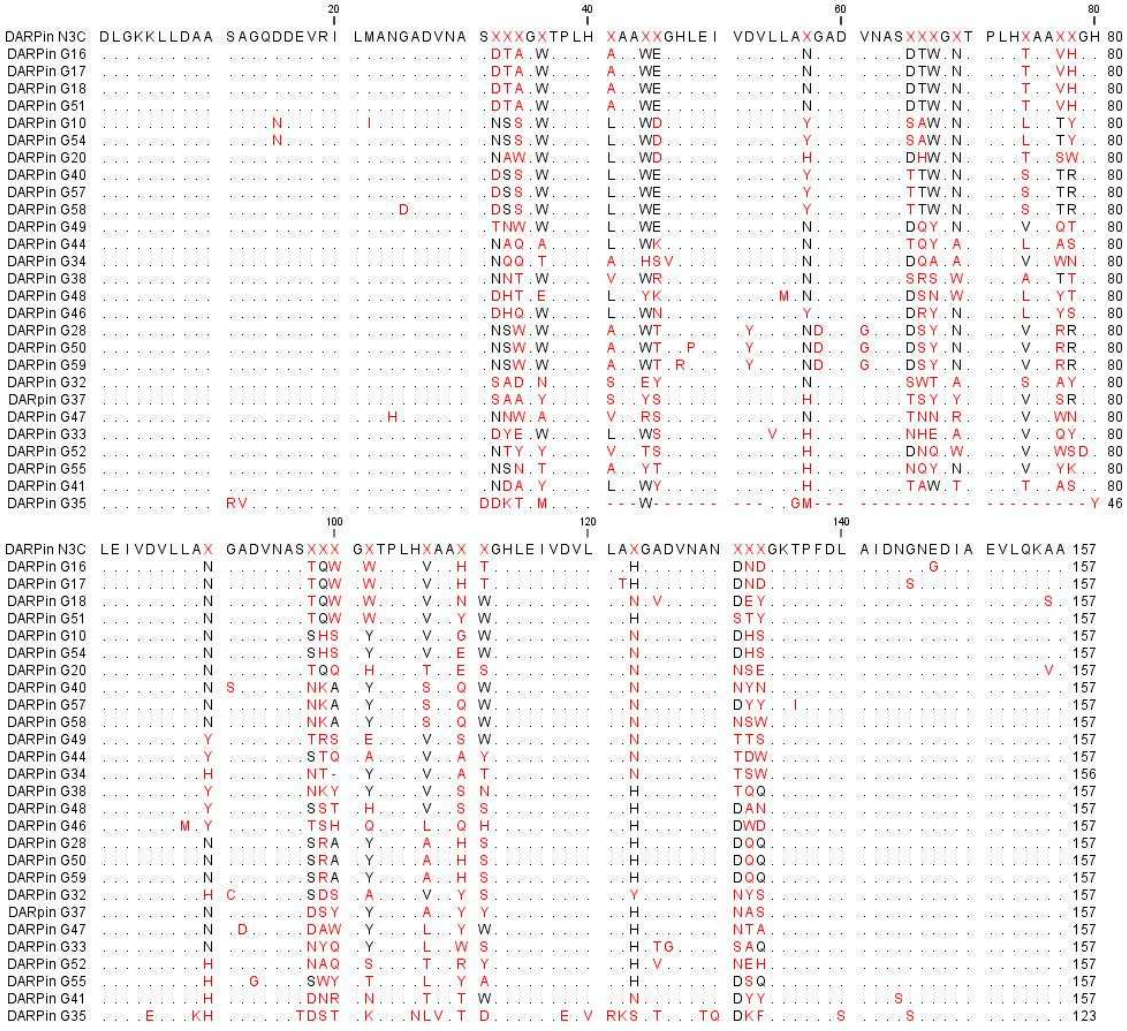

Figure 33 Alignment of DARPins selected by Ribosome Display for GLIC.

The first sequence, named DARPin N3C, corresponds to the consensus. The X marks randomized positions in the library. The dots show identical residues.

The selected and sequenced DARPins contain similar residues in the variable parts. Some of them only differ in a few amino acids and were thus predicted to bind to the same epitope (e.g DARPin G10 and G54 or G16 and G17). The DARPins were overexpressed in MC1061 cells and purified by Ni-NTA chromatography. The His-tag was subsequently cleaved with the HRV 3C protease and removed by binding to Ni-NTA resin and the purified DARPins were analyzed by size exclusion chromatography. For high-throughput screening of the DARPins, an analytical column on a HPLC system was used. Initially, GLIC was loaded to calibrate its elution behavior. Subsequently all the DARPins showing a monodisperse peak on SEC, were mixed with GLIC and loaded to investigate the migration behavior of the complex. In Figure 34 an overlay of size exclusion profiles of GLIC and of GLIC mixed with the DARPin G10 is shown. Together with the DARPin, the peak containing GLIC, shifts towards lower elution volumes corresponding to a higher molecular weight, strongly indicating co-migration of both proteins. Co-migration on SEC was also confirmed by the two bands observed on SDS-PAGE. The small shoulder in the SEC indicates dissociation of the two proteins during size exclusion or alternatively a variable binding stoichiometry of the complex.

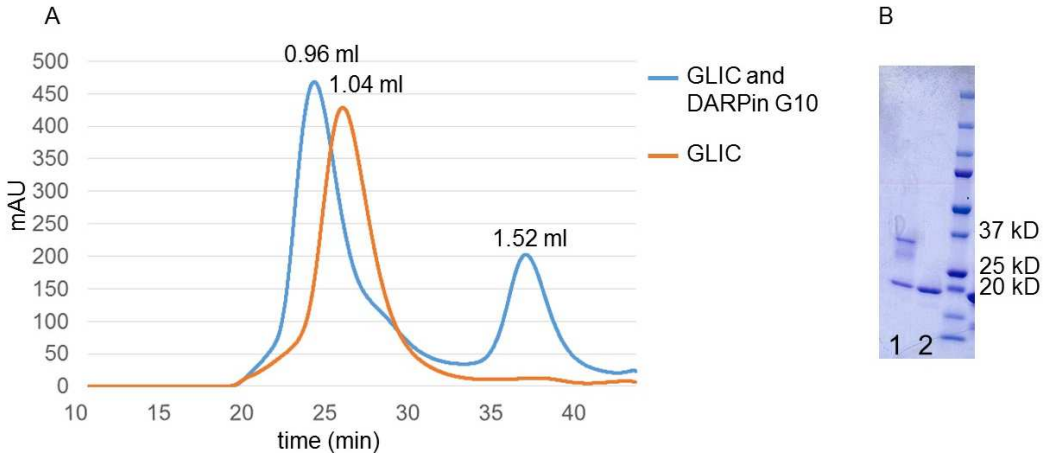

Figure 34 Overlay of elution profiles of GLIC and GLIC mixed together with DARPin G10.

A) The blue and the orange curves depict the absorbance at 280 nm of GLIC and a GLIC-DARPIN complex respectively. The retention volume of the first peak of the blue curve of 0.96 ml is shifted towards higher molecular weight compared to the orange curve at 1.04 ml, indicating co-migration of GLIC and the DARPin. The second peak with a retention volume of 1.52 ml shows excess DARPin. B) SDS-PAGE confirms the co-elution of GLIC and the DARPin. 1: Fraction of the first peak of the blue curve showing GLIC between 37 kD and 25 kD and the co-migrated DARPin at 20 kD. 2: Fraction of the second peak of the blue curve showing excess DARPin at 20 kD.

In Figure 35, the HPLC elution profiles of GLIC mixed with DARPins G46, G52, G54 and G57 are shown. In all cases a peak shift towards higher molecular weight is observed, implying co-migration of the complex. This expectation was confirmed by SDS-PAGE where in the first peak both proteins are detected. The first elution peak of GLIC mixed with the DARPin G52 (Figure 35, B) shows a shoulder thus suggesting the presence of a protein complex that is slightly bigger because it is shifted towards lower retention volume. This could be due to the binding of oligomeric DARPins to GLIC or due to further oligomerization of the complex.

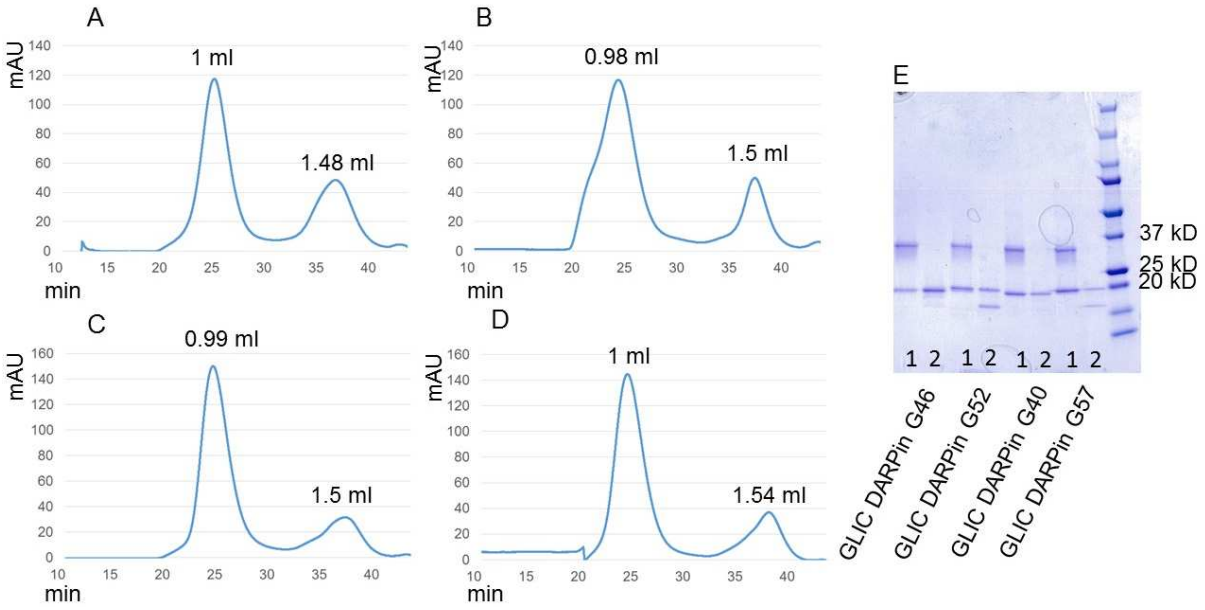

Figure 35 Size exclusion profiles of GLIC DARPin complexes.

Size exclusion profiles on an analytical column. A) GLIC co-eluting with DARPin G46 in a peak with a retention volume of 1 ml. The excess DARPin elutes at 1.48 ml B) GLIC co-eluting with DARPin G52 with a peak with a retention volume of 0.98 ml. The excess DARPin elutes at 1.5 ml. C) GLIC co-eluting with DARPin G40 with a peak with a retention volume of 0.99 ml. The excess DARPin elutes at 1.5 ml. D) GLIC co-eluting with DARPin G57 with a peak with a retention volume of 1 ml. The excess DARPin elutes at 1.54 ml. E) A SDS-gel with fractions from the respective HPLC runs of different GLIC and DARP complexes. The upper band between 37 kDa and 25 kDa corresponds to GLIC and the lower band at 20 kDa to the DARPin. 1: Fraction of the first elution peak, where co-migration of GLIC and DARPin strongly indicates complex formation. 2: Fraction of the second peak, containing excess DARPin.

For co-crystallisation experiments, GLIC and DARPins were expressed and purified separately. SEC-purified and concentrated proteins were mixed in a 1:2 molar ratio and subjected to another round of size exclusion chromatography to confirm their co-migration. In Figure 36 a size exclusion profile of GLIC in complex with DARPin G18 on a preparative Superdex 200 column is shown. Two separate peaks correspond to the GLIC-DARPin complex and to unbound DARPin at retention volumes of 10.76 ml and at 16.56 ml, respectively. The peak composition was confirmed by SDS-PAGE. The peak corresponding to the complex was collected, concentrated to 7-10 mg/ml and used for crystallization screening. Not all GLIC-DARPIN complexes did elute as a single monodisperse peak, which indicates possible dissociation or heterogeneity of the complex. This could lower the molar ratio of DARPin to GLIC in fractions used for crystallization screening. For this reason, for crystallization experiments, GLIC and DARPins were purified individually and mixed prior to crystallization in a 1:1.2 molar ratio. Although the DARPins are in slight molar access, a similar crystallization behavior as for the pure complex was expected. In complexes with DARPins G16, G18, G46 and G57 crystals could be observed in different

conditions at low and high pH, whereas no crystals were observed at the same conditions in controls only containing the respective DARPins.

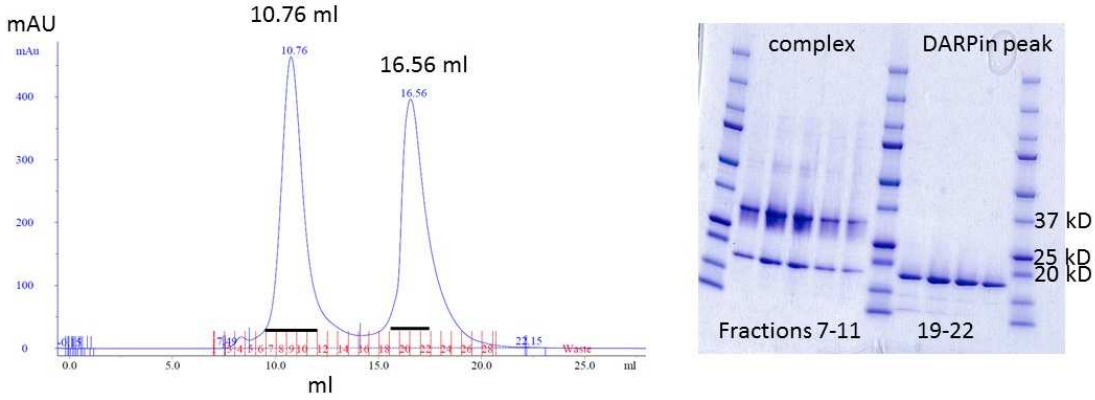

Figure 36 Size exclusion profile of co-migration of GLIC and DARPin G18 for crystallisation.

Chromatogram of the GLIC–DARPin G18 complex run on a Superdex S200 column. The black bars indicate the fractions which were loaded for SDS-PAGE. Two peaks with an elution volume of 10.76 ml and 16.56 ml are visible. The first peak corresponds to the GLIC-DARPIN G18 complex, as confirmed by SDS PAGE where a band between 37 kD and 25 kD and a second band below 20 kD are visible. The upper band corresponds to GLIC, the lower one to DARPin G18. The unbound DARPin, which was loaded in excess, elutes at a volume of 16.56 ml, as confirmed on the SDS-gel where in fractions 19-22 only the DARPin is present.

In Figure 37 selected crystals and their corresponding diffraction pattern are shown. The crystals grown at low pH conditions turned out to contain only GLIC. Crystals at higher pH diffracted poorly and were not suitable for further analysis.

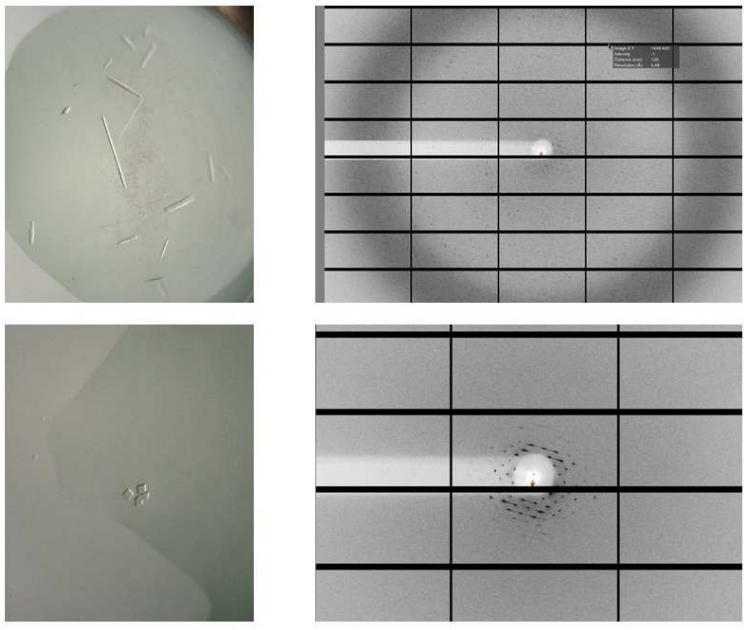

Figure 37 Crystals obtained for GLIC DARPin complexes.

Top) Crystals grown in 1 M Ammonium formate, 0.05 M Na- Acetate, pH 4.5, 10 % PEG 4000, diffracted to 3.5 Å. Molecular replacement revealed that crystals only contained GLIC. Bottom) Crystals grown in 0.2 M Potassium phosphate, 0.05 M glycine pH 9.4, 10 % PEG 4000 showed poor diffraction properties.

Although the co-crystallization approach of the DARPins-GLIC complex has so far not allowed to obtain crystals of the complex at high resolution, a possible impact of the binder on the function of GLIC was investigated. The activation and ion conduction properties of GLIC can be investigated by two-electrode voltage-clamp electrophysiology with *Xenopus laevis* oocytes expressing the protein on the plasma membrane. To test if the His-tagged DARPins bind to exposed parts of GLIC on the oocyte surface and thus possibly alter its function, binding assays have been performed. Oocytes were injected with mRNA coding for GLIC and the protein was expressed for 2 days. Afterwards the oocytes expressing the protein and non-injected oocytes as control, were incubated with purified His-tagged DARPins and after 3 washing steps, bound DARPins were detected with an anti-His-antibody. As for scFvs, no binding was detected, thus indicating that the recognized epitope may either be buried in the membrane or that the DARPins bind to the intracellular part of the protein. To exclude a small number of bound DARPins that would result in a low signal, GLIC expressing oocytes were again incubated with His-tagged DARPins and after 1 washing step, glutaraldehyde, a chemical crosslinking agent was added [115]. If DARPins were able to bind to exposed parts of GLIC they might be covalently crosslinked and it would be possible to preserve the complex after extraction of GLIC. Unfortunately also in this case no signal due to bound DARPins was observed in a Western blot, in agreement with the negative result from the oocyte surface ELISA.

GLIC is activated by protons with a half maximal activation (EC_{50}) at pH 4.8. Its structure was determined at low pH in a presumably conductive conformation, but Ribosome Display to select specific DARPins was performed at high pH where GLIC is supposed to be in a non-conductive conformation. To investigate whether the binding of the selected DARPins to GLIC is dependent on the pH, an ELISA with immobilized GLIC was performed. The incubation with the DARPins was followed by a washing step with buffers covering a pH range from 8 to 4.5. The bound DARPins were subsequently detected with a HRP-conjugated antiHis$_6$-antibody. The results suggest a strong pH dependence of binding, since no signals could be detected below pH 4.75 whereas at all higher pH values all DARPins showed significant signals (Figure 38). Interestingly, the DARPins G16 and G20 show a maximum at pH 4.8 and reduced signals at pH 7 and 8, even though the selection was carried out at pH 7.5.

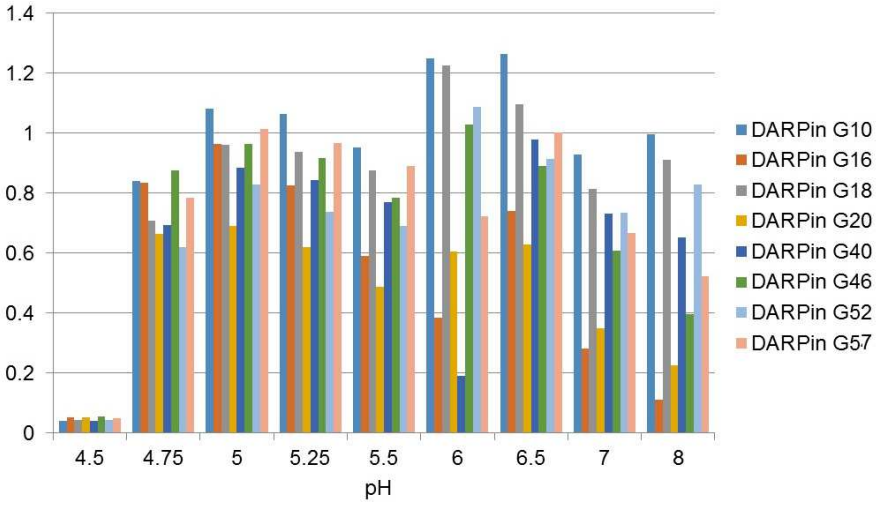

Figure 38 pH dependent ELISA of GLIC DARPin complexes.

After binding to the immobilized target protein, the DARPins were washed with a buffer at different pH ranging from 4.5 to 8 and the bound DARPins detected with an antiHis$_6$-antibody.

To estimate the binding kinetics of DARPins to GLIC and to classify the binders according to their affinity, a surface plasmon resonance (SPR) experiment was performed. For that purpose Avi-tagged and biotinylated GLIC was coated on a ProteOn™ NLC Sensor Chip, containing immobilized neutravidin and the DARPins were subsequently applied at different concentrations. The recorded data was globally fitted using the 1:1 Langmuir kinetic model, expecting a single DARPin binding site on each subunit. In all cases, the fits are poor and only allow for a semi-quantitative estimation of binding affinities. In Figure 39 three SPR profiles are shown with DARPin G28 binding with low µM, DARPIN G52 with sub- µM and DARPin G18 with nM affinity.

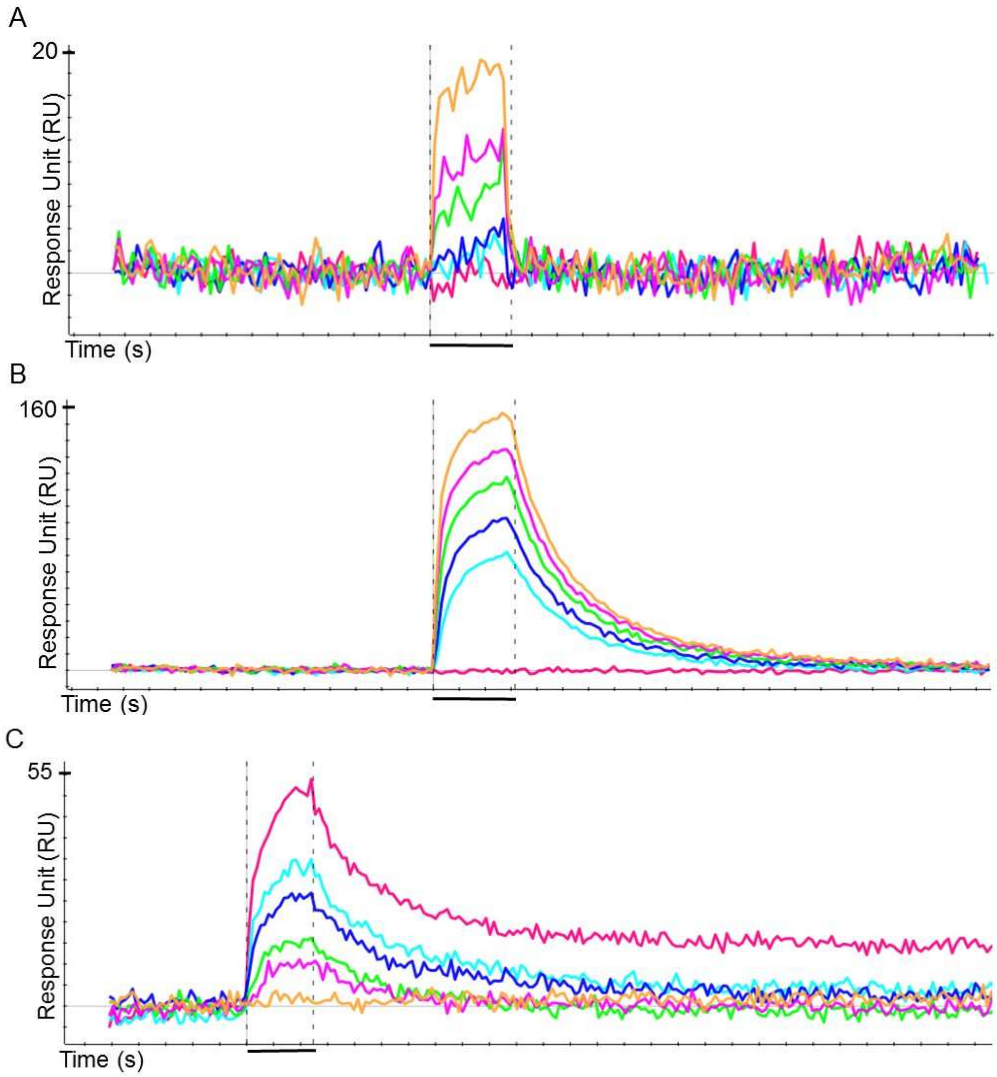

Figure 39 SPR sensorgrams of DARPin G28, G18 and G52.

SPR sensorgrams of three DARPins are shown. The X-axis corresponds to the time, in seconds, and the Y-axis to the response unit (RU). The first dotted line indicates the start of the application of the DARPins at different concentrations (for G28 and G18: yellow: 600 nM, pink: 300 nM, green: 150 nM, dark blue) 75 nM, light blue 37 nM, red) 0 nM, for G52: pink: 600 nM light blue) 300 nM dark blue) 150 nM green: 75 nM red) 37 nM orange) 0 nM) and was used for a fit of the association rate constant. The second line marks the beginning of DARPin washout used to determine the dissociation rate constant. The black bar corresponds to 60 seconds for A) and B). For C) the black bar corresponds to 120 seconds. A) DARPin G28. B) DARPin G18. C) DARPin G52.

The poor fits are potentially caused by DARPin binders, which, instead of being washed out, show rebinding to the immobilized ligand on the chip. This rebinding could be diminished by reducing the analyte concentration [103]. The DARPins G10 and G46 could not be measured by SPR, but co-elution experiments with GLIC on SEC suggest binding affinities below 1 µM. Reported binding affinities of DARPins to membrane proteins range between 9-173 nM [54], whereas for the soluble GFP, a DARPin with a K_D of 160 pM was selected [116]. Generally, DARPins bind soluble proteins with K_Ds ranging between 4-10 nM [117]. Despite the comparably high binding affinities and the promising biochemical properties of selected DARPins, the original purpose of obtaining crystals of the complex in a different conformation diffracting to high resolution or of generating modulators of channel function that are accessible from the extracellular side was not achieved. The lack of a functional phenotype could also be due to the hindered permeability of the binder across the extracellular vitelline layer surrounding a *X. laevis* oocyte, and binding could thus be investigated by characterizing GLIC expressed in HEK-293 cells.

2.1.3.2 DARPins selected for ELIC

The structure of ELIC was determined in a supposedly closed or non-conductive conformation and so far no structure of ELIC in a different conformation could be obtained. In an attempt to close this gap in our structural understanding, three different strategies of Ribosome Display were applied to select binders specifically recognizing ELIC in different states. The agonist propylamine, potentially stabilizes an open or desensitized conformation, and the antagonist acetylcholine or the absence of any binder a closed conformation. A total of four rounds of Ribosome Display were performed for each condition with increasing stringency of the washing step and a decreasing number of PCR amplifications after each round of selection. After the fourth round, the DARPins were cloned into the expression vector and expression was carried out in E. coli MC1061 cells. Subsequently a single clone ELISA was performed to detect specific ELIC binders. As previously, wells coated with neutravidin were used as control. Since for these selections, the few obtained binders showed a certain degree of unspecific binding, the procedure was repeated with ELIC in the absence of any ligand. After the single clone ELISA, which followed the selection, the DARPins showing a significant signal over background were sequenced and subsequently characterized.

In Figure 40 a sequence alignment of the selected DARPins is shown. In total 33 different sequences were identified for the three selections. Some sequences appeared more than once. Six DARPins did contain framework mutations in the third internal repeat, which contains mostly leucines and threonines. Also a few DARPins lacking one or more internal repeats were selected (e.g DARPin E 16).

The selected DARPins were overexpressed in MC1061 cells and purified by Ni-NTA chromatography. After cleavage of the His-tag with HRV 3C protease and its removal by binding to Ni-NTA resin, the DARPins were subjected to size exclusion chromatography on a Superdex 200 column. In contrast to the DARPins selected for GLIC, the DARPins selected for ELIC showed unexpected elution behavior (Figure 41). Most DARPins seem to form oligomers and therefore did not elute as a single monomeric peak. Peaks with a low retention volume can hardly be separated from the elution peak of ELIC and it would thus be difficult to judge if the proteins co-migrate or if they only co-elute without binding with a high affinity to the channel. Consequently these oligomeric DARPins were not used for further investigation by surface plasmon resonance or co-crystallization.

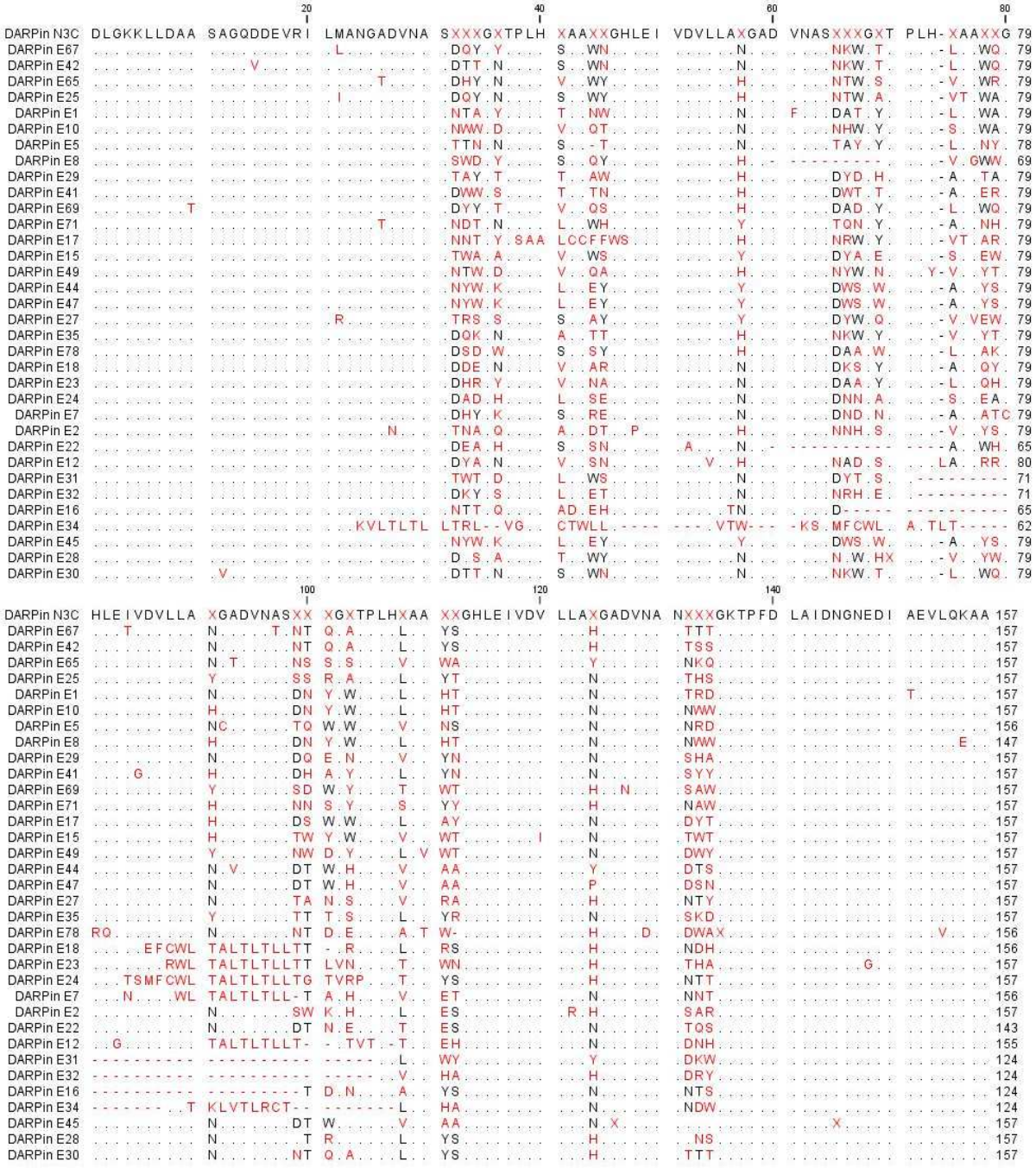

Figure 40 Alignment of DARPins selected for ELIC.

The first sequence, named DARPin N3C, corresponds to the consensus sequence. X indicates randomized positions in the library, the dots identical residues.

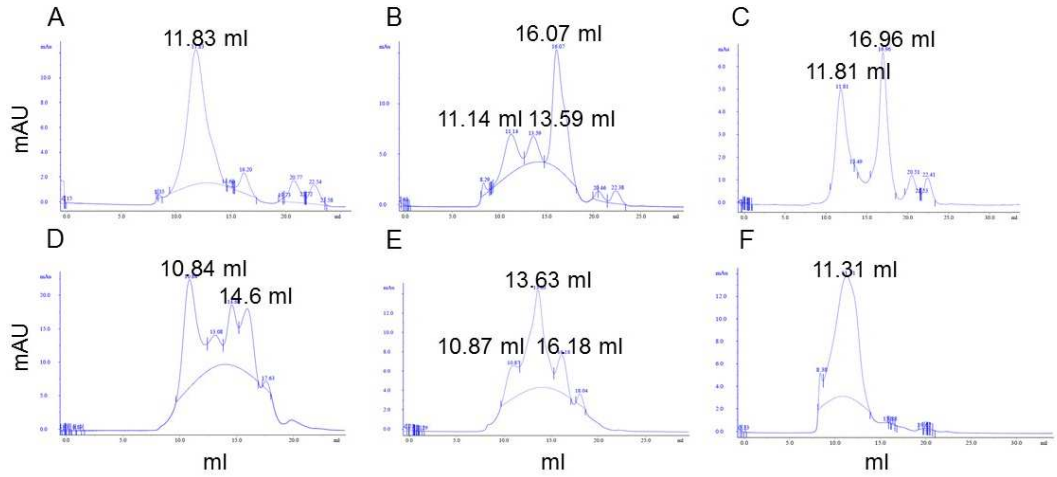

Figure 41 Size exclusion chromatogram of DARPins selected for ELIC.

The blue curve shows the absorption at 280 nm. The Superdex S200 elution profiles of six selected DARPins are shown. A) DARPin E27, B) DARPin E28, C) DARPin E32, D) DARPin E25, E) DARPin E45, F) DARPin E47.

To probe whether stable monomers can be separated from higher oligomers, the monomeric fraction of DARPins eluting as 2 peaks was reinjected on a SEC column. In Figure 42, the fraction of DARPin E42 eluting at 15 ml was reinjected on the Superdex 200 column but the resulting chromatogram again shows a polydisperse behavior with a second peak appearing at lower elution volume.

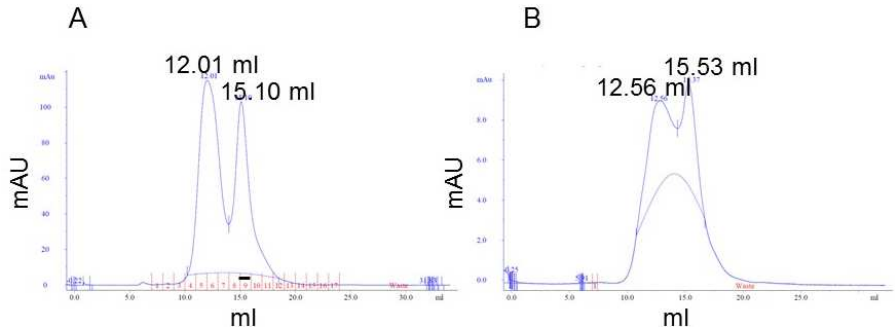

Figure 42 Size exclusion profiles of DARPin E42 and the reinjection of fraction 9.

A) Size exclusion profile of Darpin E42 after purification. Fraction 9 (black bar) corresponding to a monomeric protein was reinjected to the Superdex S200 column and again eluted as polydisperse peak with two maxima (B).

Although the gel filtration profile of the two DARPins E30 and E41, show, that these binders form oligomers, they elute in peaks with retention volumes that could be separated from a complex peak if mixed with ELIC. After purification, the DARPins were mixed at a 1:1.2 molar ratio with purified ELIC and subjected to size exclusion chromatography (Figure 43). It appears, that the DARPin E 30 causes aggregation of ELIC as manifested in the large void peak in the respective chromatograms with a retention volume of 8 ml (Figure 43, B). The SDS-PAGE shows that ELIC is present in the first 8 fractions, in the void peak and in the peak with a retention volume of 11.68 ml. The DARPin is partially eluting in the fractions of the peak at 11.68 ml and mainly in the last peak with the highest retention volume. Although the addition of the DARPins appears to induce aggregation of ELIC, no DARPins were found in the void peak. These findings suggest, that the two proteins do not co-migrate and thus the

DARPins have a binding affinity of lower than 1 µM. The DARPin E41 elutes in a single peak at 13.9 ml, which indicates a formation of oligomers (Figure 43, C). In the size exclusion profile of ELIC in complex with the DARPin E41 (Figure 43, D) a single peak is observed containing both proteins as confirmed by SDS-PAGE but, although the DARPin was loaded in excess, no peak with a retention volume corresponding to the size of a DARPin was detected. In this case it is possible, that this DARPin comigrates with ELIC, but there is also evidence, that the DARPin could be present in oligomers with similar retention volume and coincidentially elutes with the protein.

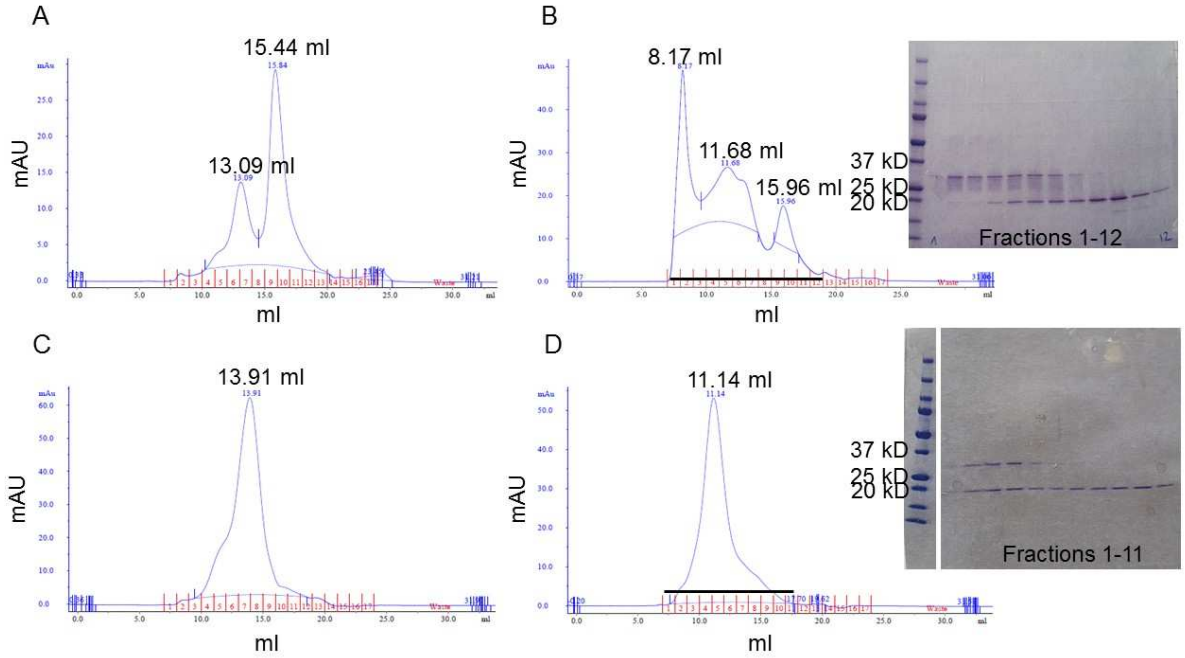

Figure 43 Size exclusion chromatogram of ELIC mixed with DARPins.

A, C) size exclusion chromatogram of the DARPins E30 and E41. B, D) size exclusion chromatogram of the DARPins mixed with ELIC. The black bar indicates the fractions that were loaded on SDS-PAGE. The bands between 37 kD and 25 kD correspond to ELIC whereas the bands at 20 kD correspond to the DARPins.

Despite the little promising SEC data, the interaction of DARPins E30 and E41 with ELIC was subsequently investigated by surface plasmon resonance. The DARPins were loaded at different concentrations and their binding characteristics monitored. Not only in the lanes where biotinylated ELIC was immobilized but also in the control lanes where no protein was coated, significant signals were obtained. In Figure 44 the SPR sensorgrams of the DARPin E41 are shown. The signals of a control lane, where no protein is coated, is compared to the lane with immobilized target protein. Both sensorgrams are very similar and show a fast binding and very slow washout of the ligand that is probably due to nonspecific interactions to the matrix. Although in every cycle of the Ribosome Display a prepanning step was performed to dispose of unspecific, hydrophobic and neutravidin binders, such DARPins with this infavourable characteristic have been selected.

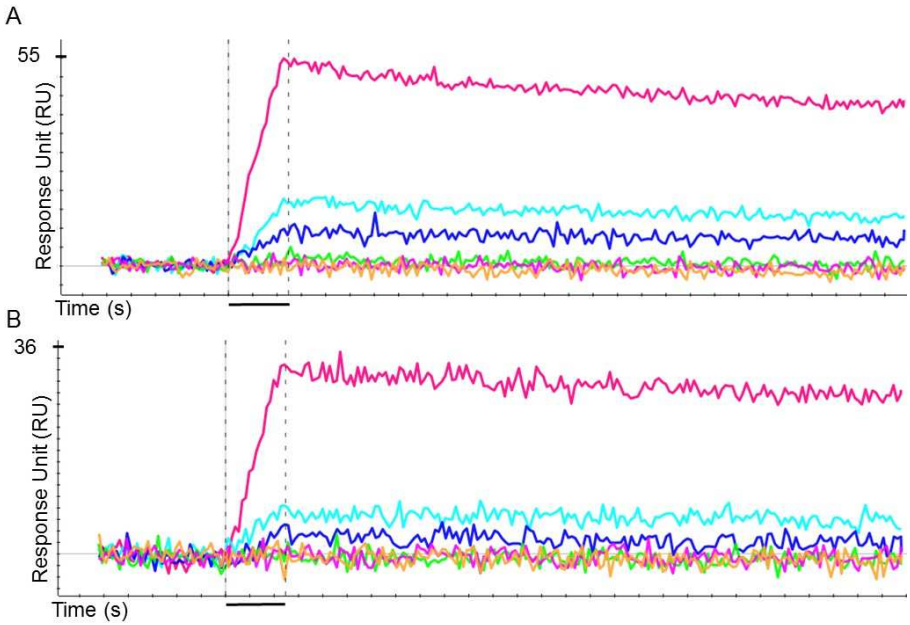

Figure 44 SPR sensorgrams of DARPin E41.

The SPR sensorgrams of the DARPin E41 in controls (A) and in conditions containing immobilized ELIC (B) are shown. The first dotted line indicates the loading of the DARPin at different concentrations (shown in unique colours, yellow) 600 nM, pink) 300 nM, green) 150 nM, dark blue) 75 nM, light blue 37 nM, red) 0 nM). The second line marks the start of the wash-out. The black bar corresponds to 120 seconds.

In summary, several DARPins targeting ELIC have been selected by Ribosome Display. Although a DARPin library of the second generation was used, which was specially designed for membrane proteins [111], all of the selected DARPins show unfavorable biochemical characteristics such as oligomerization and the formation of soluble aggregates. Interestingly this behavior was not observed in the selection of the related channel GLIC. Since these DARPins cannot be used for a structural or functional investigations of ELIC, a different strategy to select other binders was followed. In the next chapter the selection of nanobodies targeting ELIC is described. For that purpose, Alpacas were immunized with the target protein and the DNA of the variable part of their heavy chain antibodies was cloned into a library. Subsequently, Phage Display with this targeted nanobody library was performed to identify promising binders.

2.1.4 Alpaca Immunization and Nanobody selection by Phage Display

To produce nanobodies that specifically bind to the respective targets, alpacas were immunized with freshly purified ELIC. After 4 injections every two weeks, the B-lymphocytes containing the mRNAs of the entire population of immunoglobulins including conventional and heavy chain only antibodies, were collected from the blood. After reverse transcription, the DNA encoding for nanobodies, was cloned into a Phage Display library, which was subsequently used for 2 cycles of Phage Display with Avi-tagged detergent purified target protein. During the second selection round, the stringency of the washing was increased and afterwards a total phage ELISA was performed to monitor the enrichment of binders during the two rounds of selection compared to the initial library.

After the Alpaca immunization and the subsequent Phage Display, a total phage ELISA was performed to determine the enrichment of binders during the two rounds, compared to the library constructed after

the immunization. In Figure 45 a 10-fold enrichment compared to round zero (which corresponds to the library or the input phages) and round 2 can be observed. No big signal with round 2 phages was detected with the negative control, consisting of other membrane proteins, injected in the same animal.

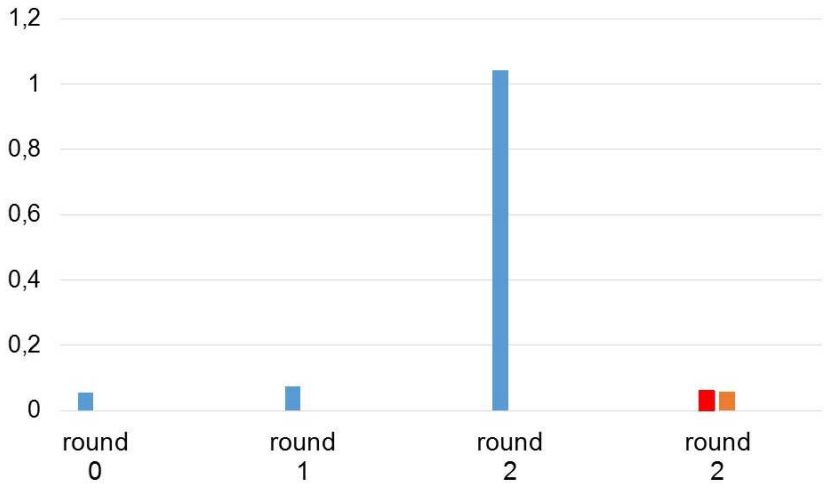

Figure 45 Total phage ELISA with nanobodies selected for ELIC.

Compared to round 0 (library, input phages) and round 1 a ten-fold enrichment of the signal after round 2 can be observed (blue bars). Round 2 phages showed no signal to other membrane proteins (red and orange bar), which were injected into the same animal.

E. coli cells were subsequently infected with round 2 phages and a single clone ELISA was performed. The nanobodies providing a significant signal were sequenced and subsequently analysed. In Figure 46 an alignment of sequences of the nanobodies is shown. Remarkably, the differences appear not only in the complementary determining regions (CDRs), as expected, but also in the framework.

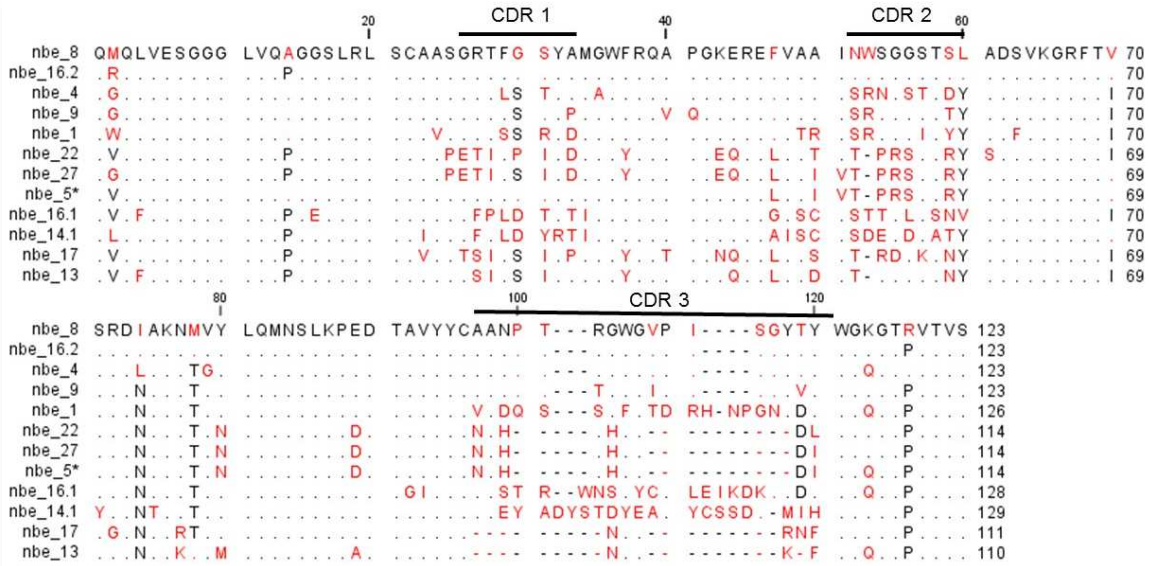

Figure 46 Alignment of nanobodies selected for ELIC.

Identical residues are depicted as dots. The complementary determining regions (CDRs) are indicated by the black bars. Besides variations in the CDRs there are also mutations in the framework of the nanobodies.

The nanobodies coding for these sequences were subsequently cloned into the expression vector, carrying an N-terminal PelB signal sequence, a His-tag, MBP and the HRV 3C cleavage site, and the protein was expressed and purified. After affinity purification on Ni-NTA resin, cleavage of the His-tagged MBP with HRV 3C protease and a second Ni-NTA column purification step the nanobodies were analyzed by size exclusion chromatography. All selected nanobodies elute as a single monodisperse peak. Purified nanobodies were mixed with purified ELIC and the co-migration of both proteins was investigated by SEC. Peak fractions were collected and analyzed by SDS- PAGE. In Figure 47 the size exclusion chromatograms of ELIC with the nanobodies 8, 9, 4, 16.1 and 16.2 and a SDS- gel with the corresponding peak fractions are shown. It is apparent, that the nanobodies 8, 9, and 16.2 co-elute with ELIC, as manifested by the 2 bands on the SDS- gel, whereas the nanobodies 4 and 16.1 do not co-migrate, since only ELIC was detected in a collected fraction of the first peak. Following this initial characterization, the preparations of ELIC-nanobody complexes were scaled-up and subjected to broad crystallization screening. Despite the promising biochemical behavior no crystals were identified for any of the three complexes.

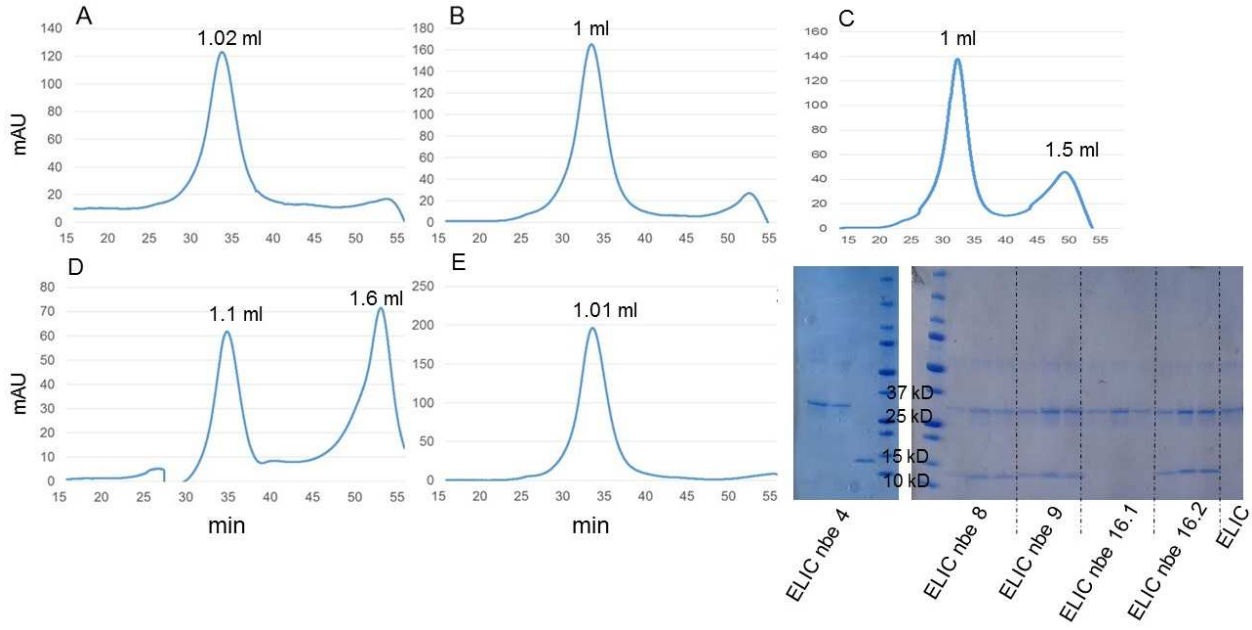

Figure 47 HPLC chromatogram of nanobodies and ELIC

A-E) Examples of nanobodies tested for co-migration with ELIC. ELIC in complex with A) nanobody 8, B) nanobody 9, C) nanobody 4, D) nanobody 16.1, E) nanobody 16.2. SDS-PAGE of the first peak. A band running between 37 kD and 25 kD corresponds to ELIC (see also the last lane on the gel that only contains ELIC), and a band between 10-15 kD to the nanobody.

The purified nanobodies were subjected to surface plasmon resonance (SPR) to evaluate the binding kinetics and to classify the nanobodies according to their affinities to ELIC. Avi-tagged and biotinylated ELIC was coated on a ProteOn™ NLC Sensor Chip and the nanobodies were applied in different concentrations (Figure 48). From the association and the dissociation properties, the binding affinity can be calculated. The data was fitted, using the 1:1 Langmuir kinetic model, expecting one nanobody binding site per subunit. Nanobody 1 has an estimated binding affinity of more than 1 µM, which is supposed to be the limit for co-migration on a SEC column (Figure 48, A). Nanobodies 8 and 9 show binding affinities of about 80 and 100 pM, respectively (Figure 48, B and C).

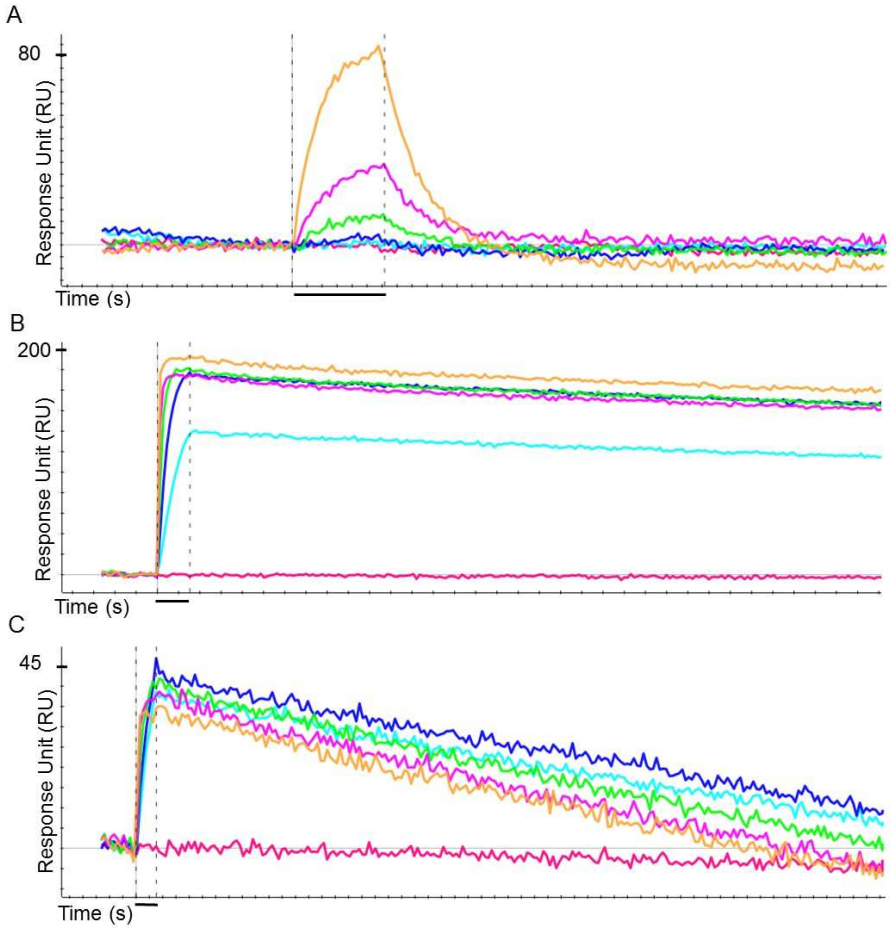

Figure 48 SPR sensorgrams of the nanobodies 1, 8 and 9.

SPR sensorgrams of 3 nanobodies (nbe 1, 8 and 9) are shown. The X-axis corresponds to the time, measured in seconds and the Y-axis to the response unit (RU). The first dotted line indicates the loading of the DARPin at different concentrations (shown in unique colors: yellow, 900 nM, pink, 450 nM, green, 225 nM, dark blue, 112 nM, light blue, 56 nM, red, 0 nM). The second line marks the start of the wash-out. The black bar corresponds to 120 seconds. A) SPR sensorgram of nanobody 1. B) SPR sensorgram of nanobody 8, C) SPR sensorgram of nanobody 9.

The relatively poor fit of the SPR sensorgrams of the nanobodies 8 and 9 could be due to non-specific binding. Similarly to the DARPins selected for ELIC, the nanobodies showed a high degree of unspecific binding as indicated in Figure 49. When comparing the signals of the control lanes, where no protein was coated, with those were the biotinylated target protein ELIC was immobilized, a similar behavior was detected. It appears, that the nanobody interacts with the surface of the chip consisting of neutravidin and alginate (www.biorad.com). Neutravidin was present during Phage Display which could have led to the selection of neutravidin-binding nanobodies, although a prepanning step was always performed to prevent this.

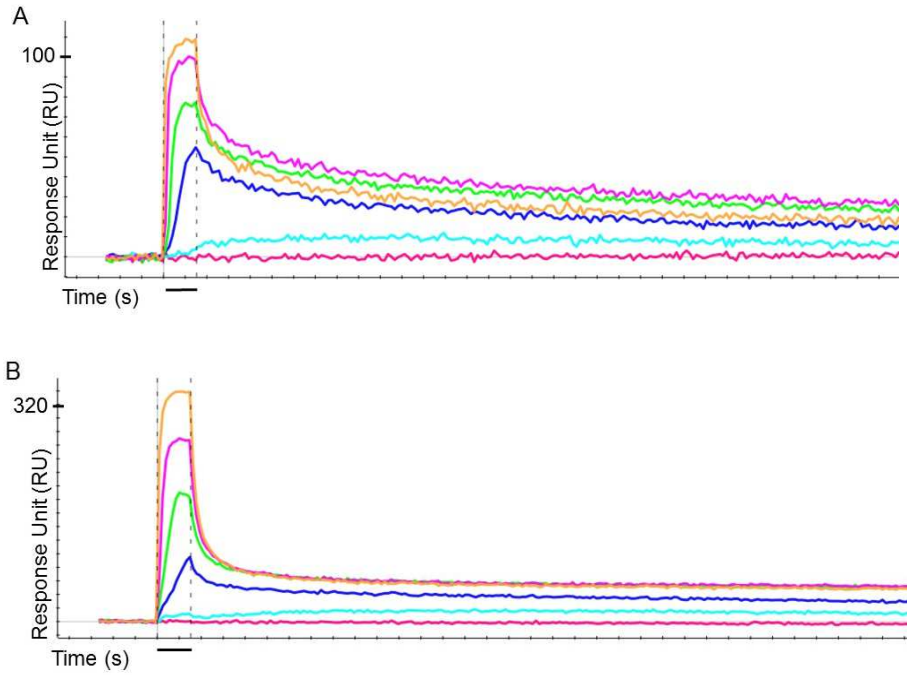

Figure 49 SPR sensorgram of nanobody 4

SPR sensorgram of nanobody 4. The first dotted line indicates the loading of the DARPin at different concentrations (shown in unique colors: yellow, 900 nM, pink, 450 nM, green, 225 nM, dark blue, 112 nM, light blue, 56 nM, red: 0 nM). The second line marks the start of the wash-out. The black bar corresponds to 120 seconds. A) Signal of nanobody 4 in control lane where no protein was immobilized. B) Signal of nanobody 4 in lane with immobilized target protein ELIC.

With the attempts to generate binders to ELIC, twelve nanobodies were identified which specifically recognize the membrane protein, following the immunization of Alpacas and the subsequent selection by phage display. Nine of these binders could be expressed and purified and show promising biochemical characteristics. Four of them bind ELIC with affinities below 1 µM and thus co-migration on a size exclusion chromatography. Although no crystals of the complex with ELIC were obtained, the nanobodies could potentially be used for future experiments investigating a possible impact on the function of the channel. For this purpose binding of YFP-fused nanobodies could be generated to detect binding in HEK-293 cells expressing the channel. Binding to an intracellular epitope could be detected by co-expression of ELIC with the nanobody, binding to an extracellular epitope by addition to the outside. A functional effect could be investigated by patch-clamp electrophysiology in the inside-out or outside-out configuration.

2.1.5 Summary

In the previous chapters the attempts to generate binders to the prokaryotic pLGICs ELIC and GLIC from three different structural frameworks have been described. These attempts allowed the successful selection of 10 different single-chain variable fragments (scFvs) and 27 different designed ankyrin repeat proteins (DARPins) recognizing GLIC by Phage and Ribosome display, respectively. Binding was confirmed by ELISA, size exclusion chromatography, surface plasmon resonance (SPR), and complexes were used for crystallization screening. Four out of the 10 selected scFvs showed a binding affinity (K_D) lower than 1 µM and thus co-migrated as complex with GLIC on size exclusion

chromatography. Since the pentameric GLIC (185 kD plus the detergent micelle) is much bigger than the monomeric scFv (25 kD), the complex can be efficiently separated from the unbound binder. If the scFv binds to GLIC with a low enough K_D, the resulting protein complex is bigger than GLIC and a shift in the elution volume can be observed, which indeed the case was. Co-elution was confirmed by SDS-PAGE, where the target protein and the binder are both present in the corresponding elution peak. Despite broad screening it was not possible to co-crystallize any scFv-GLIC complex. Since in these cases not even crystals of the isolated membrane protein were observed, the complex may have stayed intact even at low pH where GLIC readily crystallizes. The scFvs have a 14 amino acid long linker, connecting the two variable parts, which might prevent effective crystal formation. To avoid this flexibility, the 4 scFvs that bind with a high affinity to GLIC, were cloned into Fab fragments in order to obtain a more stable molecule for crystallization. Similar binding affinities to the target protein were confirmed by size exclusion chromatography and SPR. Although no crystals were observed in co-crystallization assays either, these larger Fab fragments binding to GLIC can potentially be used as tools for single particle electron microscopy.

Specific protein binders can also have an impact on the function of the targeted protein [53-55], by either occupying an agonist binding site or preventing conformational changes. However, no binding of the scFvs to GLIC expressed on *X. laevis* oocytes could be detected, indicating that the epitope is not accessible to the outside, and thus no functional experiments could be performed.

The 27 DARPins, selected against GLIC by Ribosome Display from a DARPin library of the second generation [111], were characterized with respect to their binding properties. A subset of eight DARPins showed high binding affinities in the nanomolar range. With some DARPin-GLIC complexes it was possible to obtain crystals at neutral and high pH, all of them diffracted poorly as it is the case with crystals with GLIC alone grown at high pH.

To probe a potential impact of the selected DARPins on protein function, it was investigated whether these highly affine binders were are able to bind to GLIC expressed on the *X.laevis* oocytes. Since, similarly to the experiment with the scFvs, no binding was detected, it thus appears that the epitope is not accessible from the outside of the oocyte and it may instead either be buried in the membrane or located at the intracellular side.

Different to GLIC, the DARPins selected for ELIC all showed the formation of oligomers or soluble aggregates, which is common for membrane protein binders [54, 57, 81]. By using a DARPin library of the second generation [111] the amount of such binders ideally should be reduced. Because of these unfavorable biochemical properties, only 2 DARPins were subjected to surface plasmon resonance to quantify their binding behavior. As expected, they both bind unspecifically also to lanes were no target protein was immobilized. Nanobodies selected by immunization of Alpacas followed by 2 rounds of phage display, show favorable biochemical characteristics and have high binding affinities, but some of them also show some degree of unspecificity during surface plasmon resonance (SPR), similar to the DARPins for ELIC. Since after the immunization of the alpaca, 2 rounds of Phage Display with the target protein immobilized via neutravidin were performed, it is possible that some nanobodies were selected which bind to neutravidin despite the prepanning step that should remove such binders from the pool.

Since the binder approach to determine the structure of the two target proteins ELIC and GLIC in a different conformation was unsuccessful, a different strategy to characterize the gating mechanism of pLGICs was followed. The binding site of the agonist is located between two subunits at the extracellular domain. After binding, a conformational change has to be transduced over a long distance to the transmembrane part where the pore opens. The interface between the extracellular and the intracellular domains of the proteins is therefore supposed to play an important role in signal transduction. In the following section, the impact of mutations of residues located in this interface region are presented.

2.2 Functional characterization of GLIC and ELIC

The functional properties of the pentameric ligand gated ion channels GLIC and ELIC expressed in *X.laevis* oocytes can be characterized by two-electrode voltage clamp (TEVC) electrophysiology. With this technique changes in ion conduction following the application of agonist can be recorded. During this process, a conformational change of the channel is triggered by agonist binding in the extracellular part to a site located between two subunits. This binding leads to a conformational rearrangement in the transmembrane domain resulting in channel opening by a so far unknown allosteric process. In 2004, Bouzat and colleagues identified regions in the interface between the extracellular and transmembrane domains which play an important role in channel gating. Chimeras of the acetylcholine binding protein (AChBP) and the pore domain of the serotonin receptor only showed activation, when the β1-β2 loop, the β6-β7 loop and the β8-β9 loop, located at the extracellular part, were exchanged with the corresponding loops of the homologue forming the pore. This underlines the importance of the coupling of these loops with the α2-α3 loop from the transmembrane part for function [44]. Previously, several amino acids located in these loops and in close proximity in the interface were mutated to alanine and the effect on function was analyzed. (Figure 51, see also Ph.D. thesis of Carlo Bertozzi, UZH 2014). As part of the work of this thesis, several residues were analyzed more thoroughly and the combined data was described in a publication (see publication "*Signal transduction at the domain interface of prokaryotic pentameric ligand-gated ion channels*" in the Appendix).

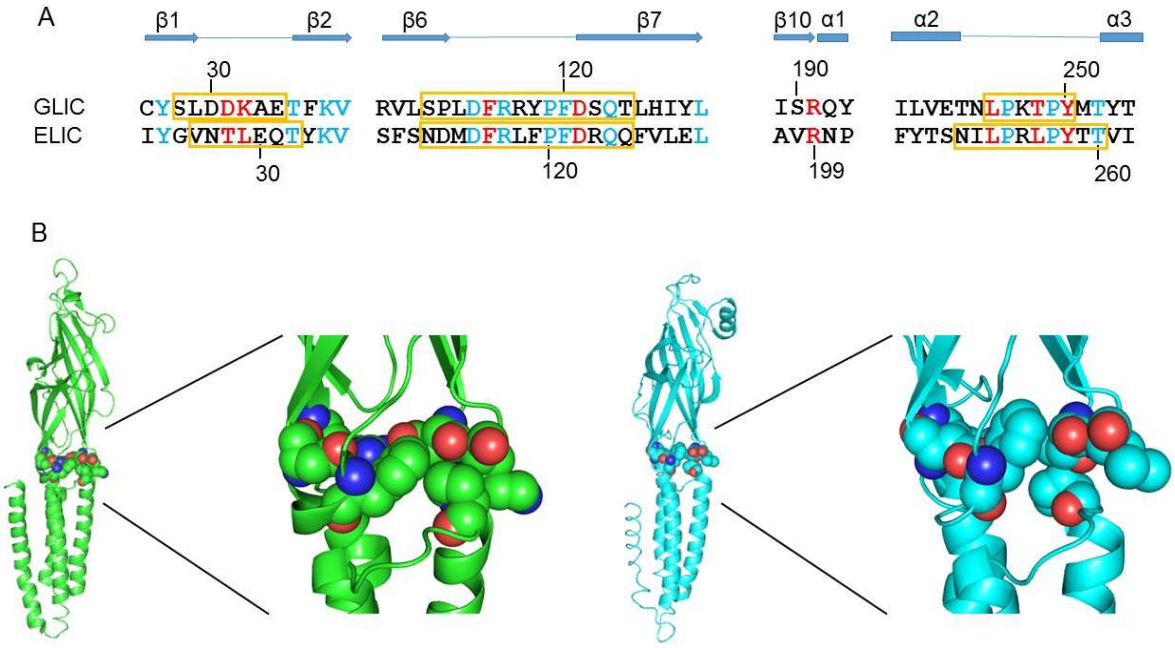

Figure 50 Domain interface of GLIC and ELIC.

A) Sequence alignment of GLIC and ELIC. Mutated residues are colored in red. Identical residues in blue. Secondary structure elements and residue numbering are shown. The yellow boxes highlight the residues that were characterized and described in the publication in the Appendix. B) Cartoon representation of a monomeric subunit of GLIC and ELIC. The residues mutated in the domain interface of GLIC (green) and ELIC (cyan) are shown as spheres. The figure was created with Pymol.

In a set of experiments the maximum response of the protein at high agonist concentration was correlated with the expression level at the plasma membrane. The correlation between currents and

surface expression was investigated in a semi-quantitative manner and mutants were identified that do no longer respond to agonist despite their correct folding and targeting to the plasma membrane. For functional analysis by two-electrode voltage-clamp (TEVC) electrophysiology, the mRNA coding for GLIC and ELIC fused to an N-terminal hemagglutinin-tag, was injected into defolliculated oocytes. The time dependence of expression of the correctly folded channels was investigated with an oocyte surface assay where the hemagglutinin-tag was detected by an antibody after 1, 2 and 3 days of injection of the mRNA coding for the corresponding protein. For WT and for most of the mutants analyzed in this study, highest expression levels were observed 2 days after injection. All subsequent experiments, such as two electrode voltage clamp recordings to measure the evoked currents upon ligand exposure, and oocyte surface assays were thus performed at this stage. To investigate the correlation between expression of the channels and activity measured by TEVC, for each oocyte the amount of expressed proteins detected by a surface assay was related to the maximal current evoked after application of the agonist (Figure 51). The more protein is expressed on the oocyte, the higher the maximal current should be. Supposing all proteins on the surface are functional and activated by the applied ligand and all the fused hemagglutinin-tags are bound by the antibody, a linear dependence of expression and current response can be expected. In Figure 51, TEVC electrophysiology measurements of the wild type proteins, subtracted by the background signal of non-injected cells, are shown. For oocytes expressing wild type GLIC, a weak correlation between the signal observed in the oocyte expression test and the maximal current response can be observed, at least for low to medium expression levels (Figure 51, A). For oocytes expressing ELIC, a similar weak correlation was observed (Figure 51, B). However, the scattering of data points in both cases is quite large, which could be due to proteins that conduct ions but, for sterical reasons do not bind to the hemagglutinin-antibody, or which could also reflect different levels of desensitized proteins.

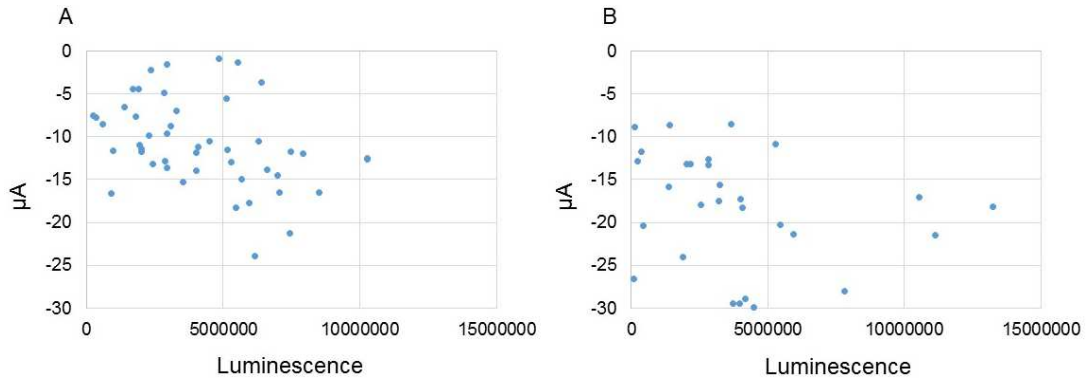

Figure 51 Correlation of maximal current and expression in oocytes.

The expression of GLIC and ELIC wild type in *X.laevis* oocytes was quantitated by a surface assay detecting the fused hemagglutinin tag. The maximal current (in µA) of each oocyte was measured by two electrode voltage clamp electrophysiology and correlated to the amount of expression (luminescence). A) Maximal currents versus expression of GLIC WT in oocytes. B) Maximal currents versus expression of ELIC WT in oocytes.

2.2.1 The β6–β7 and the α2-α3 loop

The β6–β7 loop from the extracellular domain of the protein (termed cys-loop in eukaryotes) is highly conserved within the family and was shown to play an important role in channel gating of glycine receptors [118]. In this study, two residues of this loop, were identified whose mutation to alanine had a

severe impact on channel activation in both homologues, GLIC and ELIC. In Figure 52, the residues which were mutated are shown as spheres in a cartoon representation.

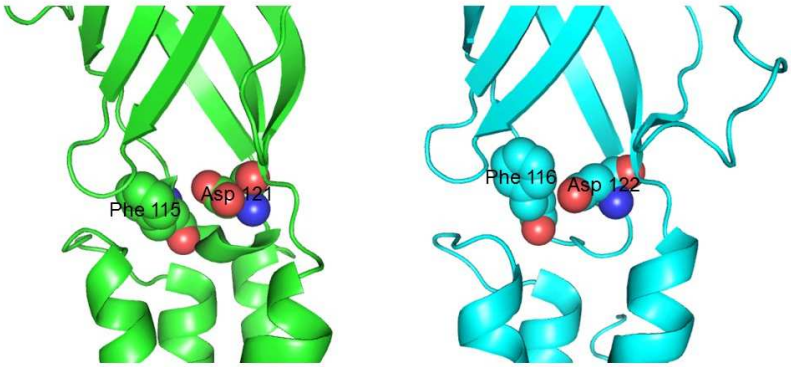

Figure 52 The β6–β7 loop of GLIC and ELIC.

Cartoon representation of the phenylalanine and aspartate in the β6–β7 loop of GLIC (green) and ELIC (cyan). The Figure was created with Pymol.

In GLIC the mutation of aspartate at the position 121 and the phenylalanine at the position 115 resulted in loss of function phenotypes, as characterized by TEVC electrophysiology were the evoked currents are compared with those of the wild type channel and those of non-injected oocytes (Figure 53, A). To make sure that the channels are folded correctly and expressed on the plasma membrane of the oocyte, a surface assay was performed, where a hemagglutinin tag was detected, and the expression levels were compared to WT (Figure 53, C). The mutant Phe115 showed robust expression which means that the channel is correctly folded and transported to the plasma membrane of the oocyte, whereas the D121A mutation has led to a slightly reduced expression level. Both Phe115 and Asp121 are important for channel gating as indicated by the lack of currents in TEVC electrophysiology. In ELIC, the F116A mutant was expressed to a similar extend on *X. laevis* oocytes than the corresponding wild type measured by an oocyte surface assay. Similarly to GLIC, the D122A mutant of ELIC showed reduced expression levels. Upon application of the agonist, no current was evoked by either mutant (Figure 53, B and D) thus underlining a similar importance of these residues for channel gating also for this homologue.

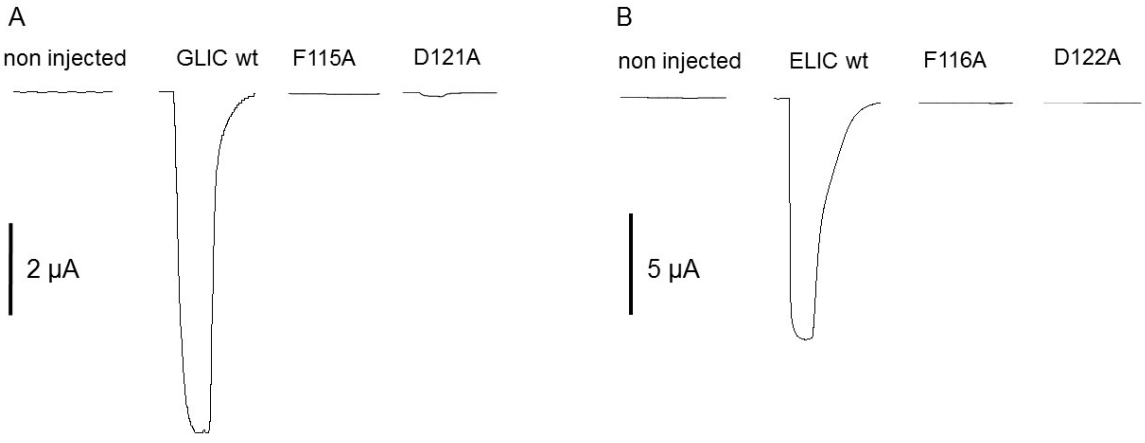

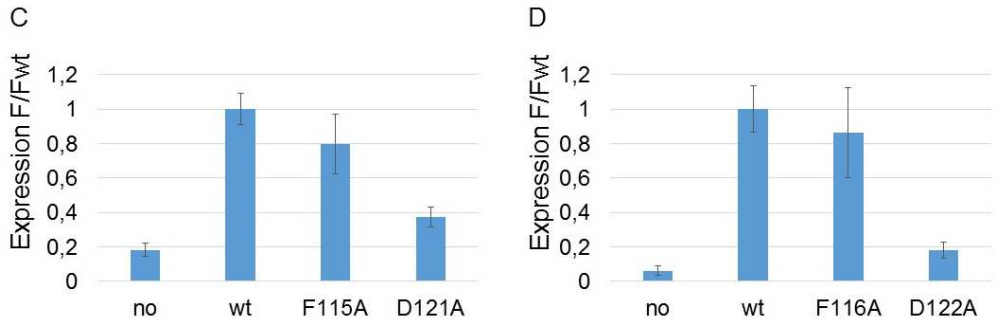

Figure 53 Maximal currents and expression of GLIC and ELIC mutants.

A) Maximal current of representative *X.laevis* oocytes expressing GLIC wild type, and mutants F115A and D121A compared to non-injected oocytes. Currents were measured at pH 4 and the voltage was clamped at -40 mV. B) Maximal current of *X.laevis* oocytes expressing ELIC wild type, and mutants F116A and D122A compared to non-injected oocytes. Currents were measured in response to application of 25 mM cysteamine and the voltage was clamped at -40 mV. C) Oocytes surface expression of the 2 mutants compared to the wild type GLIC and non-injected oocytes. D) Oocyte surface expression of the two mutants compared to ELIC wild type and non-injected oocytes. For each construct, at least 10 oocytes were measured and normalized to wild type, the errors are standard errors of the mean (SEM).

The β6–β7 loop (cys-loop) of the extracellular domain interacts with the α2-α3 loop of the transmembrane domain. To investigate the influence of single residues located in the α2-α3 loop on channel gating, they were mutated to alanine and analyzed by two-electrode voltage clamp electrophysiology. *X. laevis* oocytes expressing the mutations L245A, T248A, Y250A of GLIC and L253A, L256A, Y258A of ELIC, did not show any current response after application of the corresponding agonists at high concentrations, indicating that they are indispensable for channel function. To ensure that the mutations did not lead to a misfolded channel that would not be transported to the plasma membrane of the oocyte, a surface assay was performed to quantify the expression levels and compare them to the corresponding wild type protein, which was measured in the same experiment with the same batch of oocytes. The GLIC mutants all show robust expression, the threonine mutant (T248A) even expresses twice as much as GLIC WT (Figure 54, A). A similar behavior is observed for corresponding ELIC mutants where the leucines Leu253 and Leu 256 express similar or even better than WT. Only the Y258A mutant shows slightly reduced signals during the surface assay, but is still significantly higher than non-injected oocytes (Figure 54, B).

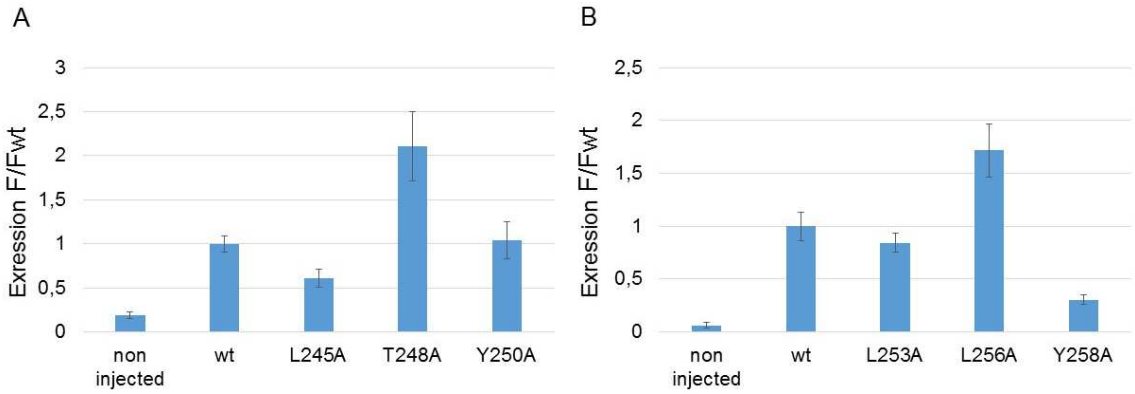

Figure 54 Expression of mutants in the α2-α3 loop of GLIC and ELIC.

A) Expression of 3 GLIC mutants in *X. laevis* oocytes compared to the wild type. All mutants show robust expression levels. B) Expression of 3 mutants of ELIC expressed in *X. laevis* oocytes compared to the wild type. Whereas the

mutants L253A and L256A expressed robustly, the mutant Y258A only shows 30% of the wild type signal. Data show the mean of at least 10 oocytes and are normalized to wild type. The errors are SEM.

2.3.2 Salt bridge

The β1–β2 turn of the extracellular domain of GLIC is stabilized by a conserved salt-bridge between an aspartate (Asp31) from the β1–β2 turn and an arginine (Arg191) of the β10-α1 linker (Figure 55). In ELIC this salt-bridge is absent and the conserved negatively charged residue, which forms this interaction in GLIC, is a polar threonine at position 28. In the structure of the non-conducting conformation of ELIC there is no contact between the conserved Arg199 and Thr28 (Figure 55). The salt bridge observed in GLIC is supposed to play an important role in channel gating in the nAChR and its formation was proposed to be the key event for channel opening [42, 119].

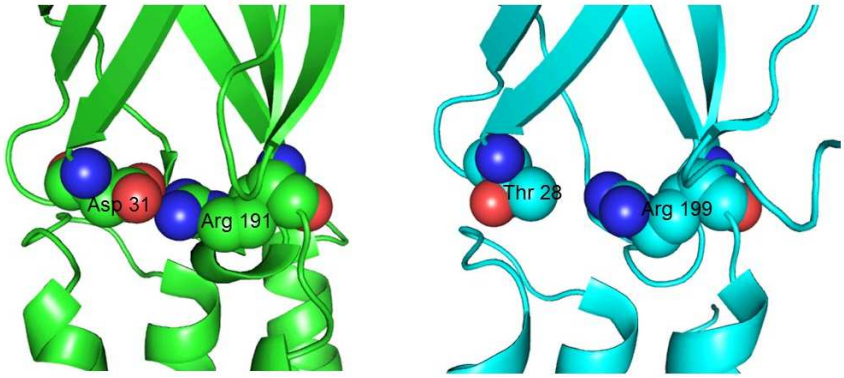

Figure 55 Salt bridge in the interface of GLIC and ELIC.

Cartoon representation of the salt bridge in the domain interface of GLIC (green) and ELIC (cyan). In GLIC Arg191 and Asp31 are forming a salt bridge. This connection is disrupted in ELIC, where the equivalent position in the β1-β2 turn contains a threonine (Thr28). The Figure was created with Pymol.

The mutation of the residues in the β1-β2 loop (Asp31) and in the β10-α1 linker (Arg191) of GLIC to alanine caused a lack of response in TEVC electrophysiology measurements (Figure 56, A). The mutation of the corresponding residue in the β10-α1 linker (Arg199) in ELIC also shows a similar loss of function phenotype. However, unlike in GLIC, the ELIC mutation T28A, located in the β1-β2 loop, shows low currents upon application of the agonist, which indicates that this position might be less critical in ELIC for channel opening than in GLIC (Figure 56, B). To prove, that the channels are correctly folded and expressed on the *X. laevis* oocyte membrane, a surface expression assay was performed where a hemagglutinin-tag fused to the channels was detected by an antibody. When comparing the signals of the mutated GLIC channel to the wild type protein and to non-injected oocytes, it is apparent, that the mutation of the Arg191 resulted in a defective channel, which is not expressed on the plasma membrane, whereas the D31A mutant shows comparable expression levels as the wild type channel (Figure 56, C). In ELIC, the mutant channels T28A and R199A show reduced expression on the *X. laevis* membranes compared to the wild type protein, thus suggesting a potential impact of the mutation on folding (Figure 56, D). The correlation of expression and maximum current of the threonine mutant T28A will be discussed later.

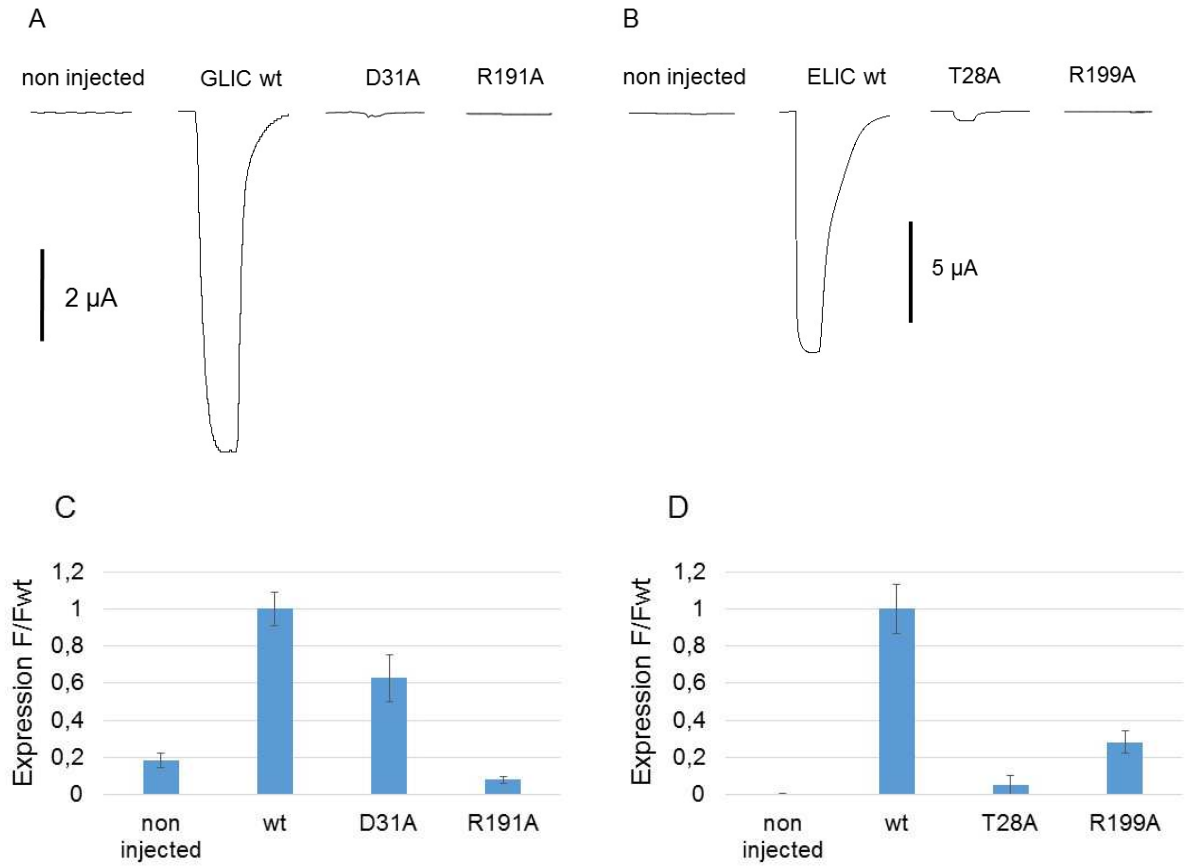

Figure 56 Maximal currents and expression of the residues involved in a salt bridge in GLIC and ELIC.

A) Maximum current response of *X. laevis* oocytes expressing GLIC wild type and the Asp31 and Arg191 mutant compared to non-injected oocytes. Currents were measured at pH 4 and the voltage was clamped at -40 mV. B) Maximum current response of *X. laevis* oocytes expressing ELIC wild type and the Thr28 and Arg199 mutant compared to non-injected oocytes. Currents were measured in response to addition of 25 mM cysteamine and the voltage clamped at -40 mV. C) Surface expression of the mutants D31A and R191A in *X. laevis* oocytes compared to wild type GLIC. D) Surface expression of the mutants T28A and R199A in *X. laevis* oocytes compared to wild type ELIC. Data show averages of at least 9 oocytes and are normalized to wild type, errors are SEM.

In acetylcholine receptors it was found, that single mutations of the residues participating in a salt bridge between the corresponding sites, which reverses their charge, resulted in reduced gating equilibrium constants, whereas the combination of these mutations show wild type like behavior [21, 23, 120]. To investigate the impact of a similar mutation, in both homologues, GLIC and ELIC, a 'charge reversal' mutation of the salt bridge was constructed, where the positions of the involved amino acids in ELIC and GLIC were switched. The switch of Arg191 and Asp31 in GLIC has a severe impact on function while its expression in *X. laevis* oocytes is not affected. Despite the high expression level on oocytes surfaces compared to wild type GLIC (Figure 57, B), only currents similar to those of non-injected

oocytes in response to application of a buffer with low pH could be detected, suggesting that the mutation leads to a complete loss of activation (Figure 57, A).

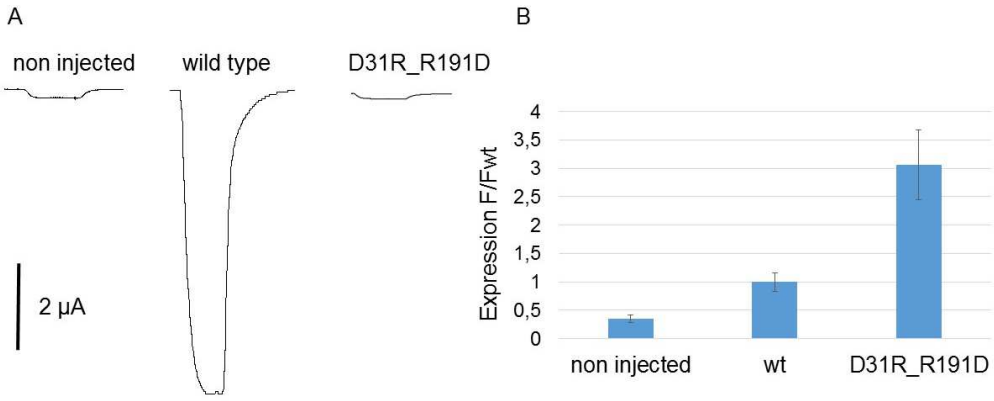

Figure 57 Two-electrode voltage clamp measurements and surface expression of *X. laevis* oocytes expressing GLIC wild type protein and the "charge-reversal" mutant.

A) Maximum current response at pH 4 with non-injected *X. laevis* oocytes, GLIC wild type and the charge-reversal mutant of GLIC. The black bar indicates a current of 2 µA. B) Expression of GLIC wild type and the mutant D31R_R191D on the surface of *X. laevis* oocytes compared to non-injected oocytes. Data show averages of at least 10 oocytes and are normalized to wild type, errors are SEM.

To investigate the potential structural rearrangements underlying the loss-of function of the charge-reversal mutant of GLIC, both mutated homologues (GLIC and ELIC) were overexpressed in *E.coli* cells following the same protocols as for the respective wild type proteins. After expression, the cells were harvested, lysed and the protein was extracted with detergents. Subsequently, the solubilized mutant proteins were purified by immobilized metal affinity chromatography (IMAC). After incubation with the HRV 3C protease to cleave the fusion protein, and dialysis into imidazole-free medium, the His-MBP fusion was separated from the channel by a second IMAC step. The concentrated flow-through fraction containing the channel proteins were run on SEC. During this purification the pentameric GLIC mutant with an elution volume of 11.7 ml could be successfully separated from the aggregation peak (Figure 58, A) whereas the corresponding mutant of ELIC was completely aggregated (Figure 58, B), as indicated by the large peak with the retention volume around 8 ml, which corresponds to the void volume of the column.

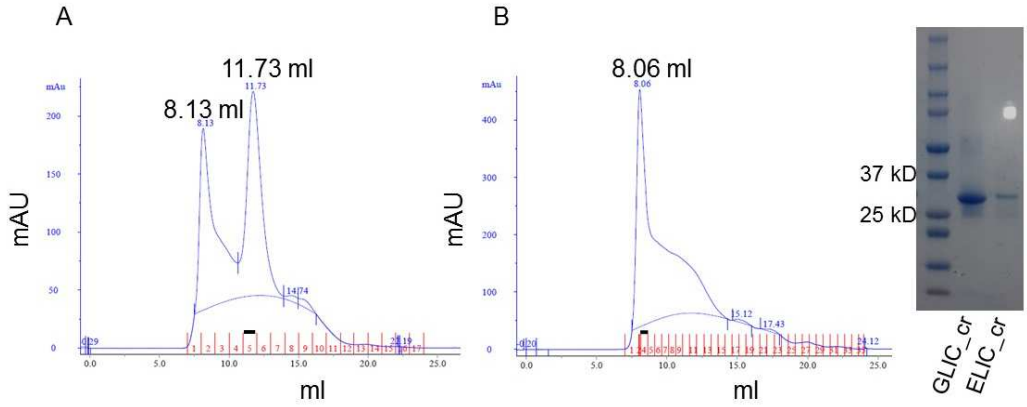

Figure 58 Size exclusion profiles of the charge reversal mutations of GLIC and ELIC.

Absorbance was measured at 280 nm. The black bars show the fractions which were loaded on the SDS-gel. A) Size exclusion chromatogram of GLIC D31R_R191D. The peak at the retention volume of 11.73 ml corresponds to the protein, as confirmed by SDS-PAGE. The peak at 8.16 ml corresponds to the void volume of the column. B) Size exclusion chromatogram of ELIC T28R_R199D. The protein appears to be aggregated, since only one peak at the void volume of 8.06 ml is observed.

After size exclusion chromatography, the fractions containing the "charge-reversal" mutant of GLIC were collected and concentrated up to 7.5 mg/ml and subjected to broad crystallization screening. The mutant was successfully crystallized in the known crystallization conditions of GLIC (225 mM $(NH_4)_2SO_4$, 50 mM sodium acetate, pH 4.0 and 4.5, 9–12% PEG 4000 and 0.5 mg/ml *E. coli* lipids). Crystals were harvested and cryo-protected by soaking in mother liquor containing additional 30% ethylene glycol and data was collected at the Swiss Light Source of the Paul Scherrer Institute. The crystal structure of the double mutant was determined at 3.2 Å. Although the molecule in most parts shows comparably small differences compared to wild type GLIC, the exchange of the two amino acids, causes a large conformational change at a site distant form the mutation. In the pore lining α-helix 2 significant differences are observed. In Figure 59, the superimposition of the charge reversal mutant and GLIC wild type shows the tilt of α-helix 2 with respect to the orientation in the WT.

The C-terminal part of this helix (Figure 60 B, blue) is tilted towards the pore and appears to close it, which might be the cause of the loss of ion conduction. Interestingly the electron density at the mutated region shows that the residues that have been exchanged in the mutant, may be involved in similar interactions as found in wild type (Figure 60).

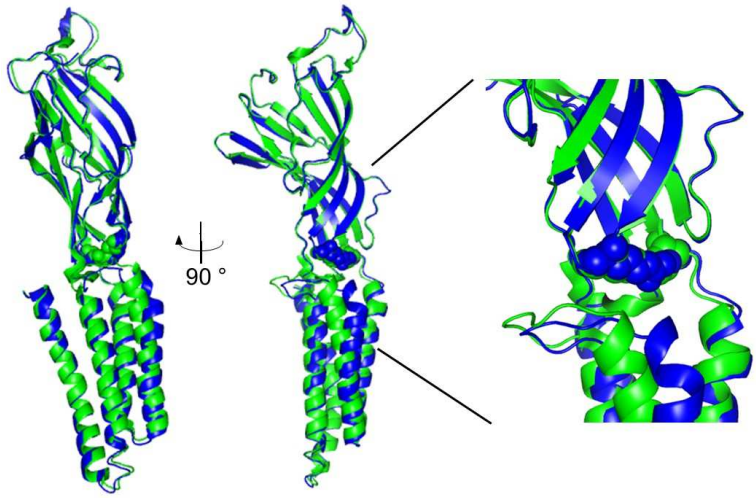

Figure 59 Superimposition of charge reversal mutant and GLIC wild type.

Superimposition of one subunit of GLIC (green) and the charge reversal mutant (blue) in two different orientations. The mutated residues are shown as spheres. The Figure was created with Pymol.

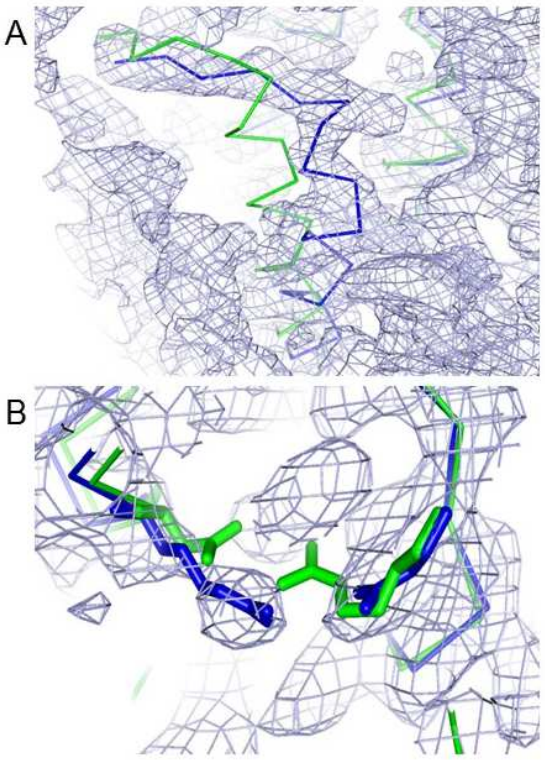

	GLIC charge reversal
Data collection	
Space group	C121
Cell dimensions	
a, b, c (Å)	180.56, 134.93, 160.47
α, β, γ (°)	90, 101.8, 90
Resolution (Å)	19.97-3.1 (3.211 - 3.1)
Completeness*	0.98
R work*	0.2542 (0.3958)
R free*	0.2886 (0.4539)
Refinement	
Resolution (Å)*	19.92-3.1 (3.211-3.1)
No. reflections*	67337 (6331)
No. atoms	
Protein	12'605
B-factors	78.7
Protein	1550
R.m.s. deviations	
Bond lengths (Å)	0.003
Bond angles (°)	0.84

* Values in parentheses are for highest resolution shell

Figure 60 Electron density and statistics of the charge reversal mutation of GLIC.

Electron density of the charge reversal mutant of GLIC where the positions of residues Asp31 and R191 involved in a salt bridge have been exchanged. A) Superimposition of one subunit of GLIC wild type (green) and the charge reversal mutant (blue). $2F_o$-F_c electron density of the charge reversal mutant (calculated at 3.1 Å and contoured at 1σ) superimposed on the structure α2 helices of the mutant (blue) and wild type GLIC (green). B) The residues of GLIC wild type (green) and the charge reversal mutant (blue) are depicted, indicating a potential interaction that has been observed in WT. C) Data collection and refinement statistics of the GLIC charge reversal mutant.

As shown before, the mutation of Asp 31 to alanine prevents channel activation of GLIC (Figure 56, A). In contrast, the mutation of the equivalent position in ELIC (T28A) can still be activated but shows lower maximal currents. In Figure 61, maximal currents of the mutant T28A and T28D, where a residue is introduced that is present in other family members (such as GLIC), are shown in comparison to non-injected and oocytes expressing ELIC wild type. All measurements were performed with the same batch of oocytes and expression was quantified in the same round of experiments. Compared to ELIC WT, both the alanine and the aspartate mutants show lower maximal current response. These findings support the assumption, that also the threonine at this position is important for function but that the impacts on function of mutations are not as severe as observed for the equivalent position in GLIC. Interestingly the reduced currents, resulting from the introduction of a possible partner for a salt bridge with the arginine from the β10-α1 suggest that the mutation might have either decreased the expression level, the single channel conductance or the maximum open probability of the channel.

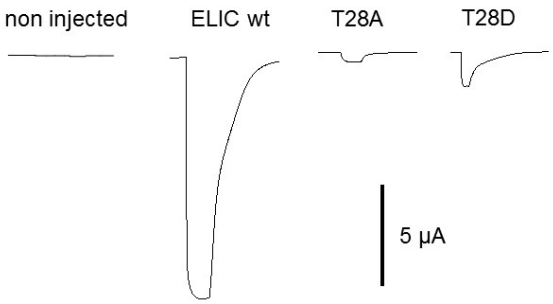

Figure 61 Maximal currents of ELIC mutants in the β1- β2 turn.

Maximum currents of *X. laevis* oocytes injected with ELIC and the two Thr28 mutants in comparison with non-injected oocytes. Currents were measured at 25 mM cysteamine and the voltage clamped at -40 mV. The black bar shows currents of 5 µA.

To investigate the density of proteins on the surface of *X. laevis* oocytes, the expression levels of ELIC WT and the two mutants of Thr28 were quantified (Figure 62, A). The T28D mutant has a comparable expression level to the wild type protein, whereas the T28A mutant expresses at lower levels. As shown above, both mutants can still be activated by the agonist cysteamine. Since in case of T28A, fewer mutant channels are expressed on the oocyte surface, the maximum currents are consequently reduced. To further relate the expression levels to the evoked maximum currents the ratio of both signals was evaluated and compared to WT. For both mutants the ratio of activity to the expression level is much lower than in case wild type ELIC (Figure 62, B) indicating that the presence of the threonine is important for channel function and that the substitution to either alanine or an aspartate (the residue that is present in GLIC) may either decrease the single channel conductance or the maximum open probability of the channel. Since the single channel conductance of T28D is unaltered (see publication "*Signal transduction at the domain interface of prokaryotic pentameric ligand-gated ion channels*" in the Appendix), it is likely that the maximum open probability is reduced.

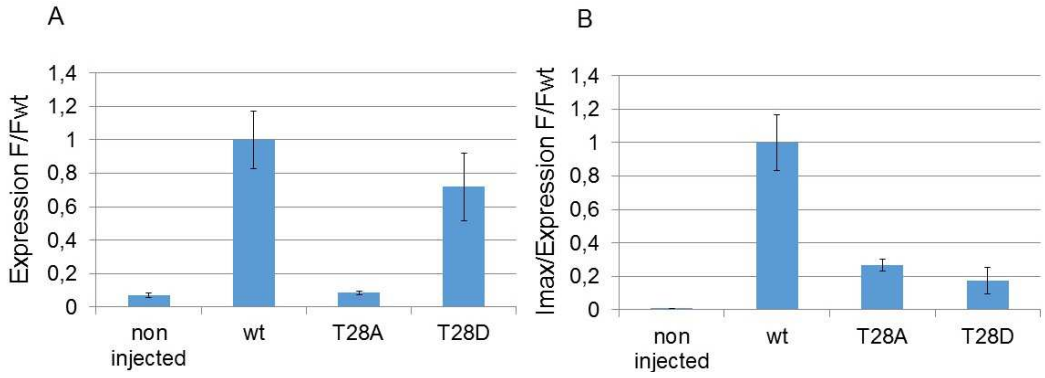

Figure 62 Expression and Imax/Expression of ELIC wild type and Thr28 mutants.

A) Expression of ELIC wild type, and the mutants T28A and T28D on *X. laevis* oocytes, compared to non-injected oocytes. B) Ratio of the evoked current to the expression level. At least 10 oocytes were measured and are normalized to wild type. Errors are SEM.

To quantify the correlation between expression of the channels and activity measured by TEVC electrophysiology in single cells, for each oocyte the amount of expressed proteins, detected by a surface assay, was related to the maximal current evoked after application of the agonist (Figure 63).

The two mutants show a different correlation of expression and activity compared to the wild type protein (Figure 63, A). Although the amount of expression of the T28D mutant is comparable to wild type, as indicated by the similar distribution of the luminescence signal, the evoked maximal currents after agonist application are significantly reduced. In contrast, the alanine mutant is poorly expressed and consequently shows very low currents, in line with the analysis of the average current density shown above (Figure 63, B). Taken together, this findings emphasize the importance of the threonine at this position for channel activation in ELIC.

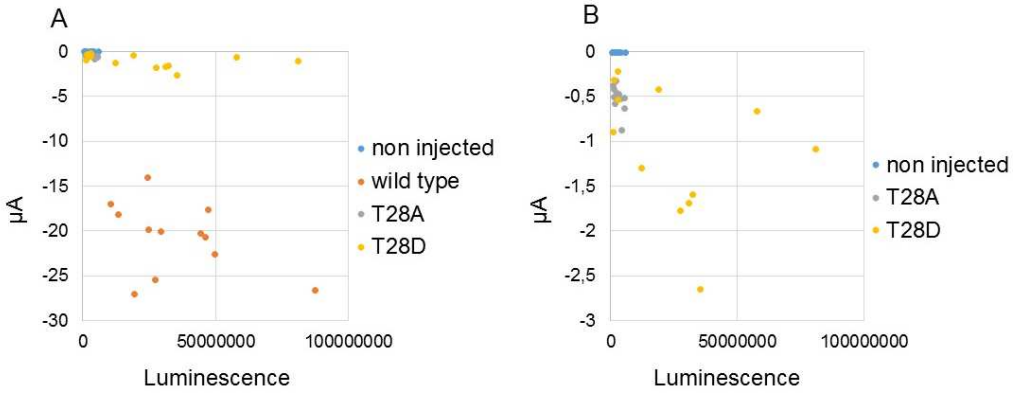

Figure 63 Correlation of maximal current and expression.

The expression of ELIC wild type and mutants of Thr 28 in *X. laevis* oocytes was quantitated by a surface assay detecting the fused hemagglutinin tag. The maximal current of each oocyte was measured by two electrode voltage clamp (µA) and correlated to the amount of expression (luminescence). A) Non-injected oocytes (blue) were compared to oocytes expressing the wild type channel (orange), the T28A mutant (grey) and the T28D mutant (yellow). B) Same representation with magnified y-axis and wild type ELIC data omitted.

Although both mutants appear to have a similar maximum open probability, the potency of agonist is highly enhanced in T28D whereas it is decreased in T28A (see publication "*Signal transduction at the domain interface of prokaryotic pentameric ligand-gated ion channels*" in the Appendix). To investigate possible structural rearrangements in the ELIC mutant T28D, the mutant was recombinantly expressed in *E.coli*. After lysis of the cells, the protein was extracted in the detergent UDM and purified by IMAC. After cleavage with the HRV 3C protease the His-MBP fusion protein was removed by an additional IMAC step and the concentrated protein was subjected to SEC (Figure 64). A peak with a retention volume of 11.8 ml corresponded to ELIC, as confirmed by SDS-PAGE.

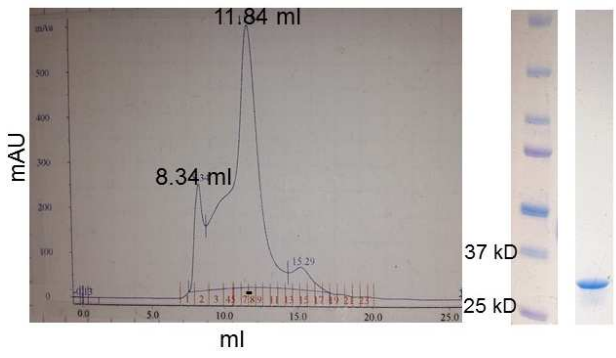

Figure 64 Size exclusion profile of ELIC T28D

Size exclusion chromatogram of the mutant ELIC T28D. Whereas the void peak elutes at 8.34 ml, the peak corresponding to the ELIC T28D elutes at 11.84 ml. The black bar shows the fraction which was loaded on SDS-PAGE.

The purified ELIC mutant was subsequently supplemented with 0.05 mg/ml *E.coli* lipids and crystallized at a concentration of 7.8 mg/ml in in 1 M $(NH_4)_2SO_4$, 0.05 M ADA pH 6.5, 11 % - 16 % PEG4000 and 0.05 M ADA pH 6.5, 0.1 M $LiSO_4$, 0.1 M $NaSO_4$, 11 %- 16 % PEG4000 with and without addition of cysteamine. Crystals were harvested, cryopotected by addition of 30% Ethyleneglycol and flash frozen in liquid propane. Data was collected at the X06SA beamline at the Swiss Light Source of the Paul Scherrer Institute and structures were subsequently determined at 4.5 Å in the absence and 9.5 Å in the presence of the agonist cysteamine. In both cases they showed the already known non-conductive state of the protein (although in case of the ligand complex, the resolution is too low to make a definitive assignment). Thus, regardless of the strong impact of the mutant on channel function, ELIC crystallized in the usual non-conductive conformation which underlines the stability of this state (Figure 65).

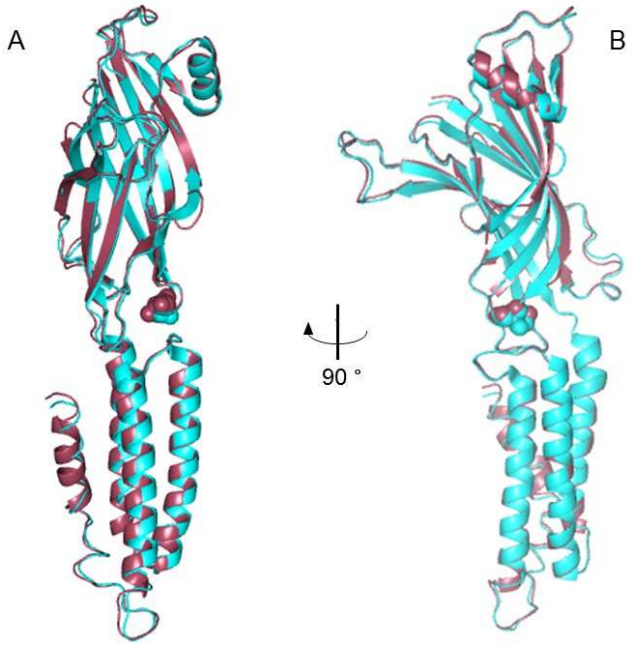

	ELIC T28D	ELIC T28D/ligand
Data collection		
Space group	$P2_1$	$P2_1$
Cell dimensions		
a, b, c (Å)	105.5, 267.0, 110.2	106.8, 264.8, 108.7
α, β, γ (°)	90.0, 110.5, 90.0	90.0, 110.5, 90.0
Resolution (Å)	50-4.5 (4.6-4.5)	50-9.5 (9.7-9.5)
R_{merge}*	9.3 (189.2)	4.9 (113.7)
I / σI *	13.1 (1.9)	14.9 (1.9)
Completeness (%) *	99.7 (99.5)	98.5 (99.8)
Redundancy *	12.0 (1.6)	6.9 (6.8)
Refinement		
Resolution (Å)	20-4.5	20-9.5
No. reflections	33,699	3,186
R_{work}/R_{free}	23.7/27.1	27.5/28.9
No. atoms		
Protein	25,060	-
Ligand/ion	-	-
B-factors		
Protein	289	-
Ligand/ion	-	-
R.m.s. deviations		
Bond lengths (Å)	0.003	-
Bond angles (°)	0.6	-

* Values in parentheses are for highest resolution shell

Figure 65 Cartoon representation of ELIC wild type and T28D mutant and statistics

A) Superimposition of a single subunit of the ELIC wild type (cyan) and the T28D mutant (red). The mutant channel shows the same non-conducting conformation. B) Statistics of the crystallized mutant channel with and without agonist.

2.2.3 The tip of the β1-β2 loop

In GLIC, as well as in the agonist-bound structure of GluCl, the β1-β2 turn of the extracellular domain and the α2-α3 loop of the pore domain are in direct contact. In GLIC, a lysine at the tip of the β1-β2 turn interacts with a conserved proline of the α2–α3 loop via the protein backbone. In ELIC, where the tip of the β1-β2 turn is formed by a leucine, and in other channels residing in a non-conductive conformation, such as the ligand-free GluCl, the contact is broken and these residues are approximately 7 Å apart from each other (Figure 66).

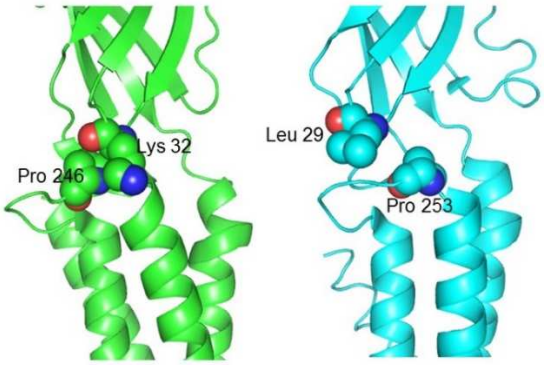

Figure 66 Cartoon representation of the domain interface of GLIC and ELIC.

In GLIC (green) the lysine, located at the tip of the β1-β2 loop interacts with a proline in the α2-α3 loop. In ELIC (cyan) the tip of the β1-β2 loop is occupied by a leucine, which makes no direct contact with the proline located in the α2-α3 loop. The Figure was created with Pymol.

To examine the importance of this interaction for activation, the tip residues Lys32 in GLIC and Leu29 in ELIC, were mutated to either alanine or glycine. Additionally, to prevent any interactions between the two domains, in another set of mutants, these residues were deleted. The mutant channels were subsequently expressed in *X. laevis* oocytes and characterized by TEVC electrophysiology and with an oocyte surface expression assay. Both assays were carried out in parallel with the same batch of oocytes to have comparable signals. Upon mutation of the residue at the tip of the turn to alanine, both mutant channels can still be activated by agonists, but with a much lower maximum current compared to the wild type protein. The mutation to glycine results in nearly complete loss-of-function in both proteins (Figure 67). If deleted in ELIC, the dL29 mutant can still be activated, whereas the corresponding deletion in GLIC causes a nonfunctional channel. The correlation of expression to the maximum evoked current of the mutants of Lys32 in GLIC and Leu29 in ELIC, show, that all mutations impact gating to variable degrees (Figure 67, A-D).

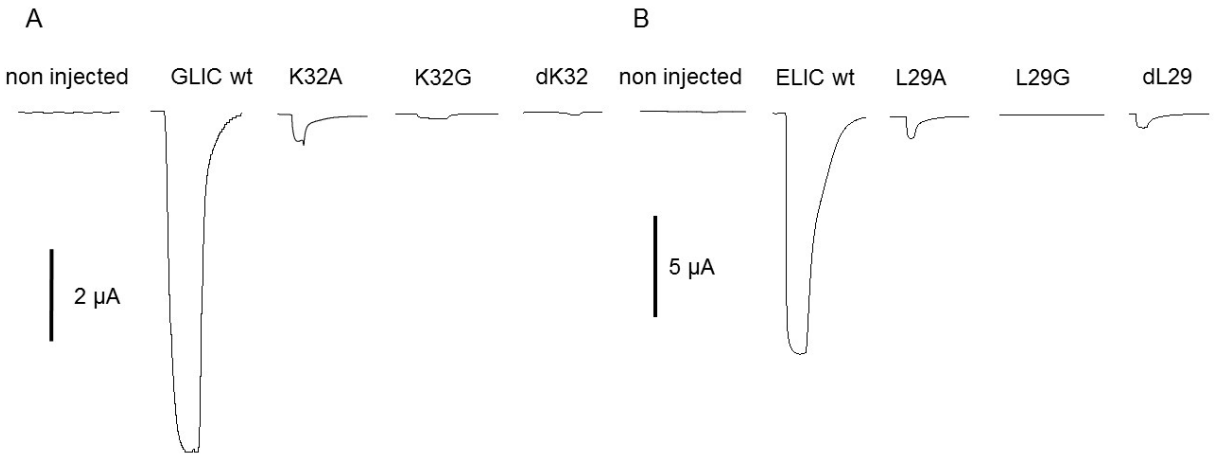

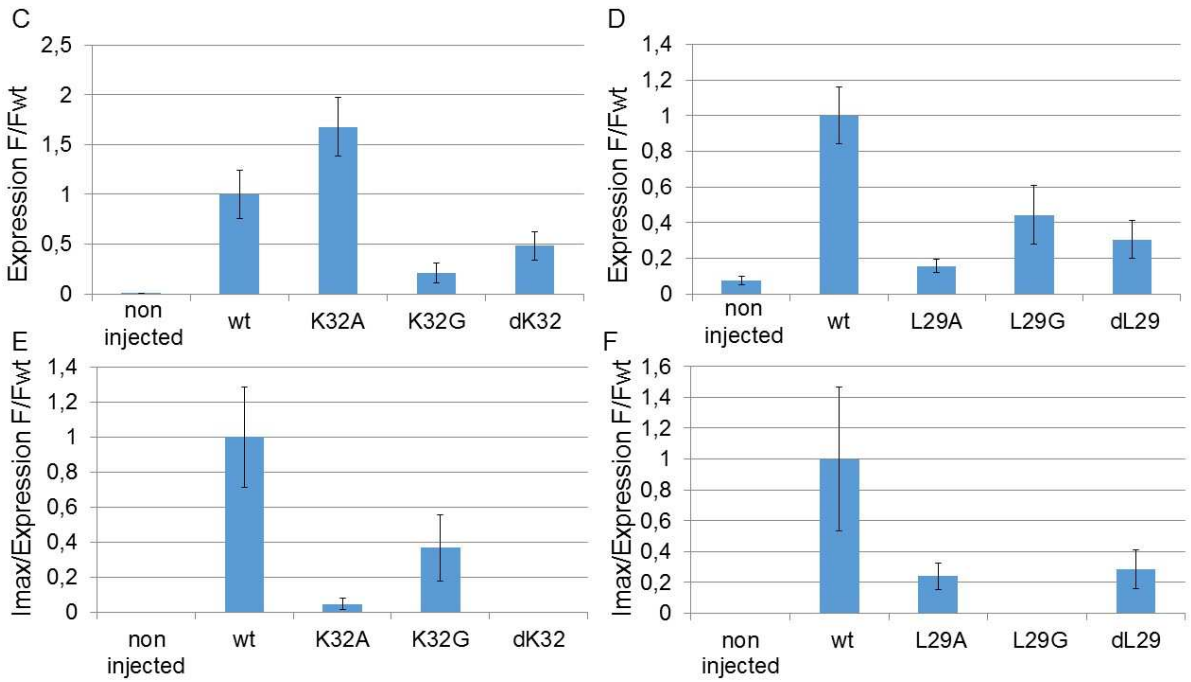

Figure 67 GLIC wild type, Lys32 mutants and ELIC wild type and Leu29 mutants.

A) Maximum currents of *X. laevis* oocytes expressing GLIC wild type and different mutants of Lys32 compared to non-injected oocytes. Currents were measured at pH 4 and the voltage was clamped at -40 mV. The black bar indicates currents of 2 µA. B) Maximum currents of *X. laevis* oocytes expressing ELIC wild type and different mutants of Leu29, compared to non-injected oocytes. Currents were measured at 25 mM cysteamine and the voltage was clamped at -40 mV. The black bar indicates currents of 5 µA. C) Expression of GLIC wild type and the mutants K32A, K32G and deletion of K32 on the surface of *X. laevis* oocyte detected by an anti-hemagglutinin-antibody. D) Expression of ELIC wild type and the mutants L29A, L29G and deletion of L29 on the surface of *X. laevis* oocyte detected by an anti-hemagglutinin- antibody. E) Relationship between expression and activity of GLIC wild type in comparison to the mutants K32A, K32G and the deletion of K32. F) Relationship between expression and activity of ELIC wild type in comparison to the mutants L29A, L29G and the deletion of L29. Data show averages of at least 10 oocytes and are normalized to wild type, the errors are SEM.

In Figure 67, C, the expression levels of GLIC WT and mutants on oocyte membranes compared to non-injected oocytes is shown. The mutant K32A even expressed at a higher level than wildtype, whereas the glycine mutant K32G and the deletion dK32 show reduced expression levels. By correlating these levels with the maximum current evoked during TEVC measurements, the alanine mutant, which showed the highest expression levels results in a strongly decreased activity. The normalized activity in the glycine mutant is about 40 % of the WT, but considering the low expression this value has to be taken with caution (Figure 67, D). Also for ELIC mutants the expression levels are reduced compared to the wild type protein, particularly in the alanine mutant L29A, which only shows about 20% of the expression of WT. When related to the maximum current, the normalized activity of the alanine mutant L29A as well as the deletion mutant dL29 is about 30% of the wild type protein (Figure 67, E).

To correlate expression and activity on the level of individual cells, for each oocyte the maximum currents evoked by WT and mutant channels measured by TEVC electrophysiology was plotted against the expression level measured by a surface assay (Figure 68). Compared to their expression the current response of the 3 mutants is generally small (Figure 68, A). Although the K32A mutant of GLIC has a similar expression level as the WT, as seen by the similar distribution, the currents are significantly

reduced. A similar relationship is observed for ELIC mutants (Figure 68, B). These findings underline the importance of these tip residues for function in both homologues.

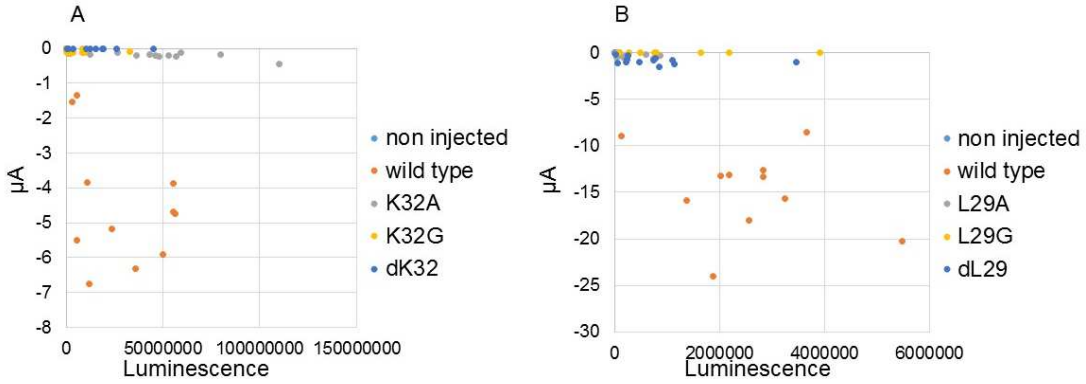

Figure 68 Correlation of maximum current and expression of mutants of the tip of the β1- β2 turn.

A) The expression of GLIC wild type (red), and the tip mutants K32A (grey), K32G (yellow) and the deletion dK32 (dark blue) in single *X. laevis* oocytes was quantified by a surface assay detecting the fused hemagglutinin tag. The expression is shown in comparison to non-injected oocytes (light blue).The maximum current of each oocyte was measured by two electrode voltage clamp and related to the expression level. B) Correlation of expression and maximum currents for ELIC wild type (red) and the tip mutants L29A (grey), L29G (yellow) and the deletion dL29 (dark blue) for single *X. laevis* oocytes expressing the respective constructs.

2.2.4 Summary

By mutation of residues located in the domain interface between the extracellular and the transmembrane domain of GLIC and ELIC and subsequent characterization by biochemical and electrophysiological methods, several positions were identified to play an important role in channel gating. For GLIC, mutations causing a loss of function protein lie in the β1-β2 loop (D31), in the β6-β7 loop (F115) and in the α2- α3 loop (D121, L245A, T248A, Y250A), whereas the mutation of a conserved arginine at position 191 (β10-α10 linker) resulted in a misfolded protein. These findings underline the importance of those residues for channel gating. Mutating the tip residue of the β1-β2 loop (K32) to alanine or glycine, the channel activation is affected but not prevented. Only if the leucine is deleted, the channel function is impaired. For ELIC a similar picture can be drawn. Residues resulting in a loss of function protein when mutated lie in the β6-β7 loop (F116), in the β10-α1 linker (R199) and in the α2-α3 loop (D122, L253A, L256A, Y258A). The residues in the β1-β2 loop (T28 and L29) show a slightly different behavior when mutated. Whereas in GLIC the D31 (in the β1-β2 loop) forms a salt bridge with the arginine at position 191, in ELIC this connection does not exist. The mutation of the corresponding residue (T28) to alanine causes reduced maximum currents in TEVC measurements. The introduction of an aspartate at this position, thereby providing a possible partner for a salt bridge results in reduced currents as well. The crystal structure of this mutant protein still shows the familiar non-conductive conformation, despite the big impact on function. In GLIC a charge reversal mutant of the salt bridge was created, where the arginine (R191) and the asparagine (D31) were switched, which resulted in a channel with impaired function and a tilt of the pore lining helix in the crystal structure. In ELIC a similar switch of the arginine in the β10-α1 linker (R199) with the mutated T28D in the β1-β2 loop caused the protein to aggregate. Similar to GLIC, the tip residue of the β1-β2 loop (L29) of ELIC was mutated to alanine and glycine and in another step, deleted. Whereas the alanine mutant and the deletion show reduced currents, the glycine mutant results in a loss of function protein.

In this study, several residues were identified to play an important role in channel gating. Notably, the residues causing a loss of function when mutated to alanine, all lie in the in close proximity to each other, indicating that the intactness of this region, the total charge and the interaction between residues are mandatory for function. Since most mutations in both homologues, GLIC and ELIC, showed similar phenotypes the importance of this conserved part of the protein is accentuated.

3. Discussion

After the discovery that the nicotinic acetylcholine receptor (nAChR) from the electric organ of *electrophorus electricus* converts a chemical input into an electrical output [121], this protein and homologous pentameric ligand gated ion channels (pLGICs) were studied extensively by biochemical and electrophysiological methods. Thirty-five years later, prokaryotic homologues were identified [24, 41] leading to the first structure determination of a full length pLGIC [26, 27, 32] at high resolution.

The structure of the prokaryotic homologue GLIC from *Gloebacter violaceus* was determined in a supposedly open conformation, whereas ELIC from *Erwinia chrysanthemi* was crystallized in a nonconductive state [26, 27, 32]. Because so far it was not possible to determine the structure of GLIC and ELIC in another conformation at high resolution, a part of this work was devoted to the selection of specific binding protein, which could stabilize the ion channels in a defined state [57]. Most proteins described here were identified *in vitro* from synthetic libraries. Ribosome and Phage Display allowed the successful selection of 10 different single-chain variable fragments (scFvs) and 27 different designed ankyrin repeat proteins (DARPins) recognizing GLIC. For GLIC, the selection was carried out at slightly basic pH in conditions where the protein is supposed to adopt a non-conductive state. Certain binders should therefore specifically bind the agonist-free conformation of the target protein, which was partly confirmed by an ELISA. The same strategy to select binders that recognize the ligand bound open conformation of ELIC was not feasible, since ELIC cannot be activated in detergent solution. Although, proteins binding to this channel were successfully identified, most DARPins and some nanobodies, which were selected for ELIC show unfavorable biochemical characteristics and unspecific binding.

3.1 Selection of specific binding proteins

By using a synthetic library encoding for scFvs a total of 10 unique binders targeting GLIC were selected by Phage Display. In this selection, the protein scFv A was the dominating species that was identified 33 times in different clones, whereas other binders, such as scFv H, were found only once. This behavior could correlate with the binding affinity of the respective scFv to its target. The stronger a scFv binds, the more likely the associated phage can be rescued and used for infection of the bacteria in the next round of selection. Surprisingly, the quantification of binding affinities by SPR revealed that the 4 scFvs, which were found to co-elute with GLIC on SEC, all bind with affinities in the same range. An alternative explanation for the prevalence of scFvA during selection could be a bias of the original library for this scFv. Although the comparison of the sequences of the randomized CDR3 of the scFvs that bind with low K_D to the targeted GLIC, does not show a clear preference for certain amino acids, trends are apparent. In general, it appears that glutamine, leucine and threonines located in the heavy chain CDR 3 are important for binding, whereas in all selected scFvs hydrophobic residues in the heavy chain CDR 3 are overrepresented (Table 1). Furthermore the DPL16 light chain seems to more suited for binding GLIC than the DPK22 light chain, because only one scFv was selected carrying this chain. Despite the high affinity and specificity of the selected scFvs to GLIC and a broad screening of crystallization conditions, no crystals of a scFv-GLIC complex were obtained, even at low pH in conditions where GLIC normally crystallizes, which suggests that the scFvs prevent crystallization. Since binding of the scFvs appears to be pH independent, the epitope may not involve protonatable residues and may also not undergo large pH-dependent conformational changes. Whereas the comparison of the structure of GLIC crystallized at low pH and a locally closed conformation of a mutant of the same protein shows significant structural differences only in the pore region, bigger conformational changes occur when GLIC is crystallized at neutral pH where it is supposed to be in a non-conductive conformation. A collective quaternary reorganization is observed in the extracellular domain involving radial and tangential motions affecting not only the C-loop (agonist binding site) but also the β7-β8 loop (B-loop, Figure 69) [26, 35, 36].

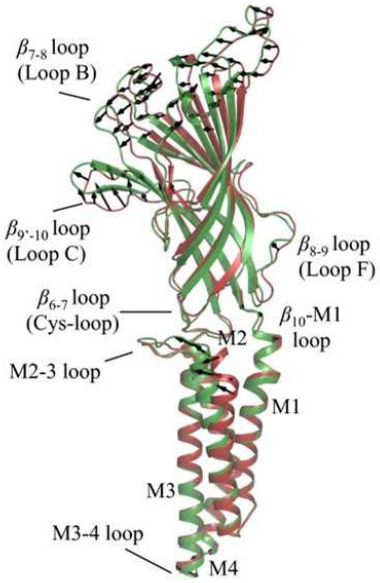

Figure 69 Side view of a full-length monomer of GLIC

Superimposition of the open pH 4 (green) and closed pH 7 (red) GLIC structures, the black arrows show the direction of the motion from the closed form to the open form. Adapted from [36].

Another reason for the poor crystallization properties of the complex could be related to the flexible linker connecting the two variable parts of a scFv, which may interfere with the formation of crystal contacts. In order to decrease the protein flexibility for co-crystallization, the scFvs were cloned into a Fab scaffold. Although the Fabs bind with similar affinities, co-crystallization experiments were also in this case not successful. However, because of their bigger size, Fab fragments can be used as tools for single particle electron microscopy by increasing the molecular weight of the protein-complex. This strategy was used in a recent structure of an ABC transport protein determined by electron cryo-microscopy [122].

Another promising scaffold for protein binders are DARPins [78], which in this study were selected by Ribosome Display. The 27 DARPins, selected for GLIC from a DARPin library of the 2nd generation [111], were characterized with respect to their binding properties. All selected DARPINS contained a N3C scaffold and eight of them showed high binding affinities in the nanomolar range. In Figure 70, their sequences are aligned.

```
                                  20                                  40                                  60                                  80
DARPin N3C  DLGKKLLDAA SAGQDDEVRI LMANGADVNA SXXXGXTPLH XAAXXGHLEI VDVLLAXGAD VNASXXXGXT PLHXAAXXGH 80
DARPin G10  ..........  .....N....  ..I.......  .NSS.W....  L..WD.....  .....Y....  .....SAW.N  ...L..TY..  80
DARPin G40  ..........  ..........  ..........  .DSS.W....  L..WE.....  .....Y....  .....TTW.N  ...S..TR..  80
DARPin G57  ..........  ..........  ..........  .DSS.W....  L..WE.....  .....Y....  .....TTW.N  ...S..TR..  80
DARPin G46  ..........  ..........  ..........  .DHQ.W....  L..WN.....  .....Y....  .....DRY.N  ...L..YS..  80
DARPin G20  ..........  ..........  ..........  .NAW.W....  L..WD.....  .....H....  .....DHW.N  ...T..SW..  80
DARPin G16  ..........  ..........  ..........  .DTA.W....  A..WE.....  .....N....  .....DTW.N  ...T..VH..  80
DARPin G18  ..........  ..........  ..........  .DTA.W....  A..WE.....  .....N....  .....DTW.N  ...T..VH..  80
DARPin G52  ..........  ..........  ..........  .NTY.Y....  V..TS.....  .....H....  .....DNQ.W  ...V..WSD.  80

                                 100                                 120                                 140
DARPin N3C  LEIVDVLLAX GADVNASXXX GXTPLHXAAX XGHLEIVDVL LAXGADVNAN XXXGKTPFDL AIDNGNEDIA EVLQKAA 157
DARPin G10  ........N. .......SHS .Y....V..G W.........  ...N......  DHS.......  ..........  .......157
DARPin G40  ........N. S......NKA .Y....S..Q W.........  ...N......  NYN.......  ..........  .......157
DARPin G57  ........N. .......NKA .Y....S..Q W.........  ...N......  DYY..I....  ..........  .......157
DARPin G46  ......M.Y. .......TSH .Q....L..Q H.........  ...H......  DWD.......  ..........  .......157
DARPin G20  ........N. .......TQQ .Y....T..E S.........  ...N......  NSE.......  ..........  .....V.157
DARPin G16  ........N. .......TQW .W....V..H T.........  ...H......  DND.......  .....G....  .......157
DARPin G18  ........N. .......TQW .W....V..N W.........  ...N.V....  DEY.......  ..........  .....S.157
DARPin G52  ........H. .......NAQ .S....T..R Y.........  ...H.V....  NEH.......  ..........  .......157
```

Figure 70 Alignment of DARPins with high affinity to GLIC.

The top sequence (DARPin N3C) corresponds to the consensus sequence. X indicates randomized positions in the library, the dots identical residues.

The DARPins G16, G18 and G51 contain identical residues in the randomized position of the internal repeats, but different residues in the N-terminal cap, which could indicate that the internal repeats bind the same epitope. Interestingly, whereas the DARPins G16 and G18 co-migrate with GLIC on a size exclusion column, G51 does not, despite the high sequence conservation, which underlines the importance of the contribution of residues of the N-terminal cap for binding (Figure 71).

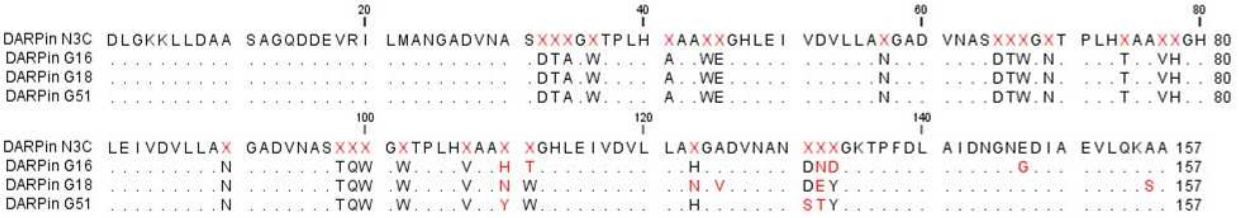

Figure 71 Alignment of DARPin G16, G18 and G51

The top sequence (DARPin N3C) corresponds to the consensus sequence. X indicates randomized positions in the library, the dots identical residues.

The DARPins selected for GLIC by Ribosome Display, bind specifically at neutral or slightly basic but not at acidic pH, as confirmed by ELISA. This pH dependence could either be due to the involvement of ionic interactions, which would be weakened upon protonation, or be dependent on the state of the channel, assuming that in the detergent solubilized state, GLIC can adopt different conformations [49, 51]. Supposing that GLIC shows a similar activation mechanism as other pLGICs, during binding of the ligand in the C-loop region, the loop would cap the binding site thereby transmitting a signal to the transmembrane part to promote channel opening [123]. If the DARPins bind to the extracellular (ECD) part of GLIC, they could specifically recognize an agonist-free conformation of the ligand binding domain, but the oocyte binding assays did not show any evidence for binding from the extracellular side. Attempts to express DARPins as YFP fusions together with GLIC in HEK-293 cells did not show any enrichment of YFP to the membrane, thus also the binding to the intracellular part of GLIC could not be demonstrated. Future experiments could use HEK-293 cells expressing GLIC to probe binding of purified YFP-DARPins from the outside. Although a similar experiment with *X. laevis* oocytes did not show any binding, the difference of the membrane composition of HEK-293 cells and the absence of the vitelline layer, a thick layer of extracellular matrix, might ease the access of the binders to their site. If binding of DARPins or other specific protein binders would be detected in a binding assay, a potential effect on channel function by either occupying an agonist binding site or preventing conformational changes upon channel gating [53-55], could be explored by patch-clamp electrophysiology.

Almost all DARPins selected by Ribosome Display to recognize ELIC, showed formation of higher oligomers and unspecific binding to the protein. Since Ribosome Display was performed in presence of neutravidin, or in the last round with streptavidin coated beads, it could be that binders were selected against avidin, despite the fact that each cycle was preceded by a prepanning step to prevent binding to this protein. From the DARPins sequences, the cause for unspecific binding or oligomerization is not immediately apparent, since most of them contain similar residues at randomized positions as the DARPins selected for GLIC. Only few of the binding proteins were found to contain long insertions.

The nanobodies, which were obtained by immunization of alpacas with the protein of interest followed by the generation of a phage display library and selection by Phage Display show better biochemical properties than the DARPins. Selected nanobodies were monomeric and co-eluted with ELIC on SEC

after complex formation. However, during SPR analysis, it was found that certain nanobodies bind unspecifically to the chip surface consisting of avidin and alginates, resulting in a high background even in the absence of ELIC. Because it was suggested that the conformational changes in ELIC do not symmetrically affect all subunits and that pLGICs can adopt different conformations even in the absence of any ligand [49, 51], it could be, that conformational changes in ELIC are rapid and that the protein does not remain long enough in a single state to be recognized by specific binders.

Since, similar as for the binders recognizing GLIC, it was not possible to investigate the binding of the nanobody to ELIC expressed on *X. laevis* oocytes, a possible impact of the nanobodies on the function of ELIC will have to be studied by patching of HEK-293 cells expressing the channel.

Although in the course of this thesis the selection of several different specific binders targeting GLIC and ELIC *in vitro* and *in vivo* was successful, none of them allowed to obtain crystals of sufficient quality for structure determination. Since no impact of these binders on the function of the target protein could be detected either, because they were not binding to the channels expressed in *X.laevis* oocytes, a different approach to investigate the gating mechanism was used as described in the next chapter.

3.2 Functional characterization of GLIC and ELIC

Previous studies have identified the interface between the extracellular and the transmembrane domains of pentameric ligand-gated ion channels as an important part of the channel opening process, since it may transduce conformational changes in the extracellular domain in response to agonist binding to the pore region [42, 43, 124]. The domain interface is highly conserved among pro- and eukaryotic family members. Overall, the prokaryotic homologues GLIC and ELIC share less than 30% of identical amino acids. The biochemical and electrophysiological investigation of GLIC and ELIC mutants of various positions in the domain interface of the extracellular and the transmembrane domain allowed the identification of residues that had a similar functional effect on both channels. Several residues at the interface located on loop regions in either domain were mutated and the expression on the surface of *Xenopus laevis* oocyte was quantified with a biochemical assay recognizing a tag exposed to the outside. In parallel the functional behavior of the mutants was analyzed by two-electrode voltage clamp electrophysiology. Most mutants showed similar expression levels in oocytes as the corresponding wild type protein, thus suggesting that the channels, despite the mutation, fold properly. None of the alanine mutants showed increased basal activity without application of agonist, which can be explained by either a possible stabilization of a non-conductive conformation of the channel or by a potential uncoupling of the extracellular and the transmembrane domain. Calorimetry experiments with two non-activatable ELIC mutants demonstrate, that the mutant proteins show comparable ligand binding affinities as the wild type protein, which suggests that the mutations do not interfere with ligand binding and instead affect channel gating (see publication "*Signal transduction at the domain interface of prokaryotic ligand-gated ion channels*" in the Appendix).

Despite the low sequence identity between GLIC and ELIC, most of the mutations had a similar impact on channel function in both homologues, thus indicating, that both proteins share a common signal transduction mechanism that may be general for the family. The amino acids that, if mutated, cause a loss of function in both homologues, mainly cluster at two regions of the channels, namely in the β6-β7 loop of the extracellular domain and in the α2-α3 loop of the transmembrane part. Mutations of conserved residues of the β1-β2 loop and the connection between β10 and α1 also have a strong impact on function. In Figure 72 a sequence alignment of loops at the interface of GLIC, ELIC, the acetylcholine receptor α7nAChR and the glycine receptor is shown, where the conserved parts of the proteins are apparent.

Figure 72 Sequence alignment of the domain interface

Sequence alignment of the domain interface of GLIC, ELIC, α7nAChR and GlyR. Residues are coloured according to the following properties: Red, conserved residues; green, similar residues; orange, mutations causing a loss of function; blue, mutations reducing maximum currents and expression; violet, mutation causing misfolding of the protein.

The findings presented in this work are supported by previous studies of the glycine receptor where the central role of the highly conserved β6–β7 loop (cys-loop in eukaryotes) for channel gating was demonstrated. Mutations causing a decrease in function of the GlyR concern the same positions that, upon mutation, resulted in a loss-of-function of the prokaryotic homologues [118]. The β6–β7 loop interacts with the α2-α3 loop of the pore domain and a mutation in the latter was identified to be crucial for function of the α7-nAChR [125]. Mutations in this loop inhibit channel function but have no effect on ligand binding [125] . A different study using chimeras of the acetylcholine binding protein and the serotonin receptor underlines the importance of these loops for function as well [124]. In the acetylcholine receptor the β6-β7 loop is interacting not only with the α2-α3 loop but also with residues from the β1-β2 turn and the β10-α1 linker [43], which emphasizes the importance of this part of the protein for channel gating. In GLIC the aspartates of the β1-β2 turn (D31) and the β6-β7 loop (D121) interact with Arg 191 of the β10- α1 linker. Mutation of these aspartates to alanine cause a loss of function phenotype, similarly to the mutation of equivalent aspartates in the β6-β7 loop of the nAChR, the glycine and the serotonin receptor, which all had a similar impact on gating by preventing channel activation [120, 126-128]. For GLIC, the mutation of the arginine of the β10-α1 linker, that is part of the salt bridge, results in a misfolded protein, which is not transported to the surface of the oocyte as confirmed by an oocyte surface assay. This finding underlines the importance of this ionic interaction for channel folding and gating similar to studies with the nAChR and other pLGICs [129].

In ELIC the residue equivalent to the aspartate in the β1-β2 loop is a threonine (Thr 28), which is not capable of forming a salt bridge with the arginine in the β10-α1 linker. Whereas in ELIC the alanine mutations of corresponding amino acids of the β6-β7 loop and the β10-α1 linker (i.e. Asp122 and Arg199, respectively) resulted in a loss of function protein, the T28A mutation resulted in lower maximum currents measured by TEVC electrophysiology. This indicates that during channel opening the polar side chain of the threonine plays an important role. By mutating this threonine to an aspartate, a negatively charged amino acid present in other family members including GLIC, a possible partner for formation of a salt bridge between the β1-β2 loop and the β10-α1 linker was introduced. In this study it was shown that in this mutant the maximum current upon agonist application is low, and after correlating it to the expression level obtained from the oocyte surface expression assay, it appears that the maximum current response is only 20 % of the values obtained for the wild type channel. This indicates that channels might already be in a desensitized state, which could account for the low maximum response of the mutant expressed in *X. laevis* oocytes. Assuming that the T28D mutation establishes an ionic interaction between the aspartate and R199, as observed in GLIC, it could lead to destabilization of the resting state and therefore result in a higher potency of the agonist. This was confirmed in isothermal titration calorimetry (ITC) experiments with the mutant T28D, which showed an increased affinity to the agonist compared to wild type. For T28D also the half maximal effective concentration

(EC_{50}) of channel activation, measured by two-electrode voltage clamp, was shifted towards lower agonist concentration. Furthermore, residual activity even without agonist was observed in patch clamp recordings (see publication "*Signal transduction at the domain interface of prokaryotic pentameric ligand-gated ion channels*" in the Appendix), which suggests that ELIC can undergo conformational changes leading to channel opening even without agonist as predicted by the Monod, Wyman and Changeux model [50, 51, 123]. Supposing that the T28D mutation shifts the probability of the channel residing in different states, the hypothesis that a fraction of the channels is already desensitized, and thus does not contribute to the measured currents, is plausible. Taken together these findings suggest that the basic side chain of the arginine is mandatory for function in all channels, whereas the mutation of the polar threonine in ELIC, although important for function, does not inhibit channel gating completely.

The big increase in the ligand affinity observed in functional investigations made the T28D mutant an attractive candidate for studying a different conformation of the channel. Thus, the crystal structure of the T28D mutant at 4.5 Å resolution was determined. In this crystal structure, no tight salt bridge could be observed, which would have changed the conformation of the channel and the protein instead showed the known non-conductive state of wild type. Although the exact relation of the of the ELIC structure to functional states (closed, desensitized or an intermediate) is not known, the structures of the glycine receptor bound to its antagonist and GluCl without any ligands resemble ELIC [32, 38] [130], which makes its assignment as a resting state plausible. Since ITC and crystallization experiments are conducted with detergent purified protein whereas the functional investigations are carried out in a membrane, differences in channel behavior can be attributed to the absence of a lipid environment.

The mutation of the corresponding residue in the β1-β2 loop of GLIC (D31A) resulted in a complete loss of function of the channel, thus underlining the importance of an acidic site chain at that position to form a salt bridge between the β1-β2 turn and the β10-α1 linker in this channel. Assuming that, analogous to ELIC T28A, the affinity of the mutant channel (D31A) to the ligand is decreased, it might still be possible to activate this non-functional GLIC mutant at even lower pH.

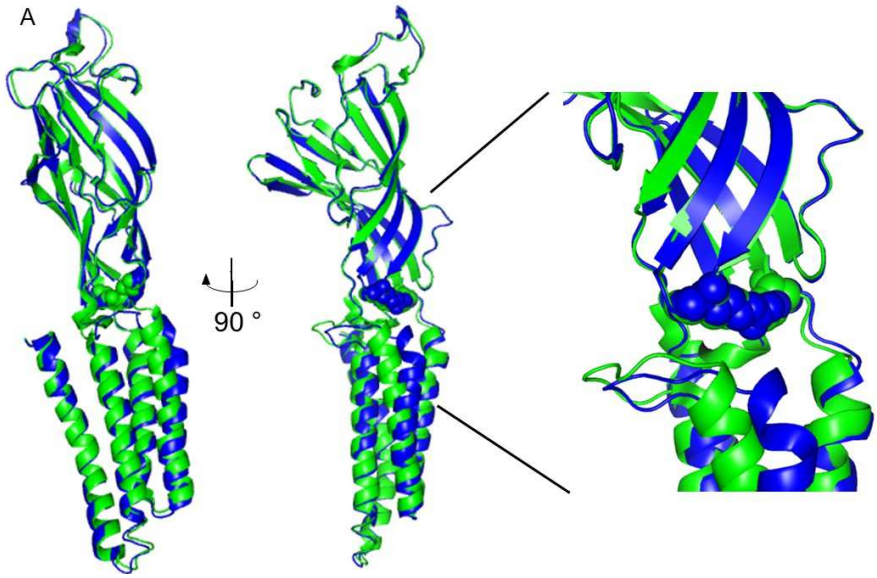

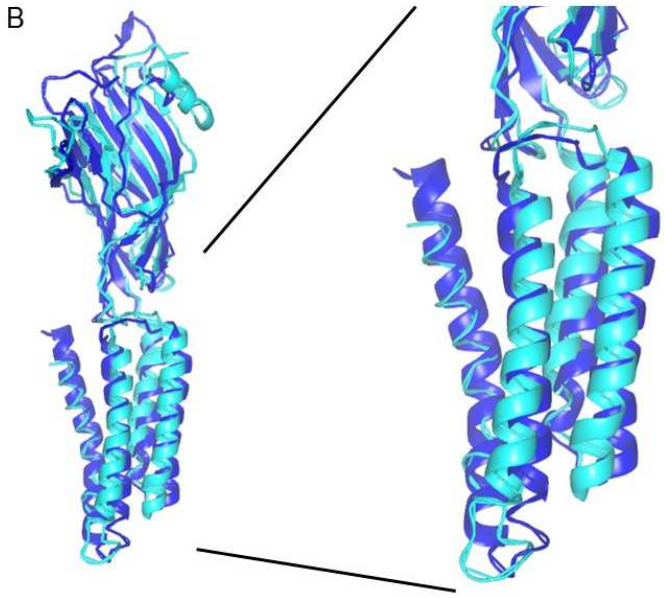

Figure 73 Superimposition of the GLIC charge reversal with GLIC WT and ELIC WT

A) Superimposition of one subunit of GLIC (green) and the charge reversal mutant (blue) in two different orientations. A close-up of the interface is shown left. Mutated residues are displayed as spheres. B) Superposition of a subunit of the charge reversal mutant (blue) and ELIC (cyan) with a close-up of the pore domain shown left. The Figure was created with Pymol.

To further investigate the importance of the described ionic interaction, double mutations of ELIC and GLIC were constructed, where the positions of the interacting acidic and basic residues was switched (charge-reversal mutation). Similar charge-reversing mutations have been previously studied in the acetylcholine receptor, where the single mutants had reduced gating equilibrium constants whereas the double mutant showed wild-type like gating characteristics [21, 23, 120]. Whereas the ELIC charge reversal mutant, when expressed in *E. coli*, could not be purified, due to aggregation of the protein, the GLIC mutant was crystallized at conditions with low pH and the structure was determined at 3.2 Å. This structure revealed striking differences in the pore region compared to GLIC WT. In GLIC WT and in the agonist bound structures of the glycine and glutamate receptor (GlyR and GluCl, [10, 37]), the α2-helices show the same, apparently open, conformation, whereas in the charge reversal mutant the C-terminal part of the α2-helix seems to have collapsed towards the symmetry axis, thereby blocking the pore (Figure 73, A). A comparison of this GLIC mutant with ELIC shows that the upper part of the α2-helix of the charge reversal mutant is oriented similarly to that of ELIC (Figure 73, B) but the lower part is less bent.

Interestingly the structure of this charge reversal mutant resembles previously crystallized GLIC mutants. Both the P246G and the Y250A mutant of GLIC show a similar orientation of the pore lining helix, which is partially unfolded close to the α2-α3 linker and tilted, thereby obstructing the channel. Comparable conformations, termed “locally-closed”, were also observed for GLIC mutants were the cysteines in the β1-β2 and the α2-α3 loop were crosslinked and of a structure of GLIC crystallized at neutral pH. In Figure 74 a superimposition of the charge reversal mutant of GLIC and the P246G mutant as well as with a cysteine crosslinked mutant are shown. Whereas these mutants all have a similar orientation of the pore lining helices, their functional behavior is different. The charge reversal mutation of GLIC results in a loss-of-function, whereas the P246G mutant can still be activated (see publication

"*Signal transduction at the domain interface of prokaryotic pentameric ligand-gated ion channels*" in the Appendix, [36]). Thus, although the salt bridge interaction is preserved in the charge reversal mutant, the pore is in a closed conformation and cannot be activated by lowering the pH.

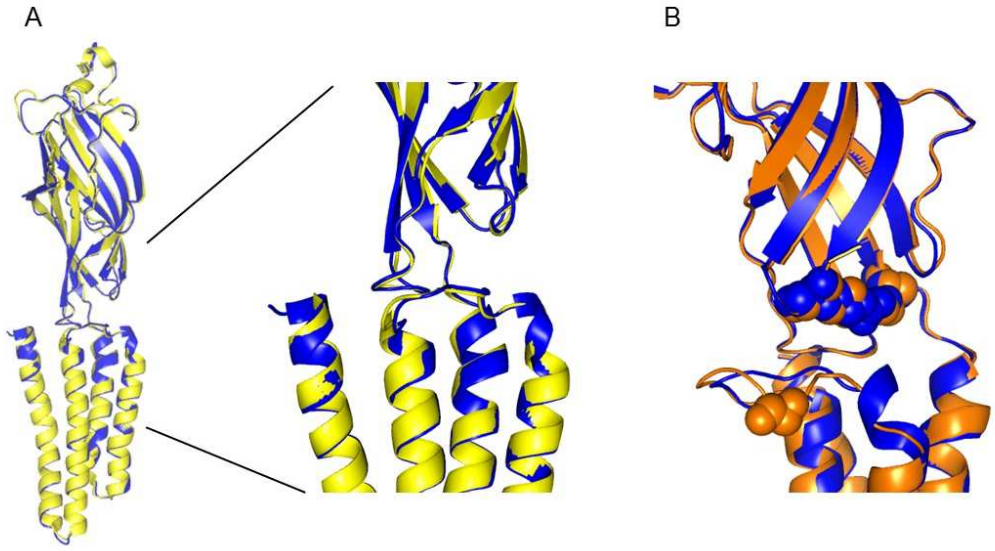

Figure 74 Superimposition of the charge reversal mutant with the locally closed conformation of GLIC and P246G

A) Superimposition of a subunit of the charge reversal mutant (blue) and the locally closed conformation (H11'F, LC1 subtype) of GLIC obtained by cysteine crosslinking between the β1-β2 and the α2-α3 loop. B) Close-up of the interface of a superposition of a subunit of the charge reversal (blue) and the P246G mutant (orange). Mutated amino acids are shown as spheres. The Figure was created with Pymol.

Although the above-mentioned salt bridge is present in structures of GLIC and of the nicotinic actelylcholine receptor and its formation and disruption is important for channel gating [26, 42], it is probable not involved in the main pathway of gating. This is underlined by findings of mutation analysis of the nAChR where the corresponding residues were mutated (charge changing and charge reversal) but still show activation [119].

In the position next to the described aspartate, at the tip of the β1-β2 loop of the extracellular domain, a lysine (K32), interacts via its backbone with a highly conserved proline (P256) in the α2-α3 loop of the pore domain. In ELIC, containing a leucine (L29) at the equivalent position, this interaction is not formed. Since equivalent interactions are present in other pLGICs that were crystallized in presumably open conformations and not in structures adopting a non-conductive state, it was assumed, that this interaction may play a role in channel gating [26, 52]. The mutation of the proline to alanine resulted in channels that still could be activated, although with a lower maximal response than the wild type protein. The mutation of the tip residues in the β1-β2 loop to glycine caused a loss of function phenotype in ELIC whereas the corresponding mutation in GLIC was functional. Whereas the deletion of the lysine in GLIC resulted in inactive channels, in ELIC, the deletion of the equivalent residue L29 only caused a reduction in the maximal current. These findings suggest that the interaction between the tip of the β1-β2 loop and the proline in the α2-α3 loop is not the predominant transducer of conformational rearrangements upon agonist binding to the transmembrane part, since even drastic mutations do not abolish activation.

In summary, the data presented in this thesis and in an accompanying publication demonstrate that channel activation cannot be reduced to a single critical contact between the two domains of the protein.

Instead, this process involves several residues that cluster at the interface between the extracellular- and the pore domain, which all play an important role in gating. Generally, it could be shown that the loops and linkers that were suspected to play a central role in eukaryotic channels are also essential for the prokaryotic homologues GLIC and ELIC. The detailed effects of equivalent mutations in heteropentameric eukaryotic receptors might be less drastic because subunits that were not mutated could compensate for the change. Despite these differences, it appears that the gating mechanism is conserved within pLGICs and the prokaryotic homologues GLIC and ELIC thus can be used as model system for the investigation of functional properties that are general for the family.

4. Methods

4.1 Buffers and media

Barth's solution:	88 mM NaCl, 1 mM KCl, 1 mM CaCl2, 0.33 mM Ca(NO3)2, 0.82 mM MgSO4, 10 mM Na-Hepes (pH 7.4)
EB:	50 mM Tris-acetate pH 7.5 at 4 °C, 150 mM NaCl, 50 mM EDTA
Minimal medium:	54 g Na_2HPO_4, 24 g KH_2PO_4, 4.02 g NaCl, 7.98 g NH4Cl, pH 7.4, MgSO4, CaCl2, Glucose
ND96:	93.5 mM NaCl, 2 mM KCl, 1.8 mM CaCl2, 2 mM MgCl2 and 10 mM Hepes (pH 7.4)
Lysogeny Broth (LB):	5 g yeast extract, 10 g tryptone, 5 g NaCl per liter
PBS:	137 mM NaCl, 2.7 mM KCl, 10 mM Na_2HPO_4, 2 mM KH_2PO_4, pH 7.4
TBS:	0.05 M Tris, 150 M NaCl, pH 7.6
Terrific broth (TB):	12 g tryptone, 24 g yeast extract, 4 ml glycerol per liter, supplemented with 0.17 M KH_2PO_4 and 0.72 M K_2HPO_4
TYE:	10 g bacto tryptone, 5 g yeast extract, 8 g NaCl, 15 g agar per liter
WBT:	50 mM Tris-acetate, pH 7.5 at 4 °C, 150 mM NaCl, 50 mM MgAc
WBT (E):	50 mM Hepes, pH 7.5, 150 mM NaCl, 50 mM MgAc
2YT:	16 g bacto tryptone, 10 g yeast extract, 5 g NaCl per liter

4.2 Expression and purification

4.2.1 GLIC and ELIC

GLIC cloned in a pBX_His_MBP_3C vector was transformed into competent MC1061 cells and grown at 37 °C in Terrific Broth (TB) medium supplemented with 100 µg/ml ampicillin. By addition of 0.04 % L-arabinose, overexpression of GLIC was induced overnight at 20 °C. All the following steps were carried out at 4 °C. The cells were harvested, resuspended in a buffer (50 mM Hepes pH 8, 150 mM NaCl) containing 1 mg/ml lysozyme, protease inhibiors (EDTA free, Roche), 40 µg/ml DNase and 1 mM $MgSO_4$ and lysed with an Emulsiflex C3 high-pressure homogenizer (Avestin) at 35 kpsi. The membranes were harvested by ultracentrifugation with a 45 TI rotor (Beckmann) at 40,000 rpm for 1 h and the overexpressed GLIC was extracted with a buffer (50 mM Hepes pH 8, 150 mM NaCl) supplemented with 1 % DDM (n-Dodecyl-β-D-Maltoside, Anatrace).

ELIC was expressed and purified according to the procedure described previously (Hilf 2008). Competent BL21 cells were transformed with a pet26b vector carrying the gene for ELIC. They were grown in M9 minimal medium at 37 °C and overexpression was induced by addition of 0.2 mM IPTG overnight at 20 °C. All the following steps were carried out at 4 °C. The cells were harvested, resuspended in a buffer (50 mM Hepes pH 8, 150 mM NaCl) containing 1 mg/ml lysozyme, protease inhibitors (EDTA free, Roche), 40 µg/ml DNase and 1 mM $MgSO_4$ and lysed by sonication. The membranes were harvested by ultracentrifugation with a 45 TI rotor (Beckmann) at 40,000 rpm for 1 h

and the overexpressed ELIC was extracted with a buffer (50 mM Hepes pH 8, 150 mM NaCl) containing 1% UDM (Undecyl-β-D-Maltoside, Anatrace).

Both proteins were purified using the same protocol except for the difference in the detergent, 0.03 % DDM in case of GLIC and 0.145% UDM in case of ELIC. The extracted proteins were subjected to immobilized metal affinity chromatography (IMAC) purification by batch- binding to Ni-NTA beads in 15 mM imidazole for 1 h. Unspecifically bound proteins were washed away with buffer (50 mM Hepes pH 8, 150 mM NaCl) supplemented with 55 mM imidazole. The bound proteins were eluted with high amounts (400 mM) of imidazole and the His-MBP- fusion tag was cleaved off with the HRV 3C protease. After dialysis to lower the imidazole concentration, a second IMAC purification was carried out to remove the HRV 3C protease and the fusion tag. Subsequently the flow-through containing the cleaved target protein, was concentrated (Amicon, 30 kDa cut-off) up to 500 µl and subjected to a size exclusion chromatography on a Superdex S200 (GE Healthcare).

The peak corresponding to the elution volume of the target protein was collected and concentrated (Amicon, 30 kD cut-off) to the desired concentration. For Ribosome Display, ELISA and surface plasmon resonance (SPR) the proteins were expressed with an N-terminal Avi-tag (GLNDIFEAQKIEWHE). After the second Ni-NTA purification a biotinylation step (Table 2) with the enzyme BirA overnight at 4 °C was performed prior to concentration and size exclusion chromatography.

µl		Final concentration
250-500	purified protein	ca 100 µM
62.6	200 mM ATP, pH 7 (NaOH)	5 mM
8.3	3 M MgOAc	10 mM
x	biotin	1.2 fold of concentration of avi-tag
5-8	BirA (8 mg/ml)	
fill up to 2500	200 mM NaCl, 10 % glycerol, detergent	

Table 2: Pipetting scheme for biotinylation with BirA

4.2.2 Single chain variable fragments (scFvs) and Fabs

Purification with periplasmic extraction. Competent HB2151 cells were transformed with DNA coding for single chain variable fragments (scFvs) in a pHen vector and grown in 2YT medium supplemented with 0.1 % glucose and 100 µg/ml ampicillin at 37 °C. After inoculation with 1 mM IPTG, expression proceeded for 4 h at 30 °C. Subsequently the cells were harvested and resuspended in sucrose buffer (20 mM Tris pH 8, 25 w/v % sucrose, 5 mM EDTA, 4 ml per gram of pellet) and incubated for 20 min on ice. Cells were centrifuged for 30 min at 20000 rpm and the supernatant saved (sucrose fraction). The pelleted cells were resuspended with (3.5-4 ml per gram pellet) 5 mM $MgCl_2$, 1 mM PMSF and 0.6 mg per gram cells lysozyme. After incubation for 30 min on ice, the cells were centrifuged (30 min at 20000 rpm) and the supernatant was saved (lysozyme fraction). The two fractions (sucrose and lysozyme) were combined and dialyzed over night against PBS pH 7.4 at 4 °C, using 12-14 kDa MwCO. Subsequently, the dialysed sample was loaded on a Protein A column. Unbound proteins were washed with PBS buffer and the scFvs eluted with 0.2 M glycine at pH 3. One ml fractions were collected and the pH neutralized by adding 70 µl 2 M Tris pH 9. Fractions containing the scFvs were pooled, dialysed (PBS, 8000 MwCO cutoff) and subjected to a size exclusion chromatography (superdex S200, GE Healthcare).

Purification with cell lysis. The scFvs were expressed as described in the previous section. The cells were harvested, resuspended in PBS buffer containing 1 mg/ml lysozyme, protease inhibitors (EDTA free, Roche), 40 µg/ml DNase and 1 mM $MgSO_4$ and lysed by sonication. Unlysed cells and cell debris were removed by centrifugation (8000 g, 30 min, 4 °C) and the supernatant containing the scFvs was loaded on a Protein A column. Further purification proceeded as described above.

Fab fragments. The Fab fragments in a pMX9 vector were produced in MC1061 cells grown in 2YT, 0.1 % glucose and 35 mg/ml chloramphenicol at 37 °C. After inoculation with 1 mM IPTG overnight at 25 °C the cells were harvested. The purification was carried out as described for scFvs.

4.2.3 DARPins

DARPins, selected by Ribosome Display, were cloned into a pBX_His_3C vector for expression and purification. Competent MC1061 cells were transformed and grown in TB medium supplemented with 100 µg/ml ampicillin at 37 °C. After inoculation with $2x10^{-2}$ % arabinose and overnight expression at 25 °C, the cells were harvested, resuspended in a buffer (50 mM Hepes, pH 8, 150 mM NaCl) containing 1 mg/ml lysozyme, protease inhibitors (EDTA free, Roche), 40 µg/ml DNase and 1 mM $MgSO_4$ and lysed by sonication. The following steps were performed at room temperature. The supernatant was subjected to IMAC purification by batch- binding to Ni-NTA beads for 1h. The beads were washed with a buffer (50 mM Hepes, pH 8, 150 mM NaCl) containing 55 mM imidazole and the proteins eluted at high imidazole concentration. During dialysis (8000 cutoff) to lower the imidazole concentration, the His-tag was cleaved off with HRV 3C protease. A second Ni-NTA IMAC purification step was carried out to remove the HRV 3C protease and the His- tag. The flow-through containing the purified DARPins was concentrated (Amicon, 10 kD cut-off) and subjected to size exclusion chromatography on a Superdex S200 (GE Healthcare). The peak corresponding to the DARPin was collected and concentrated to the desired concentration for further experiments. By using a buffer with 15 % glycerol, the fractions containing the purified DARPins could be shock frozen in liquid nitrogen and stored at -80 °C.

4.2.4 Nanobodies

The DNA of the nanobodies selected by Phage Display following the immunization of alpacas was cloned into a pBAD vector containing an N-terminal PelB signal sequence, a His_{10}-tag, the fusion protein MPB and a HRC 3C cleavage site. Competent E.coli MC1061 cells were transformed with the vectors and grown in 2.4 L TB medium supplemented with 100 µg/ml ampicillin at 37 °C until they reached an OD_{600} of 0.8. Protein expression was induced with $2x10^{-2}$ % L-arabinose and carried out overnight at 25 °C. The cells were harvested, resuspended in a buffer (50 mM Hepes, pH 8, 150 mM NaCl) containing 1 mg/ml lysozyme, protease inhibitors (EDTA free, Roche), 40 µg/ml DNase and 1 mM $MgSO_4$ and lysed by sonication. The following steps were performed at room temperature. The supernatant was subjected to an IMAC purification by batch- binding Ni-NTA beads for 1h. The beads were washed with a buffer (50 mM Hepes, pH 8, 150 mM NaCl) containing 55 mM imidazole and the proteins were eluted at high imidazole concentration. During dialysis (8000 cutoff) to lower the imidazole concentration, the His- tag and the MPB were cleaved off with HRV 3C protease. A second Ni-NTA IMAC purification step was carried out to remove the HRV 3C protease and the His-tagged MBP. The nanobodies were concentrated (Amicon, 10 kD cut-off) and subjected to size exclusion chromatography (S200, GE Healthcare).

4.3 Selection of binders

4.3.1 Phage Display with single chain variable fragments (scFv)

The ETH-2 Gold phage library from the Neri group was used for Phage Display with GLIC. Three rounds of display were performed prior to the total phage ELISA and the single clone ELISA. The Immunotubes (Maxisorb ImmunoTM Tubes, Nunc) were coated with 5 ml of 67 nM neutravidin in 1xPBS, sealed with parafilm and incubated overnight at 4 °C. The next day, the tubes were blocked with 5 ml PBS supplemented with 0.2 % BSA for 2 h at room temperature. Approximately 500 nM of the biotinylated target protein was added in 4 ml PBS, BSA and detergent and incubated for 1 h at 4 °C. After washing the tube 3 times with PBS-detergent, 4 x 250 µl of each sub-library in PBS-detergent was incubated for 2 h at 4 °C. The tube was rinsed 10 times with PBS-detergent and subsequently the phages were eluted by adding 500 µl of freshly prepared 100 mM TEA (8 min rotating). The solution containing the specifically bound phages was poured into 250 µl of 1 M Tris pH 7.4 for neutralization. A second elution step with 500 µl of 200 mM glycine pH 2 was performed. The two elutions were combined, supplemented with 45 µl of 2 M Tris for neutralization and stored on ice until further use.

The eluted phages were heated to approximately 37 °C and 10 ml of a *E. coli* TG1 cell culture in 2xTY in the exponential grow phase (OD_{600}=0.4-0.5) were added. After incubation for 30 min at 37 °C the cells were shaken for another 30 min at 37 °C. Subsequently, the cells were centrifuged (10 min, 3300 g, 4 °C), resuspended in 1-2 ml 2xYT medium, and plated on at least 4 square TYE-glucose-ampicillin plates. A serial dilution of the cells with $10^{-1/-2/-3/-4/-5/-6}$ time concentrations was performed to proof the enrichment of binders during the selection. 10 µl aliquots were spotted on a TYE-plate supplemented with 0.1 % glucose and ampicillin. Uninfected TG1 cells served as negative control. After an overnight incubation at 37 °C, the colonies on the titration plates were counted and compared to the negative control and to plates from previous selection rounds. The number of infected TG1 cells should increase during the selection procedure. The cells that grew on the square plates were suspended in 2-3 ml 2xTY containing 15 % glycerol. Fifty ml 2xTY supplemented with glucose and ampicillin was inoculated with 10 µl of the cell suspension to an OD_{600} of 0.1 and grown at 37 °C to an OD_{600} of 0.4-0.5. Ten ml of this culture was then infected with 10 µl helper-phage (*E.coli*:helperphage 1:10) and incubated for 30 min at 37 °C. The infected cells were centrifuged (10 min, 3300 g, 4 °C) and the pellet resuspended in 10 ml 2xTY medium supplemented with ampicillin and kanamycin. 140 ml 2xTY containing ampicillin and kanamycin was inoculated with the resuspended cells and grown overnight at 37 °C.

The cells were centrifuged (10 min, 3300 g, 4 °C) and the supernatant (ca. 160 ml) was mixed with 40 ml 5xPEG/NaCl (20 % w/v PEG 6000, 2.5 M NaCl) and incubated for 1.5 h on ice. The phages were pelleted (30 min, 12000 g, 4 °C) and resuspended in 30 ml PBS. A second purification step was performed by adding 7.5 ml 5xPEG/NaCl (30 min on ice) and centrifugation for 30 min at 10000 g. To remove remaining cells, the pellet was resuspended in 2 ml PBS and centrifuged for 15 min at 10000 g at 4 °C. The supernatant contains the phages in high concentration and can be kept on ice until it is used for another selection round, for a total phage ELISA, for infecting cells for single clone ELISA or it can be frozen and stored at -80 °C.

After 3 selection rounds the purified phages were used for infecting E.coli TG1 cells and dilutions ($10^{-4/-5/-6}$) were plated on TYE-plates. Single colonies were picked, grown for 2-3 h at 37 °C in 1 ml 2xTY medium supplemented with 0.1 % glucose and ampicillin, and inoculated with 1 mM IPTG. Expression was carried out overnight at 30 °C. A crude cell extract ELISA was performed to test the scFv binding specificities (see section *Crude cell extract*).

4.3.2 Alpaca immunization and Phage Display with Nanobodies

Alpacas were immunized every second week with detergent purified target protein. After 4 injections, blood was taken and B-lymphocytes were collected. Reverse transcription of the mRNA of the entire population of antibodies and nanobodies was performed, and the DNA coding for the nanobodies was cloned into a Phage Display library. Subsequently, 2 rounds of Phage Display was performed in a 96-well plate (Nunc). Eight wells (4 for the target protein and 4 for the negative control) were coated overnight with 67 nM neutravidin in 100 µl PBS and subsequently blocked with 250 µl PBS supplemented with 2% milk for 2 h at room temperature. 44 µM of the biotinylated target protein was added to 4 of the wells in 100 µl PBS containing the appropriate detergent and incubated for 1 h at 4 °C. The wells were washed twice with PBS-detergent and 10 µl of the phage library (prepared by Y. Neldner) in 100 µl PBS supplemented with 1 % milk and the appropriate detergent were added to all wells. After incubation of 1 h at 4 °C the wells were washed 5 times and the phages eluted with 100 µl trypsin (0.25 mg/ml in PBS), and stored 30 min at room temperature. The eluted phages were transferred to a tube containing 5 µl AEBSF (5 mg/ml in H_2O) and 200 µl of this solution was used for infecting 1.4 ml TG1 cells which were grown to an OD_{600} of 0.5. After incubation of the cells together with the phages for 30 min at 37 °C, 18 ml 2xYT supplemented with 100 µg/ml ampicillin and 2 % glucose was added and grown overnight, while shaking, at 37 °C. Simultaneously, a phage titration assay was performed to gain information about the amount and enrichment of the phages. Ten µl of the eluted phages were mixed with 100 µl PBS and diluted covering a dilution series of $10^{-1/-2/-3/-4/-5}$. 90 µl of TG1 cells at an OD_{600} of 0.5 were infected with the serial dilution and 5 µl drops were plated out on LB-agar plates supplemented with 100 µg/ml ampicillin and 2% glucose. The total number of phages was calculated using following formula:

#colonies x 10 x 20 x dilution factor x 4 (correction for volume, 400 µl)

The next day, a glycerol stock (final concentration of 25 % glycerol) of the overnight grown TG1 cells, infected with the phages, was prepared and stored at -80 °C. 25 ml 2xTY supplemented with 100 µg/ml ampicillin and 2 % glucose was inoculated with 50 µl of the overnight culture and grown at 37 °C until $OD_{60\ 0}$ of 0.5. 10 ml of this culture was infected with $2x10^{10}$ M13KO7 helper phage (prepared by Y. Neldner) for 30 min at 37 °C and subsequently centrifuged for 5 min at 4000 rpm. The supernatant was removed and the cells resuspended in 50 ml 2xYT supplemented with 100 µg/ml ampicillin and 25 µg/ml kanamycin and grown overnight at 37 °C. All following steps were carried out at 4 °C. The next day, the culture was centrifuged for 30 min at 4000 rpm and the supernatant, containing the phages was mixed with 10 ml 20 % PEG6000 and 2.5 M NaCl. After incubation on ice for 30 min, the mixture was spun for 30 min at 4000 rpm and the supernatant discarded. The pelleted phages were resuspended in 1 ml PBS and remaining cells removed by centrifugation for 5 min at 14000 rpm. A second precipitation was performed by adding 250 µl of 20 % PEG6000 and 2.5 M NaCl. The sample was incubated on ice for 15 min. After centrifugation for 15 min at 14000 rpm, the supernatant was discarded and the pelleted phages were resuspended in 1 ml PBS. The phages were used for the next affinity selection round or for infection of *E.coli* TG1 cells for single clone ELISA. To test the titer of the rescued phages, a serial dilution covering 10^{-10} to 10^{-24} was made. Ninety µl TG1 cells were infected with 10 µl of the diluted phages and 5 µl plated out on LB-agar plates supplemented with 100 µg/ml ampicillin and 2 % glucose.

4.3.3 Ribosome Display (according to the protocol from M. Seeger and H. Roschitzki-Voser)

The first round of Ribosome Display was performed with immunotubes. The second and third round was carried out in a 96-well plate, and the fourth round with magnetic streptavidin-beads. We used a library

of RNA of DARPins of the second generation [111]. For the selection with ELIC, the buffer WBT (E) was used.

Surface Panning using Immunotubes

Preparation. The Immunotubes (Maxisorb ImmunoTM Tubes, Nunc) were coated with 1 ml of 66 nM neutravidin in 1xTBS (3.3 µl from a 20 µM stock per ml), sealed with parafilm and incubated overnight at 4 °C. Two immunotubes are needed for each target protein. Both tubes were blocked with 5 ml 0.5 % BSA in 1xTBS for 1 h at RT while shaking. The tubes were washed three times with 1xTBS. The TBS solution was discarded. One ml biotinylated target protein at ~ 1 µM in WBT-BSA-detergent was added to one tube and shaken for 1 h at 4 °C. Just before panning was started, the tubes were washed three times with WBT-BSA-detergent.

In vitro translation. Translation mix was prepared according to pipetting scheme (Table 3). Five times volumes for immunotubes were used. 5x 4 µl library RNA à 2.5 µg/µl was added to the translation mix. Translation was subsequently carried out for exactly 8 min 30 sec at 37 °C. The reaction was stopped by adding ice-cold WBT-BSA-detergent buffer containing 12.5 µl Heparin (200 mg/ml stock) and sample was centrifuged at 20'000 g for 5 min at 4 °C.

Translation mix	µl
Premix buffer (Red)	25
Extract	30
Stop solution	
WBT-BSA (0.5 % w/v)	220
Heparin (200 mg/ml)	2.75
Total	278

Table 3 Translation pipetting scheme for one reaction

Prepanning. The stopped and centrifuged translation mix was pipetted to the previousely blocked immunotube (without target protein) and incubated by shaking for 1 h at 4 °C.

Panning and Elution. The prepanned solution was transferred to the previousely prepared target coated and blocked immunotube and shaken for 1 h at 4 °C. The panning tube was subsequently washed 3 times with 2 ml WBT-BSA-detergent. In order to elute RNA, 500 µl EB25 with 50 µg/ml S. *cerevisiae* RNA (2 µl of a 25 mg/ml stock) per ml, was added. After addition the sample was shaken for 5 min at 4 °C. The eluate was directly pipetted into 1 ml lysis buffer of Roche RNA purification kit. A second elution step was performed and the RNA purified using the Roche high pure RNA isolation kit.

Surface Panning using 96-well plates

Preparation. The 96-well plates (Cert Maxisorb Nunc-Immuno Plates) was coated with 100 µl of 66 nM neutravidin in 1xTBS (3.3 µl from a 20 µM stock per ml). The plate was subsequently covered with plastic foil and incubated overnight at 4 °C. Four wells were used for each target protein. Wells were blocked with 250 µl 0.5 % BSA in 1xTBS for 1 h at RT while shaking. Wells were subsequently washed three times with 1xTBS and dried by removal of the supernatant. One-hundred µl of biotinylated target protein at ~ 1 µM in WBT-BSA-detergent was added to two wells and incubated by shaking for 1 h at 4 °C. Just before panning is started, wells were washed three times with WBT-BSA-detergent.

In vitro translation. The translation mix was pipetted according to pipetting scheme (table 3). Four µl library RNA à 2.5 µg/µl was added to the translation mix. The translation was carried out for exactly 8

min 30 sec at 37 °C. The reaction was stopped by addition of ice cold WBT-BSA-detergent buffer containing 12.5 µl Heparin (200 mg/ml stock) and sample was centrifuged at 20'000 g for 5 min at 4 °C.

Prepanning. The stopped and centrifuged translation mix was pipetted to the previously blocked wells (without target protein) and incubated by shaking for 1 h at 4 °C.

Panning and Elution. The prepanned solution was transferred to the previously prepared target coated wells and shaken for 1 h at 4 °C. The panning wells were subsequently washed 3 times with 250 µl WBT-BSA-detergent. In order to elute RNA, 100 µl EB25 with 50 µg/ml S. *cerevisiae* RNA (2 µl of a 25 mg/ml stock) per ml, was added. The sample was shaken for 5 min at 4 °C. The eluate was directly pipetted into 200 µl lysis buffer of Roche RNA purification kit. A second elution step was performed and the RNA purified using the Roche high pure RNA isolation kit.

Solution Panning

Preparation. RNA free 2 ml tubes were blocked overnight with 1.8 ml 0.5 % BSA in 1xTBS at 4 °C. Three tubes were needed for each target protein. For the prepanning, 20 µl of suspension of magnetic streptavidin coated beads (Streptavidin Magnetic Particles, Roche 11641778001 or Dynabeads® MyOneTM StreptavidinT1, Invitrogen 800.955.6288) are used (termed "beads" below). For the panning, 20 µl/10 µl (1st and 2nd round/ 3rd and 4th round) of beads are used. For the 3rd and 4th round, 10 µl of suspension of beads are used to determine the selection background. The suspension was blocked in TBS-BSA (100 µl per 10 µl initial suspension) overnight (or for 2 h at RT) and washed once with 1 ml WBT-BSA-detergent prior to use.

In vitro translation. The translation mix was pipetted according to the pipetting scheme (table 3). Four µl library RNA à 2.5 µg/µl were added to the translation mix. The translation was carried out for exactly 8 min 30 sec at 37 °C. The reaction was stopped by adding ice cold WBT-BSA-detergent containing 12.5 µl Heparin (200 mg/ml stock). The sample was centrifuged at 20'000 g for 5 min at 4 °C.

Prepanning. The stopped and centrifuged translation mix was added to the magnetic streptavidin coated beads dedicated for the pre-panning (equivalent of 20 µl suspension) and incubated for 1 h at 4°C.

Panning and Elution. The supernatant was transferred to a fresh tube and 1 µM/500 nM (1st and 2nd round/ 3rd and 4th round) of biotinylated target protein was added to the cleared supernatant. Incubation for 1 hour at 4°C (solution panning). In the 3rd and 4th round, a control omitting the biotinylated targets to check for background binding of the ribosomal complexes to the beads was included. The panning solution was added to the washed magnetic beads and incubated for 15 minutes. Afterwards the beads were washed three times with WBT-BSA-detergent. The washed beads were transferred to a fresh tube and the RNA was eluted using 100 µl EB25 with 50 µg/ml S. *cerevisiae* RNA (2 µl of a 25 mg/ml stock) per ml while Shaken for 5 min at 4 °C. The eluate was directly pipetted into 200 µl lysis buffer of Roche RNA purification kit. A second elution step was performed and the RNA purified using the Roche high pure RNA isolation kit.

From Reverse Transcription to RNA preparation

RNA Purification. Maximal 700 µl of the eluate mixed with lysis buffer was loaded to the column. The flow-through was discarded after spinning for 1 min at 8'000 g at 4 °C. This step was repeated until everything was loaded on the column. The column was washed with 500 µl buffer 1 and 500 µl buffer 2. Afterwards 200 µl of buffer 2 was added to the column and centrifuged for 2 min at 13'000 g. RNA was eluted with 30 µl elution buffer and centrifuged for 1 min at 8'000 g. The eluted RNA can be stored at – 20 °C or used directly for reverse transcription.

Reverse Transcription. The eluted RNA was heated up to 70 °C for 10 min. The reverse transcription reaction was pipetted according the pipetting scheme (Table 4) and 8.75 µl RNA was added. The reverse transcription was carried out for 1 h at 50 °C and later used for PCR.

2x Master mix	10 µl
Primer rev (100 µM)	0.25 µl
RNAsin (200 U/µl)	0.5 µl
Affinity Script	0.5 µl
Total	11.3 µl

Table 4 Reverse transcription pipetting scheme for one reaction

PCR on RT. The PCR reaction was mixed according to the pipetting scheme (Table 5) using the inner primers (EWT5/NC4S). 25 to 45 cycles were carried out (depending on the Ribosome Display round). The PCR product was purified on a 1.2 % agarose gel and extracted using the QIAquick Gel Extraction Kit (see manufacturer's protocol). In the last round, the primers DARPin_fx_f and DARPin_fx_r were used instead of EWT5 and NC4S for cloning into a pBX_N_His_3C_vector, which was used for the expression of the DARPins in bacterial cells.

H_2O	34 µl
DMSO	2.5 µl
10x Buffer	5 µl
dNTP (10 mM each)	2 µl
Primer for (100 µM)	0.5 µl
Primer rev (100 µM)	0.5 µl
Vent polymerase	0.5 µl
Mix with 5 µl template	45 µl

Table 5 PCR pipetting scheme for one reaction

PCR for Digestion. The PCR reaction was mixed according to the pipetting scheme (Table 5) using the inner primers (EWT5/NC4S). Twenty-five to forty-five cycles were carried out (depending on the Ribosome Display round). The PCR product was purified on a 1.2 % agarose gel and extracted using the QIAquick Gel Extraction Kit (see manufacturer's protocol).

Digestion of PCR product. The purified PCR product was digested using the restriction enzymes NcoI and HindIII for 1 h at 37 °C. The product was purified with the MinElute PCR purification Kit from QIAgen and directly eluted into the ligation mix.

Preparation of fragments for ligation. DNA fragments containing RBS (ribosome binding site) and C-terminal loop region were prepared by PCR on a pRDV- vector using the primers T7b_2 and pRDV_Nco_r or TolAk and pRDV_Hind_f for RBS-site and loop region, respectively. The fragments were digested with NcoI and HindIII respectively and purified on an 1.2 % agarose gel.

Ligation with fragments to introduce RBS and loop region. The ligation mix was pipetted according to the pipetting scheme and incubated for 45 min at room temperature. The same amount of NcoI and

HindIII fragment were used, calculated by this formula (Loop-fragment: ca 300 bp, RBS- fragment: ca 200 bp):

$$ng\ (2) = (ng\ (1) * bp\ (1)) / bp\ (2)$$

PCR on ligation. The PCR reaction was mixed according to the pipetting scheme (table 5) using the outer primers (T7B.2/TolAk). Thirty to thirty-five cycles were carried out (depending on the Ribosome Display round). The PCR product was purified on a 1 % agarose gel and extracted using the QIAquick Gel Extraction Kit (see manufacturer's protocol).

PCR for Transcription. The PCR reaction was mixed according to the pipetting scheme (table 5) using the outer primers (T7B.2/TolAk). Thirty to thirty-five cycles were carried out (depending on the Ribosome Display round). Three µl of the PCR reaction was loaded on an analytical agarose gel (0.8 %). The remaining PCR mix was not purified and directly used for the transcription.

Transcription. The transcription reaction was mixed according to the pipetting scheme (Table 6) using 22.5 µl PCR product and carried out for 2-3 h at 37 °C.

H_2O	23.5 µl
5x Buffer	20 µl
NTPs (25 mM each)	28 µl
RNAsin	2 µl
T7 Pol	4 µl

Table 6 Transcription pipetting scheme for one reaction

Transcription with Promega kit. The PCR for transcription was done as described above, but with a two-fold approach, thus doubling the PCR. The PCR was purified with the MinElute PCR purification Kit from QIAgen and eluted with 20 µl elution buffer. The transcription was carried out according to manufacturer's protocol.

RNA purification. 100 µl of UHP water and 200 µl of 6 M LiCl was added to the transcription mix and incubated on ice for 30 min. After centrifugation at 20'000 g for 30 min at 4 °C, the supernatant was discarded. The pellet was washed with 500 µl ice-cold 70 % EtOH and dried for 5 min at room temperature. The pellet was taken up in 200 µl ice cold UHP water and centrifuged at 20'000 g for 5 min at 4 °C. The supernatant was transferred to a fresh eppendorf tube containing 20µl 3M NaOAc and 500 µl of ice cold 100 % EtOH was added. The mixture was incubated at – 20 °C for at least 30 min or overnight and centrifuged at 20'000g for 30 min at 4 °C. The supernatant was discarded and the pellet washed with 500 µl 70 % EtOH. The pelleted RNA was dried in a SpeedVac apparatus for 15 min and subsequently taken up in 30 µl ice cold UHP water. The concentration of the diluted (2 µl RNA in 500 µl UHP water) RNA was measured in a photo-spectrometer. One OD unit corresponds to 10 µg/µl stock RNA, e.g. OD*10 = concentration in µg/µl. The RNA was shock-frozen in liquid nitrogen and stored at -20 °C (for long term storage at -80 °C).

RNA purification with kit. The manufacturer's protocol was followed and RNA concentration measured with a NanoDrop Spectrophotometer.

4.4 Other methods

4.4.1 Surface Plasmon Resonance (SPR)

For all SPR measurements the ProteOn XPR36 interaction array system (BioRad) of the FGCZ (functional genomics centre Zurich) was used. Biotinylated GLIC and ELIC were purified as described above. After size exclusion chromatography the protein was immobilized via the ligand channels by binding of the avi-tag to a ProteOn™ NLC Sensor Chip until an RU of ca 600 was reached. The binders to be analysed, were purified with the same buffer as the corresponding target protein and loaded in different concentrations (0 to 600 mM) via the analyte channels at a flow rate of 30 µl/min. The ProteOn manager software from BioRad was used for analysis of the signals after referencing using the interspot regions.

4.4.2 Crude cell extract

Single clones (of scFvs, DARPins or nanobodies) were inoculated in 1.2 ml medium (TB or LB) supplemented with the appropriate antibiotics at 37 °C and shaken overnight at 200 rpm. 200 µl of this culture was taken to inoculate 900 µl medium and grown for 2-3 h at 37 °C, while shaking at 200 rpm prior to induction with 1 mM IPTG or 0.002 % arabinose. The binders were expressed at 20 °C overnight, the cells harvested (3000 g, 10 min, 4 °C) and frozen at –20 °C. The cells were lysed by resuspension in 50 µl PBS with 1 % detergent or by resuspension with 50 µl PER-II by vortexing. After incubation at room temperature for 30 min, 500 µl PBS was added and cell debris pelleted by centrifugation (3000 g, 10 min, 4 °C).

4.4.3 ELISA

An ELISA plate (96-well or 384-well) was coated overnight at 4 °C with 67 nM neutravidin (in PBS, 100 µl for 96-well plates or 20 µl for 384-well plates). The wells were blocked with 250 µl or 44 µl PBS containing 1 % BSA for 1h at room temperature. 300 nM of biotinylated membrane protein (100 µl or 20 µl) was added to the wells in a PBS-BSA buffer containing the appropriate detergent and incubated for 1 h at 4 °C under gentle agitation. After washing 3 times with PBS-detergent, the binders to fused to a His- or myc-tag were added in a PBS-BSA-detergent buffer and incubated while slightly shaking for 1 h at 4 °C. Subsequently the wells were washed and the primary antibody (100 µl or 20 µl in PBS-BSA-detergent) was added and solution was incubated for 1 h at 4 °C. After 3 washing steps, the secondary antibody (conjugated with horse-radish peroxidase) was added (100 µl or 20 µl in PBS-BSA-detergent) and incubated for at least 30 min at 4 °C. After 4 washing steps, binding was detected by addition of a HRP- substrate. The reaction was stopped with 1 M HCL and absorbance was quantified at 450 nm in a Tecan infinite M1000 plate reader.

4.4.4 RNA

Constructs containing the gene of either the wild type or mutant channels preceded by the signal sequence of the chicken α7nAchR and a hemagglutinin- tag were cloned into a modified pTLN vector for expression in *X. laevis* oocytes. After linearization of the plasmid DNA by MluI, capped complementary RNA was transcribed with the mMessage mMachine kit (Ambion), purified with the RNeasy kit (Qiagen) and the concentration measured with a NanoDrop spectrophotometer.

4.5 Functional characterization of different GLIC and ELIC mutants

4.5.1 Two- electrode voltage clamp (TEVC)

Approximately 10 ng of RNA, coding for either the WT or mutant channels, was injected into defolliculated *X.laevis* oocytes. For expression, oocytes were incubated in Barth's solution supplemented with 50 µg/ml Gentamycin at 16 °C. A surface expression assay was performed after 1, 2 and 3 days after injection to analyse the highest expression levels. Two days after injection, two-electrode voltage clamp measurements were performed at 20 °C (OC-725B, Warner Instrument Corp.), the voltage was clamped at -40 mV. For ELIC, maximal currents were recorded in a bath solution containing 10 mM Hepes (pH 7), 130 mM NaCl, 2mM KCl, 0.5 mM $CaCl_2$ and 5 mM or 25 mM cysteamine. For GLIC the maximal currents were measured in a bath solution containing 10 mM Citrate (pH 4), 130 mM NaCl, 2 mM KCl, 1.8 mM CaCl2, 1 mM MgCl. Directly after recording of the maximal currents, the expression of the channels was analysed by a surface expression assay.

4.5.2 X*. laevis* oocyte surface expression assay

The *X. laevis* oocytes, previously used for TEVC, were subjected to a surface expression assay [131]. For that purpose the oocytes were placed in a 96-well plate (TPP, tissue culture testplate, flat bottom) and blocked in ND 96 solution containing 1 % BSA for at least 30 min at 4 °C. The hemagglutinin-tagged channels were labeled with 1 µg/ml rat monoclonal anti-HA antibody (3F10, Roche), in ND 96 solution containing 1% BSA for 1 h at 4°C and briefly washed 3x with ND96 solution at 4 °C. Subsequently oocytes were incubated with 0.16 µg/ml horseradish peroxidase–(HRP) coupled to a secondary antibody (HRP-conjugated goat anti-rat F(Ab)2 fragments (Jackson)), in ND96 solution containing 1% BSA for 30–60 min at 4°C. The oocytes were washed 5x for 10 min with ND96 solution at 4 °C and transferred to a white 96-well plate (flat bottom, Nunclon Delta Surface). The solution was aspirated, 30 µL of Super Signal ELISA femto (Pierce) solutions 1 and 2 was added and luminescence was quantitated in a Tecan infinite M1000 plate reader.

Appendix

PLOS | BIOLOGY

RESEARCH ARTICLE

Signal Transduction at the Domain Interface of Prokaryotic Pentameric Ligand-Gated Ion Channels

Carlo Bertozzi, Iwan Zimmermann, Sibylle Engeler, Ricarda J. C. Hilf, Raimund Dutzler*

Department of Biochemistry, University of Zürich, Zürich, Switzerland

* dutzler@bioc.uzh.ch

OPEN ACCESS

Citation: Bertozzi C, Zimmermann I, Engeler S, Hilf RJC, Dutzler R (2016) Signal Transduction at the Domain Interface of Prokaryotic Pentameric Ligand-Gated Ion Channels. PLoS Biol 14(3): e1002393. doi:10.1371/journal.pbio.1002393

Academic Editor: Pierre-Jean Corringer, Institut Pasteur, FRANCE

Received: July 29, 2015

Accepted: January 27, 2016

Published: March 4, 2016

Data Availability Statement: The coordinates of the ELIC mutants F116A, Y258A, and P254A and T28D have been deposited with the Protein Data Bank under accession codes 5HEJ, 5HEU, 5HEO, 5HEW. The GLIC mutants P246A and P246G have been deposited with the Protein Data Bank under accession codes 5HEH and 5HEG. Relevant data is also provided as supporting information file.

Funding: The research leading to these results has received funding from a grant from the Swiss National Science Foundation (grant no. 31003B_141180) to RD. The funders had no influence on the study

Abstract

Pentameric ligand-gated ion channels are activated by the binding of agonists to a site distant from the ion conduction path. These membrane proteins consist of distinct ligand-binding and pore domains that interact via an extended interface. Here, we have investigated the role of residues at this interface for channel activation to define critical interactions that couple conformational changes between the two structural units. By characterizing point mutants of the prokaryotic channels ELIC and GLIC by electrophysiology, X-ray crystallography and isothermal titration calorimetry, we have identified conserved residues that, upon mutation, apparently prevent activation but not ligand binding. The positions of nonactivating mutants cluster at a loop within the extracellular domain connecting β-strands 6 and 7 and at a loop joining the pore-forming helix M2 with M3 where they contribute to a densely packed core of the protein. An ionic interaction in the extracellular domain between the turn connecting β-strands 1 and 2 and a residue at the end of β-strand 10 stabilizes a state of the receptor with high affinity for agonists, whereas contacts of this turn to a conserved proline residue in the M2-M3 loop appear to be less important than previously anticipated. When mapping residues with strong functional phenotype on different channel structures, mutual distances are closer in conducting than in nonconducting conformations, consistent with a potential role of contacts in the stabilization of the open state. Our study has revealed a pattern of interactions that are crucial for the relay of conformational changes from the extracellular domain to the pore region of prokaryotic pentameric ligand-gated ion channels. Due to the strong conservation of the interface, these results are relevant for the entire family.

Author Summary

The pentameric ligand-gated ion channels constitute a large family of membrane proteins that are expressed in animals and certain bacteria. Their molecular architecture and function is conserved throughout the family. In mammals, they operate as receptors of the neurotransmitters acetylcholine, serotonin, GABA, and glycine and play a key role in electrical signal transduction at chemical synapses. These receptors are called ionotropic

design, data collection and analysis, decision to publish, or preparation of the manuscript.

Competing Interests: The authors have declared that no competing interests exist.

Abbreviations: Bg, background; EPR, electron paramagnetic resonance; GluCl, glutamate-gated chloride channel; GlyR, glycine receptor; HA-tag, hemagglutinin tag; HEK293, human embryonic kidney 293; HRP, horseradish peroxidase; HRV, human rhinovirus; ITC, isothermal titration calorimetry; MWC, Monod Weyman Changeux; nAChR, nicotinic acetylcholine receptor; non inj., noninjected; pLGIC, pentameric ligand-gated ion channel; PSI, Paul Scherrer Institute; SEM, standard error of the mean; SD, standard deviation; SLS, Swiss Light Source; WT, wild type.

because they open a selective ion conduction path across the membrane upon binding of the neurotransmitters to a site that is exposed to the extracellular medium. Ligand binding promotes a conformational change in the extracellular domain that is transmitted over more than 50 Å to the pore domain. Due to this long-range effect, pentameric ligand-gated ion channels have become important model systems for the study of allosteric processes, a mechanism that is of large importance for biology and entails the regulation of a protein activity by an effector that binds to a distant domain. In the present study, we investigated the role that residues in the contact region between the ligand-binding and the pore domains of two bacterial pentameric ligand-gated ion channels of known structure have in the transduction of conformational changes. Our study shows that single mutations severely influence the functional properties, with certain mutations preventing activation. The results underline the importance of highly conserved residues in the domain interface for the transmission of allosteric signals and thus likely apply also to other family members.

Introduction

During activation of a pentameric ligand-gated ion channel (pLGIC), the binding of agonists promotes the opening of a selective ion conduction pore at a distance of more than 50 Å away from the binding sites [1,2]. This process has been described by means of the Monod Weyman Changeux (MWC) mechanism of allosteric proteins, where activation can be broken down into distinct steps defining ligand binding and the shift in the equilibrium between the open and closed state of the pore [3–5]. pLGICs constitute a large family of membrane proteins that are expressed in animals and certain prokaryotes [6]. In mammals, the family encompasses ionotropic neurotransmitter receptors for acetylcholine, serotonin, GABA, and glycine, which are key players in electrical signal transduction at chemical synapses [7], whereas prokaryotic pLGICs are potentially involved in pH resistance [8,9]. All family members share a conserved molecular architecture composed of five either identical or closely related subunits. Over recent years, insight into the structural properties of pLGICs has been obtained from different sources. Electron microscopy studies of the nicotinic acetylcholine receptor (nAChR) from Torpedo electric ray have shed light on the structure of a heteropentameric receptor at medium resolution [10,11]. A recent study by single-particle electron cryomicroscopy revealed agonist and antagonist bound views of the glycine receptor (GlyR) [12]. Structures at higher resolution have been provided by X-ray crystallography for various pro- and eukaryotic family members [13–21]. Although these structures show different conformations of the channels, whose assignment to defined functional states is in certain cases still ambiguous [22], they closely resemble each other with respect to their general architecture. Each subunit consists of a predominantly β-stranded extracellular domain and an α-helical transmembrane pore, which interact via an extended interface. Both domains constitute independent folding units that, in certain cases, can be expressed as isolated proteins, thereby maintaining their respective structure observed in the full-length receptors [23–25]. The acetylcholine binding protein, which resembles the extracellular domain, even is an independent soluble protein [26]. Besides their close structural relationship, family members also share a common gating mechanism. Whereas the probability for channel opening in the ligand-free state is very low, it is increased by several orders of magnitude following agonist binding to sites in the extracellular domain located at the boundary between two adjacent subunits [1,5]. Since conformational rearrangements in this part of the protein are transduced via the domain interface to the transmembrane

pore [27], it is not surprising that the residues at this interface belong to the most conserved parts of the protein.

In this study, we were interested in the role of interactions at the domain interface for the transduction of conformational changes in pLGICs. For that purpose, we have characterized mutants of ELIC and GLIC, two prokaryotic family members, by electrophysiology, calorimetry, and X-ray crystallography. These prokaryotic channels are ideal targets for mechanistic investigations: Their detailed structures have been determined in different conformations and show compact proteins that contain the main features of pLGICs [28]. Moreover, unlike many eukaryotic pLGICs, they form functional homopentamers that have been characterized on a macroscopic and a single channel level and that exhibit a functional behavior that closely resembles family members of higher organisms [8,9,29,30]. Whereas ELIC forms a cation-selective channel with high conductance that is activated with high efficacy by the primary amines cysteamine, propylamine, and GABA [9], the cation-selective GLIC is activated by protons and inhibited by bulky positively charged compounds that also act as open channel blockers of the nAChR [8,31]. Our study has identified a cluster of interacting residues located at the β1-β2 turn, the β6-β7 loop and the pre-M1 region of the extracellular domain, and the M2-M3 loop of the pore that exert a strong influence on channel function. These residues face a tightly packed core of the subunit, suggesting that their mutual interactions are critical for the transduction of signals underlying channel activation. Our results are generally consistent with previous investigations on eukaryotic receptors, which underlines the conservation of the activation mechanism throughout the family.

Results

Alanine Scanning Mutagenesis at the Domain Interface

To investigate the role of interactions between the ligand-binding and the pore domain of pLGICs, we have selected residues in ELIC and GLIC that are either part of the domain interface or that are located in close proximity (Fig 1 and S1 Fig). In an initial screen, we have mutated these residues to alanine and expressed them in *Xenopus laevis* oocytes. Surface expression was quantified by ELISA with an antibody that recognizes a tag fused to the extracellular N-terminus of the respective protein. Most constructs showed robust expression, with few exceptions where the truncation of the side chain has led to a strong reduction of the ELISA signal (S2 Fig). To probe whether the mutated proteins would still be activated by ligands, we have measured the current response upon application of agonist by two-electrode voltage clamp electrophysiology. Whereas the majority of the investigated constructs showed response at high agonist concentration, the mutation of certain positions, although well expressed, resulted in either an apparent loss of activation or very low currents (Fig 2 and S2 Fig). In general, equivalent positions in ELIC and GLIC exhibited a similar pattern, which underlines the role of conserved residues at the domain interface for channel activation, but there were also some differences observed. In both cases, mutants with strongly compromised activation properties cluster at the loops connecting β-strands 6 and 7 (the cys-loop of eukaryotic receptors that contains the region of highest conservation) and α-helices M2 and M3 of the pore domain (the M2-M3 loop). A nonactivating phenotype was also found for certain residues of the β8-β9 loop that connect to the neighboring subunit and in GLIC, for an aspartate in the β1-β2 turn. Finally, no activation in case of ELIC and no expression in case of GLIC was observed for a strictly conserved arginine at the end of β-10 (the pre-M1 region). None of the investigated mutations showed detectable basal activity in the absence of agonists.

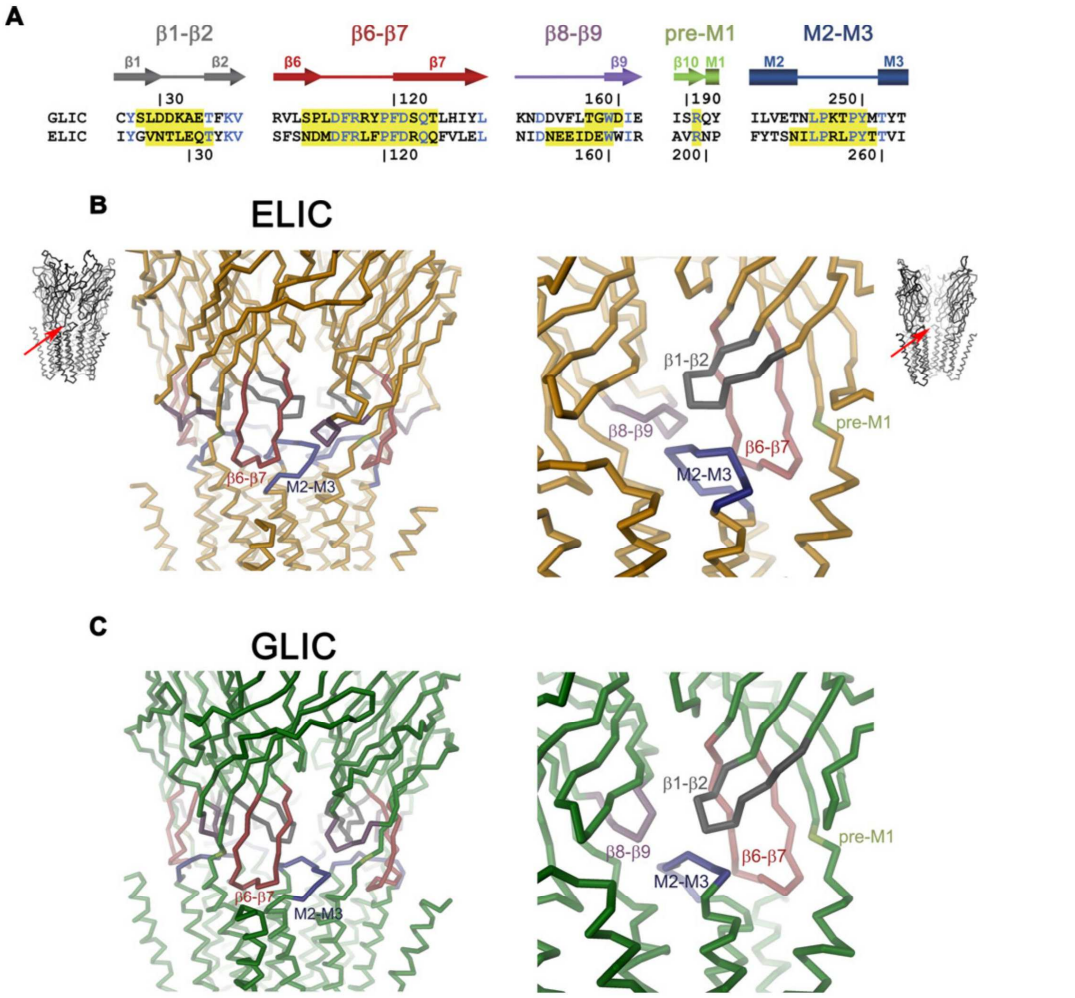

Fig 1. Domain Interface of pLGICs. (A) Aligned sequences of the domain interface of GLIC and ELIC with residue numbering shown above and below, respectively. Secondary structure elements are indicated. Identical residues are colored in blue. Residues mutated in this study in either protein are highlighted in yellow. (B) Domain interface of ELIC (Protein Data Bank entry 2VL0). The protein is displayed as Cα-trace, mutated regions are shown in unique colors, the views are indicated. Left: View at the interface from the outside. Right: View from the pore region on two adjacent subunits. (C) Domain interface of GLIC (Protein Data Bank entry 3EHZ). The protein is displayed as Cα-trace, with mutated regions shown in unique colors. The views are as in B.

doi:10.1371/journal.pbio.1002393.g001

Characterization of Nonactivating Mutants at the Domain Interface

When mapped on the structure, most mutations resulting in nonactivation by agonist point into a tightly packed core of the protein, irrespectively of their position in the sequence, thus

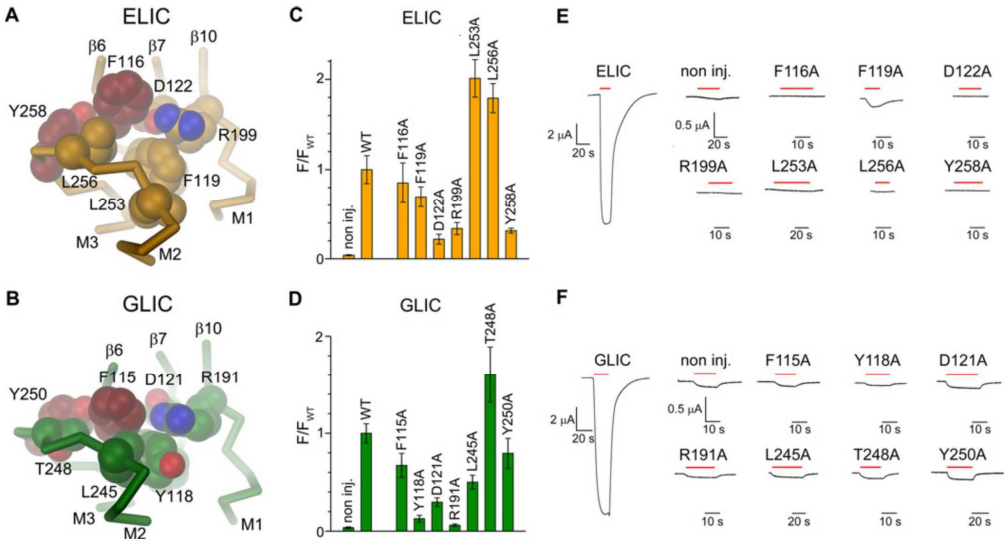

Fig 2. Nonactivating mutations at the domain interface. Cα-trace of parts of the domain interface in a single subunit of (A), ELIC and (B), GLIC with sidechains of selected nonactivating mutants shown as CPK models. The views are from within the pore (as in Fig 1B, right panel). Residues in ELIC for which alanine mutants were characterized in detail (Phe116 and Tyr258) and the corresponding residues in GLIC (Phe115 and Tyr250) are colored in red. (C–D), Surface expression of nonactivating mutants of (C), ELIC and (D), GLIC. Data show averages of 7–14 different oocytes and are normalized to wild type (WT). Background of noninjected (non inj.) oocytes was not subtracted. Errors are standard error of the mean (SEM). (E–F), Current response of a representative oocyte at high agonist concentration that was subsequently used for the analysis of surface expression. Currents were recorded at –40 mV. (E) Response in ELIC after application of 25 mM cysteamine. (F) Response in GLIC after change to pH 4. Application of agonist is indicated by a red bar. (See S1 Data for the raw data used to generate plots shown in panels C and D).

doi:10.1371/journal.pbio.1002393.g002

suggesting that any disruption of this core may interfere with channel activation (Fig 2A and 2B and S3A Fig). To exclude that these mutations cause misfolding of the protein, we have expressed several of them in *Escherichia coli*. Most mutants showed wild type (WT)-like expression levels and were stable in detergent solution. For two cases, the ELIC mutants F116A of the β6-β7 loop and Y258A of the M2-M3 loop, we have grown crystals and determined structures at 3.5 and 3.2 Å, respectively (Table 1). Both mutants crystallized in the same non-conducting conformation that has been observed in all known ELIC structures. Small structural differences in the vicinity of the respective mutations indicate local rearrangements of protein interactions due to the loss of the bulky aromatic side chains (Fig 3A and 3B, S4A and S4B Fig). The data suggests that the mutations, despite their severe phenotype on channel activation, have only a local effect on the protein structure. We have also investigated whether both mutants would at least show residual activity, and we have thus expressed them in *X. laevis* oocytes and HEK-293 cells and studied excised patches in the outside-out configuration upon fast application of agonist. Neither of the two mutants display ligand-induced channel activity in any of numerous independent recordings (Fig 3C–3E). To exclude that the two non-activating mutations have compromised the ability of the protein to recognize its ligand, we have studied agonist and antagonist binding to the detergent solubilized protein by isothermal titration calorimetry (ITC, S5 Fig). WT ELIC binds the agonist propylamine and the competitive antagonist acetylcholine with an effective dissociation constant (K_{eff}) of 8 and 2.5 mM,

Table 1. Data collection and refinement statistics 1.

	ELIC F116A	ELIC Y258A	ELIC T28D	ELIC T28D/ligand
Data collection				
Space group	$P2_1$	$P2_1$	$P2_1$	$P2_1$
Cell dimensions				
a, *b*, *c* (Å)	105.2, 267.0, 111.0	105.3, 266.6, 110.7	105.5, 267.0, 110.2	106.8, 264.8, 108.7
α, *β*, *γ* (°)	90.0, 110.2, 90.0	90.0, 110.5, 90.0	90.0, 110.5, 90.0	90.0, 110.5, 90.0
Resolution (Å)	50–3.5 (3.6–3.5)	50–3.2 (3.3–3.2)	50–4.5 (4.6–4.5)	50–9.5 (9.7–9.5)
R_{merge}*	9.0 (77.0)	8.5 (74.1)	9.3 (189.2)	4.9 (113.7)
$I / \sigma I$ *	14.2 (2.0)	15.2 (2.3)	13.1 (1.9)	14.9 (1.9)
Completeness (%) *	99.4 (99.6)	99.3 (99.2)	99.7 (99.5)	98.5 (99.8)
Redundancy *	3.4 (3.6)	3.9 (3.8)	12.0 (1.6)	6.9 (6.8)
Refinement				
Resolution (Å)	30–3.5	30–3.2	30–4.5	20–9.5
No. reflections	71,563	93,066	33,699	3,186
R_{work}/R_{free}	21.3/25.5	22.0/24.7	23.7/27.1	27.5/28.9
No. atoms				
Protein	24,880	24,980	25,060	-
Ligand/ion	-	-	-	-
B-factors				
Protein	131	97.3	289	-
Ligand/ion	-	-	-	-
R.m.s. deviations				
Bond lengths (Å)	0.002	0.003	0.003	-
Bond angles (°)	0.6	0.6	0.6	-

*Values in parentheses are for highest-resolution shell.

doi:10.1371/journal.pbio.1002393.t001

respectively (Fig 3F). Whereas the affinity for the antagonist, which stabilizes the closed state of the channel, is similar in calorimetry and electrophysiology experiments [30,32], K_{eff} of the agonist is about 20-fold higher than its EC_{50} measured in two-electrode voltage clamp recordings (EC_{50} of 450 μM in the absence of Ca^{2+}) [9], which suggests that the channel may not be fully activated in detergent solution. It is also noteworthy that the measured value is very close to the dissociation constant for propylamine to the resting state of 7.1 mM that was obtained from a detailed kinetic analysis of single channel recordings of ELIC [29]. To enhance binding of the agonist, we also carried out calorimetry experiments in the background of the mutant R91A located in the ligand binding site, which was previously shown to increase the potency of cysteamine, propylamine, and acetylcholine [9]. In accordance with electrophysiology, ITC experiments show that the K_{eff} values of ligands are decreased in the mutant R91A, although this effect is stronger for the agonist than the antagonist (Fig 3G). In the background of the mutant R91A, both nonactivatable mutants F116A and Y258A bind agonist and antagonist with similar K_{eff} as the single mutant R91A, thus emphasizing that the mutation has likely not affected ligand binding but instead interfered with channel activation (Fig 3H and 3I).

Mutation of a Conserved Salt Bridge

Similar to the phenylalanine in the β6-β7 loop, the mutation of an equally conserved aspartate in the same region (Asp122 in ELIC and Asp121 in GLIC) results in an apparent loss of activation in both proteins (Fig 2E and 2F). This residue is located just above the interface and forms

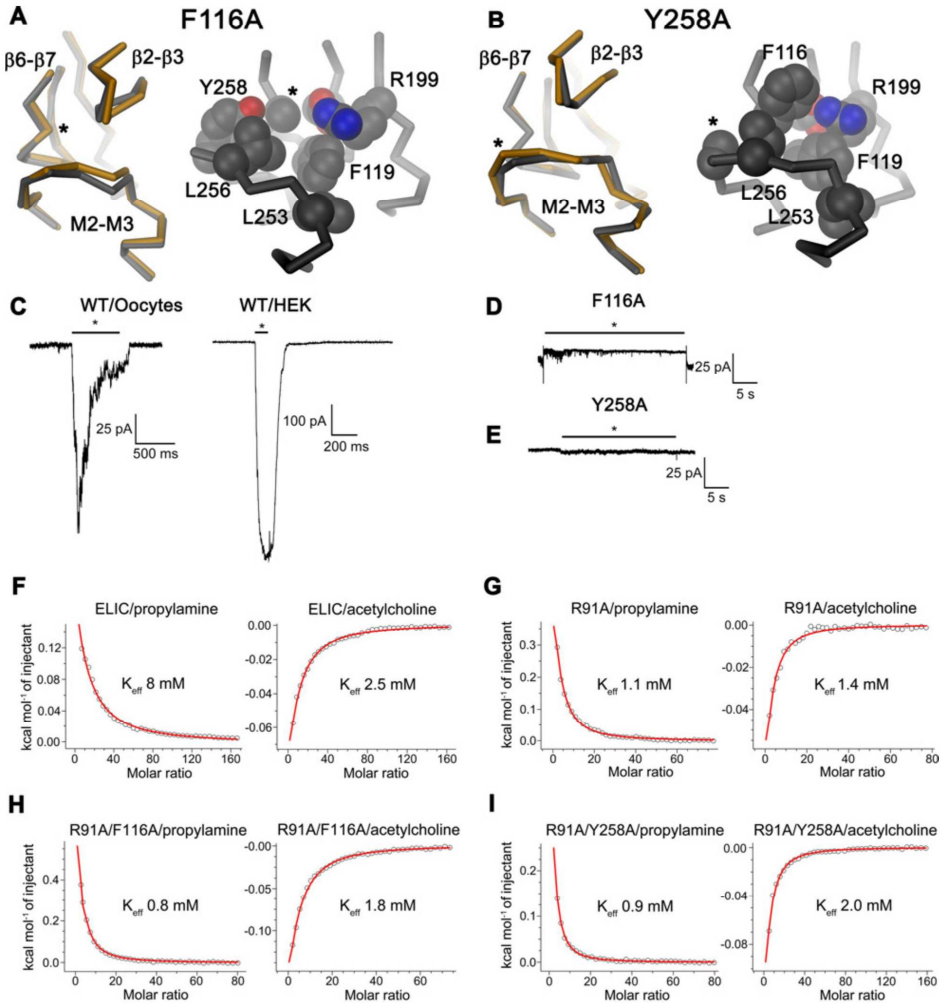

Fig 3. Characterization of two nonactivating mutants of ELIC. (A) Refined structure of the ELIC mutant F116A. Left, Cα-trace of part of a single subunit of F116A (grey) showing the domain interface superimposed on ELIC WT (orange). Right, interface of F116A with sidechains of selected residues shown as CPK models. View and selection are as in Fig 2A. (B) Analogous representation of the refined structure of the mutant Y258A. In A and B, the site of mutation is indicated by an asterisk. (C) Macroscopic currents recorded from representative patches of ELIC WT upon fast application and washout of agonist. Left, current response of a membrane patch of *X. laevis* oocytes expressing ELIC upon application of 20 mM cysteamine. Right, current recorded from a membrane patch of ELIC expressed in human embryonic kidney 293 (HEK293) cells upon application of 25 mM propylamine. The difference in magnitude of the currents is due to the higher expression of ELIC in HEK293 cells. (D) Representative current response of a membrane patch of the ELIC mutant F116A expressed in *X. laevis* oocytes upon application of 20 mM cysteamine. (E) Representative current response of a membrane patch of the ELIC mutant Y258A expressed in HEK293 cells upon application of 25 mM propylamine. C–E, Currents were recorded from excised patches in the outside-out configuration at a potential of −50 mV for HEK cell and −80 mV for *X. laevis* oocyte patches. Application of agonist by fast solution exchange is indicated by a black bar. (F–I), ITC experiments. Agonist and antagonist binding to (F), ELIC WT, (G), the ligand binding site mutant R91A, the double mutants (H), R91A/F116A and (I), R91A/Y258A. Graphs show a fit of the integrated and corrected heat upon addition of the agonist propylamine (left) and the antagonist acetylcholine (right) to a binding isotherm (red line). Experiments were repeated twice with similar results. (See S1 Data for the raw data used to generate plots shown in panels F–I).

doi:10.1371/journal.pbio.1002393.g003

a salt bridge with a conserved arginine (Arg199 in ELIC and Arg191 in GLIC) at the end of β-strand 10 at the boundary to the pore domain (Fig 4A and 4B and S3B Fig). The mutation of the respective arginine to alanine also causes a nonactivating phenotype in ELIC, whereas no expression of this mutant was observed in GLIC (Fig 2C–2F). In GLIC, Arg191 also interacts with Asp31 on β-strand 2, a position that, with respect to its negative charge, is conserved in many pLGIC subunits but not in ELIC where the respective residue is a threonine and the glutamate-gated chloride channel (GluCl) from *C. elegans* where it is a valine (S3B Fig). In GLIC, the mutant D31A is well expressed but shows no activity at pH4 (S2B Fig). In ELIC, the equivalent mutant T28A can be activated but with a 3.5-fold higher EC_{50} of agonist than WT (Fig 4C and S6A Fig). When mutating Thr28 in ELIC to aspartate, thereby introducing a negative charge that is present in many family members, the EC_{50} of channel activation shifts to a 45 times lower agonist concentration (18 μM, Fig 4C and S6B Fig). A similar increase in the affinity was observed in ITC experiments, where the agonist binds with a K_{eff} of 90 μM, a 90-fold decrease in concentration compared to WT, while the binding of the antagonist acetylcholine was unchanged (Fig 4D and S5E Fig). Patch clamp recordings already show considerable basal activity of this mutant in the absence of ligand and increased currents upon ligand application (Fig 4E), whereas no basal activity is observed in WT. The single channel conductance of the mutant is similar to WT, but the current density is lower in both two-electrode voltage clamp and patch clamp experiments (Fig 4E, S6B Fig). All experiments suggest that this mutant stabilizes a high affinity state with respect to ligand binding, and we were thus interested whether it would be sufficient to change the crystallization behavior and allow us to determine the structure of ELIC in a different conformation. While we succeeded in obtaining crystals of the T28D mutant in the same conditions, they exhibited poorer diffraction than WT and only allowed us to collect data at 4.5 Å in the absence and 9.5 Å in the presence of ligand (Table 1). The structures indicate that, despite the drastic impact on the potency of the ligand, the mutant crystallized in the familiar nonconducting conformation, which further underlines the stability of this state in a crystalline environment (S4C Fig). Collectively, our studies emphasize the importance of ionic interactions between three conserved residues located in the β1-β2 turn (GLIC Asp31, ELIC Thr28), the β6-β7 loop (GLIC Asp121, ELIC Asp122), and the pre-M1 region (GLIC Arg191, ELIC Arg199, Fig 4A and 4B) for channel activation and the stabilization of the open state.

The Contact Region between the β1-β2 Turn and the M2-M3 Loop

At the tip of the GLIC β1-β2 turn, immediately adjacent to Asp31, Lys32 interacts with a strictly conserved proline in the M2-M3 loop (Pro254 in ELIC and Pro246 in GLIC, Fig 5A and 5B). This interaction is also observed in the presumably open structures of GluCl, the GlyR, and the structures of a homopentameric $GABA_A$ receptor. Conversely, this interaction is not formed in the structures of ELIC, the ligand-free GluCl, the antagonist-bound GlyR and the structure of the 5-HT_3 receptor, where the contact is broken (S3C Fig). We thus suspected that this interaction might play an important role for the relay of conformational changes from the extracellular domain to the pore [14,28]. In all pLGICs of known structure, the interaction between the tip of the β1-β2 turn and the pore domain is mediated by the protein backbone, whereas the side chain of the respective residue points towards the channel lumen (Fig 5A and 5B and S3C Fig). In contrast to other residues in the interaction interface, this position is not conserved and contains a lysine in GLIC and the 5-HT_3 receptor and a hydrophobic amino acid in ELIC, GluCl and the $GABA_A$ receptor. When expressed in *X. laevis* oocytes, the respective alanine mutants in ELIC and GLIC can still be activated with similar EC_{50} values as the respective WT (Fig 5C and 5D, S6C and S6D Fig), although with a lower maximal current

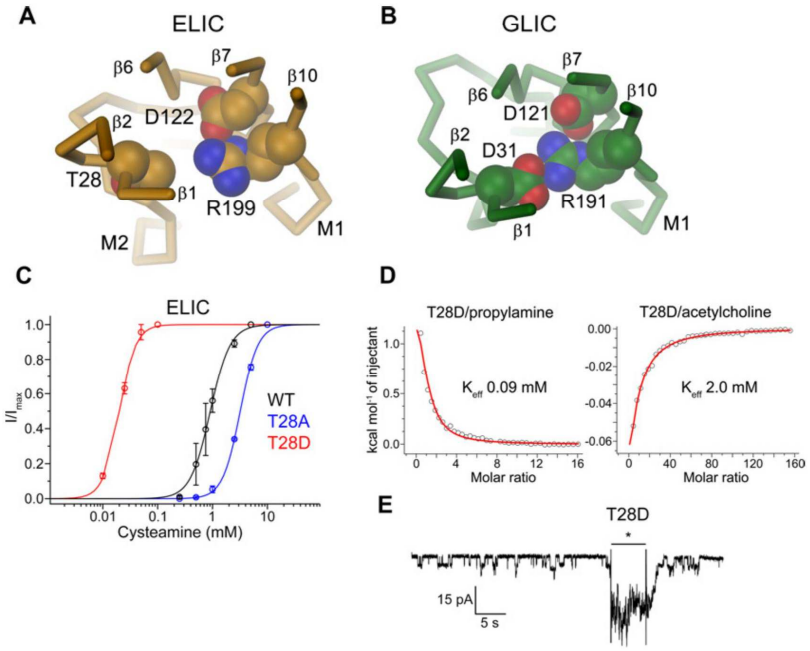

Fig 4. ELIC mutant with strongly increased potency for the agonist. Structure of the interaction region between the β1-β2 turn, a conserved arginine the end of β-10 and the β6-β7 loop in (A), ELIC and (B), GLIC. The view is from the extracellular side. Side-chains of selected residues forming a branched salt bridge in GLIC and their equivalent residues in ELIC are shown as CPK models. (C) Dose-response relationships of *X. laevis* oocytes expressing the ELIC mutants T28A and T28D measured by two-electrode voltage clamp electrophysiology. Current response of WT is shown for comparison. All currents were recorded at an outside Ca^{2+} concentration of 0.5 mM. Panels show averages of 4–6 independent measurements, solid lines show a fit to a Hill equation, errors are standard deviation (SD). (D) Agonist and antagonist binding to the ELIC mutant T28D as determined by ITC. Graphs show a fit of the integrated and corrected heat upon addition of the agonist propylamine (left) and the antagonist acetylcholine (right) to a binding isotherm (red line). (E) Patch clamp recording of the ELIC mutant T28D expressed in *X. laevis* oocytes. Currents were measured from excised patches in the outside-out configuration at –80 mV. Application of 20 mM cysteamine by fast solution exchange is indicated by a black bar. The recording shows considerable basal activity in the absence of the ligand. (See S1 Data for the raw data used to generate plots shown in panels C and D).

doi:10.1371/journal.pbio.1002393.g004

response (S2, S6C and S6D Figs). Remarkably, even a deletion mutant of L29 in ELIC showed a comparable activation pattern (Fig 5C and S6E Fig). Mutations of the conserved proline in the M2-M3 loop to alanine (P246A in GLIC and P254A in ELIC) resulted in channels that, apart from a small shift in the EC_{50} in the case of GLIC, show robust activation with similar properties as WT (Fig 5E and 5F, S6F and S6G Fig). In line with the comparably small effect in functional experiments, the crystal structure of the GLIC mutant P246A is virtually identical to WT (S7A and S7B Fig, Table 2). To avoid residual side chain interactions with the ligand-binding domain that may still be present after replacing the proline by alanine, we next investigated the mutation of the respective proline residue in both channels to glycine. In ELIC, the mutation P254G has a small but significant effect on the structure, which overall shows the frequently observed nonconducting conformation. The reorganization of the well-structured M2-M3 loop indicates a change in the conformational properties of this region (Fig 5G, S4D Fig, Table 2). The equivalent mutation P246G in GLIC results in large rearrangements when compared to WT. The structure determined at 3.2 Å shows a molecule with small differences

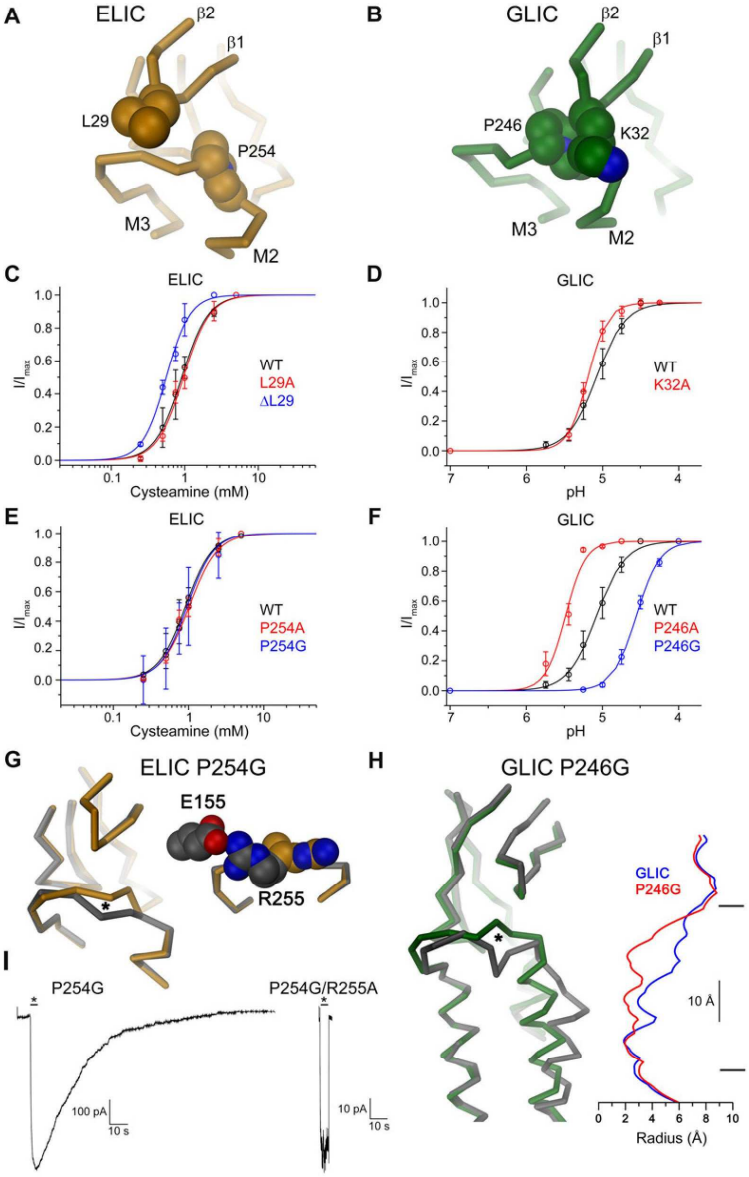

Fig 5. Interaction between the β1-β2 turn and the pore domain. Relationship between the residue at the tip of the β1-β2 turn and a conserved proline at the M2-M3 loop in (A), ELIC and (B), GLIC. The view is parallel to the membrane plane. Side chains of selected residues are shown as CPK models. (C–F), Dose-response relationships of *X. laevis* oocytes expressing mutants of either ELIC or GLIC measured by two-electrode voltage clamp electrophysiology.

Current response of the respective WT is shown for comparison. For ELIC, currents were recorded at an outside Ca^{2+} concentration of 0.5 mM. Panels show averages of 3–5 independent measurements, solid lines are a fit to a Hill equation, errors are SD. Mutants of the β1-β2 turn: (C), ELIC mutant L29A and the channel carrying a deletion of Leu29 (ΔL29). (D), GLIC mutant K32A. Mutants of the M2-M3 loop: (E), ELIC mutants P254A and P254G. (F), GLIC mutants P246A and P246G. For ELIC P254G, ligand was not removed following application due to the very slow deactivation of the channels. (G) Refined structure of the ELIC mutant P254G. Left, Cα-trace of part of a single subunit of P254G (grey) showing the domain interface superimposed on ELIC WT (orange). An asterisk marks the site of mutation. Right, structure of the M2-M3 loop of the mutant P254G and of WT with side chains of R255A and E155 from the adjacent subunit shown as CPK model. (H), Structure of the GLIC mutant P246G. Left, Cα-trace of part of a single subunit of P246G (grey) showing the domain interface and part of the pore region superimposed on GLIC WT (green). An asterisk marks the site of mutation. Right, Pore radius of GLIC (blue) and P246G (red) along the channel axis. The membrane boundary is indicated. (I) Macroscopic currents recorded from representative patches of the ELIC mutant P254G (left) and the double mutant P254G/R255A (right) upon fast application and washout of agonist. Currents were recorded from membrane patches of the respective ELIC mutants expressed in HEK293 cells in response to application of 25 mM propylamine. The difference in the deactivation rate in both mutants is apparent. (See S1 Data for the raw data used to generate plots shown in panels C-F).

doi:10.1371/journal.pbio.1002393.g005

throughout most of the protein except for the M2-M3 loop and the pore-lining helix M2, which both have undergone major conformational changes (Fig 5H, S7C Fig, Table 2). The introduced conformational freedom upon replacement of the restrained amino acid proline with the flexible glycine has resulted in the rearrangement of the M2-M3 loop and the unfolding of the C-terminal part of M2. The remainder of the helix has collapsed towards the pore axis as to maximize the hydrophobic interactions of residues at the extracellular part leading to a structure, which, most probably, prevents the permeation of ions (Fig 5H, S7D and S7E Fig). In contrast to the large conformational change in the extracellular part of the helix, its conformation at the intracellular half remained unchanged. Remarkably, this pore conformation is

Table 2. Data collection and refinement statistics 2.

	ELIC P254G	GLIC P246A	GLIC P246G
Data collection			
Space group	$P2_1$	C2	C2
Cell dimensions			
a, *b*, *c* (Å)	105.0, 266.6, 110.7	177.7, 133.9, 159.8	180.4, 134.2, 160.8
α, *β*, *γ* (°)	90.0, 109.3, 90.0	90.0, 101.1, 90.0	90.0, 102.0, 90.0
Resolution (Å)	50–3.3 (3.4–3.3)	50–3.3 (3.4–3.3)	50–3.2 (3.3–3.2)
R_{merge}*	11.5 (90.1)	10.1 (77.3)	12.2 (95.6)
$I / \sigma I$ *	12.2 (2.5)	13.1 (2.4)	9.3 (1.8)
Completeness (%) *	99.8 (99.8)	99.6 (99.6)	98.3 (82.8)
Redundancy *	5.4 (5.4)	5.3 (5.4)	4.4 (4.3)
Refinement			
Resolution (Å)	30–3.3	30–3.3	30–3.2
No. reflections	85,767	55,060	60,831
R_{work}/R_{free}	22.1/25.2	24.6/28.0	24.7/25.8
No. atoms			
Protein	25,020	12,595	12,590
Ligand/ion	-	-	-
B-factors			
Protein	109	97	101
Ligand/ion	-	-	-
R.m.s. deviations			
Bond lengths (Å)	0.003	0.003	0.004
Bond angles (°)	0.64	0.65	0.78

*Values in parentheses are for highest-resolution shell.

doi:10.1371/journal.pbio.1002393.t002

very similar to structures of GLIC obtained from cysteine crosslinking of residues at the domain interface, which were previously assigned to a locally closed conformation of the ion conduction path [33], the structures of two nonactivating mutants in the M2-M3 loop [34] and a recent structure of GLIC at neutral pH [20]. In this locally closed conformation, an interaction of a histidine residue in the pore-forming helix M2 with the backbone of the neighboring helix M3 established in the low pH crystal structure of GLIC is broken (S7F Fig). It is noteworthy that the histidine is in a position that in other family members of known structure is predominantly hydrophobic, and that it was previously proposed to be involved in the pH-dependent activation of GLIC [35,36].

Despite the strong impact of the mutation on the structure, both proteins can still be activated (Fig 5E and 5F, S6G–S6J Fig). When studied by two-electrode voltage clamp electrophysiology, the GLIC mutant P246G shows dose-dependent channel activation with an EC_{50} that is shifted by 0.5 pH units towards higher proton concentrations (Fig 5F and S6H Fig). In ELIC, the mutant P254G shows agonist-induced currents with a similar EC_{50} as WT but with a slower activation and an unusually slow deactivation of the channel upon washout of the ligand (Fig 5E, S6I Fig). This behavior can be observed in two-electrode voltage clamp recordings, where the activity of the protein after a change to ligand-free solution decays slowly (S6J Fig), and it becomes even more pronounced in macroscopic recordings of excised outside-out patches (Fig 5I, S8A–S8C Fig). The cause for this unusual deactivation phenotype was revealed in the structure of the P254G mutant of ELIC. In this structure, electron density between Arg255 on the M2-M3 loop and Glu155 located in the β8-β9 loop of the extracellular domain of an adjacent subunit indicates the formation of a strong ionic interaction that is absent in WT and that may stabilize the open conformation of the pore (Fig 5G, S4D Fig). In the background of the mutation R255A, the kinetics of channel deactivation of the P254G mutant becomes similar to WT, thus confirming the role of the interaction for the unusual functional behavior (Fig 5I and S8D Fig). The single mutation of R255A behaves similar to WT but shows faster activation and deactivation kinetics and an increased rate of desensitization (S8E–S8G Fig). Thus, to our surprise, the mutation of a conserved proline in the M2-M3 loop to glycine still promotes activation in both channels, ELIC and GLIC. These results are in contrast to the much more drastic effects that are observed in mutants of other residues at the domain interface, including several positions in the same region, where even the truncation of the side chain to alanine has apparently prevented channel activation.

Discussion

We have used a mutagenesis approach to investigate the role of the domain interface of two prokaryotic pLGICs for the transduction of conformational changes from the extracellular to the pore domain. Our study has revealed a pattern of corresponding residues in ELIC and GLIC that, if mutated to alanine, had a similar effect on either channel. Remarkably, whereas mutations in several positions have apparently prevented activation in both proteins, none of the investigated alanine mutations showed detectable basal activity in the absence of agonists. Our results suggest that the respective side chain truncations may have either stabilized a closed conformation of the channel, where the energy of ligand binding is no longer sufficient for activation, or alternatively, that they have interfered with the coupling of both domains and that the pore region that is uncoupled from the extracellular domain resides in a stable nonconducting conformation. In all cases, the mutations likely did not interfere with ligand binding but instead impeded gating, as suggested by calorimetry experiments of two nonactivating mutants of ELIC, which showed WT-like binding properties of agonists and antagonists (Fig 3H and 3I). In case of WT, the observed agonist binding affinity is lower than expected from

the EC_{50} value measured by electrophysiology [9] and instead matches the binding affinity to the resting state obtained from single channel analysis [29] (Fig 3F). It thus appears that in detergent solution, ELIC resides in a single conformation that, with respect to ligand binding, resembles a resting state. Assuming that the conformation that is probed by calorimetry is also observed in the crystal, since in both cases the protein is solubilized in the same detergent, it is unlikely that the structure of ELIC represents a desensitized state with high affinity for the ligand. The conformational rigidity of solubilized ELIC is in accordance with the fact that all currently available structures show the same nonconducting conformation of the protein, irrespectively of whether agonist is bound or mutations were introduced that have stabilized the open state as it is the case for the mutations T28D or P254G. This behavior is in line with previous observations for ELIC [9,37]. Additionally, a reduced conformational freedom in detergent solution was observed in an electron paramagnetic resonance (EPR) spectroscopy study of GLIC [38], which suggests that both proteins may require a lipid environment for full activation. Whereas the predominantly local effects of most mutations, which modulate the open to closed equilibrium of the channel, resembles the behavior of eukaryotic receptors [39], the mutation of a conserved proline (Pro254) to glycine in ELIC resulted in the formation of novel interactions between residues apart from the site of mutation that were not present in WT, causing an unusual functional phenotype that would have been difficult to explain in the absence of structure (Fig 5G).

Our studies show that mutations with a nonactivating phenotype predominantly cluster in two regions of the protein, the β6-β7 loop of the extracellular domain and the M2-M3 loop of the pore. The results are in accordance with a previous investigation of two mutations in the M2-M3 loop of GLIC [34], and they overall mirror the functional behavior of eukaryotic pLGICs [40–43]. Differences between pro- and eukaryotic channels may originate from an altered energetic relationship between distinct states, and effects may generally be less pronounced if mutations only concern one or two subunits of a heteropentameric receptor. An early study has identified a mutation in the M2-M3 loop of the homopentameric α7 nAChR, which prevents activation but not ligand binding [44]. A similar phenotype was found for a mutation of the equivalent residue of the GlyR causing Startle disease, as well as by an additional mutation located two residues upstream [45]. Based on these observations, an involvement of the M2-M3 loop in gating has been proposed [44–46]. Similarly, our study has shown that mutations of the corresponding positions in the two prokaryotic channels (T248A, Y250A in GLIC and L256A, Y258A in ELIC) have interfered with activation but not ligand binding, as suggested by the calorimetry experiments of the ELIC mutant Y258A. The same region was also investigated in the hetero-pentameric muscle nAChR. Based on the effect of mutations on the equilibrium and kinetics of the open to closed transition, a prominent role of the M2-M3 loop of the α-subunits on the activation of the channel was postulated, but in this case the positions with the strongest phenotype differ from the residues identified in this study [39,47,48]. Whereas the kinetics of ELIC and GLIC is comparably slow [9,29,49], we found that the point mutation R255A in the M2-M3 loop of ELIC not only accelerated activation and deactivation but also increased the rate of desensitization (S8E–S8G Fig). In that respect, it is interesting to note that alanine is found in the same position of the fast desensitizing α7 nAChR and that a mutation of the corresponding residue of the GlyR causes Startle disease [50]. Since in a different study the domain interface was shown to influence the desensitization rate of homomeric pLGICs [51], it appears that the same region determines activation and desensitization of the channels.

Like the M2-M3 loop, the β6-β7 loop of eukaryotic pLGICs has also been proposed to play a critical role in channel activation. Mutations in equivalent positions that interfered with activation in both prokaryotic channels decreased the agonist response of the α1 GlyR and abolished

the potentiation of currents by general anesthetics [52]. In a different study, the activation in chimeras of the α7 nAChR and the GlyR was enhanced by point mutations of residues of the β6-β7 loop that are in equivalent positions as nonactivating mutants in ELIC and GLIC [53]. A strong effect of mutations on the gating equilibrium constant was also found in the α-subunit of the nAChR [39,43,47], and strong energetic coupling of two conserved phenylalanines of the β6-β7 loop to the M2-M3 loop was proposed based on mutant cycle analysis [54].

In ELIC and GLIC, a nonactivating phenotype was found for mutations of a conserved aspartate of the β6-β7 loop (Asp122 in ELIC and Asp121 in GLIC) that interacts with an equally conserved arginine in the pre-M1 region (Arg199 in ELIC and Arg191 in GLIC). Mutations of the corresponding aspartate also interfered with activation in the nAChR [43,55], the 5-HT_3 receptor [56] or the GlyR [57]. In GLIC, the pre-M1 arginine bridges the β6-β7 loop with the β1-β2 turn by interaction with a negatively-charged residue (Asp31) that is found in most pLGIC subunits (Fig 6A, S3B Fig). The mutation of this residue to alanine prevents activation of GLIC, whereas the mutation of a threonine residing at the equivalent position in ELIC (T28A) appears to remain functional, although with decreased potency of the agonist (Fig 4C, S2 Fig). The role of this interaction in channel activation and the destabilization of the resting state is underlined by a mutation of the respective threonine to aspartate in ELIC, which strongly increases the potency for the agonist and where the channel shows increased basal activity, which is not observed in WT (Fig 4). This basal activity demonstrates that ELIC can, in principle, also open in the absence of agonist and thus underlines the validity of the MWC model also for this channel. Equivalent ionic interactions have previously been investigated in the nAChR and other pLGICs [54–56,58,59]. In one study, they were postulated to be part of a molecular pathway that plays an important role in the relay of signals from the extracellular domain to the pore region, thereby connecting ligand binding to gating [54,59]. Since similar but smaller effects were found in a different study, the central importance of this ionic interaction for channel activation was questioned [58], and it was instead proposed that the total charge of the interface rather than specific pairwise interactions may govern channel activation in the nAChR [55]. Contrary to our previous expectation [14,28], conformational changes appear not to be predominantly transduced via an interaction of the tip of the β1-β2 turn to a conserved proline in the M2-M3 loop of the pore domain (Pro254 in ELIC and Pro246 in GLIC), as mutations of this residue to alanine and glycine still permit channel activation. This is remarkable since the equivalent proline was proposed to play a prominent role in the early events of gating in the nAChR [39,48], and since in several structures of different pLGICs assigned to potentially open conformations, this interaction is present, whereas it is broken in presumably nonconducting conformations (S3C Fig). A coupling of the β1-β2 turn to a proline of the M2-M3 linker in the nAChR was previously proposed based on a model of the receptor from electron microscopy data at 4 Å [10,54,59]. However, due to a mismatch in the structural interpretation of this region, this position does not coincide with the residue investigated in this study.

The structures of different pLGICs at high resolution [12–21] provide a framework for the comprehension of the results of this study. With respect to the transmembrane domain, most known structures cluster around three distinct conformations: A presumably conducting state of the pore, which has initially been observed for a low pH crystal form of GLIC [14,15], is shared by GluCl and the GlyR in complex with their agonists and the allosteric modulator ivermectin [12,16], as well as the $GABA_A$ receptor [17] (S9 Fig). It is still debated whether these structures correspond to conducting, partially conducting, or even desensitized states [22]. A structure of the GlyR in complex with glycine has a larger pore diameter at the intracellular part of the transmembrane domain but shares a very similar pattern of interactions at the domain interface [16]. Conformations resembling the nonconducting state of ELIC were later

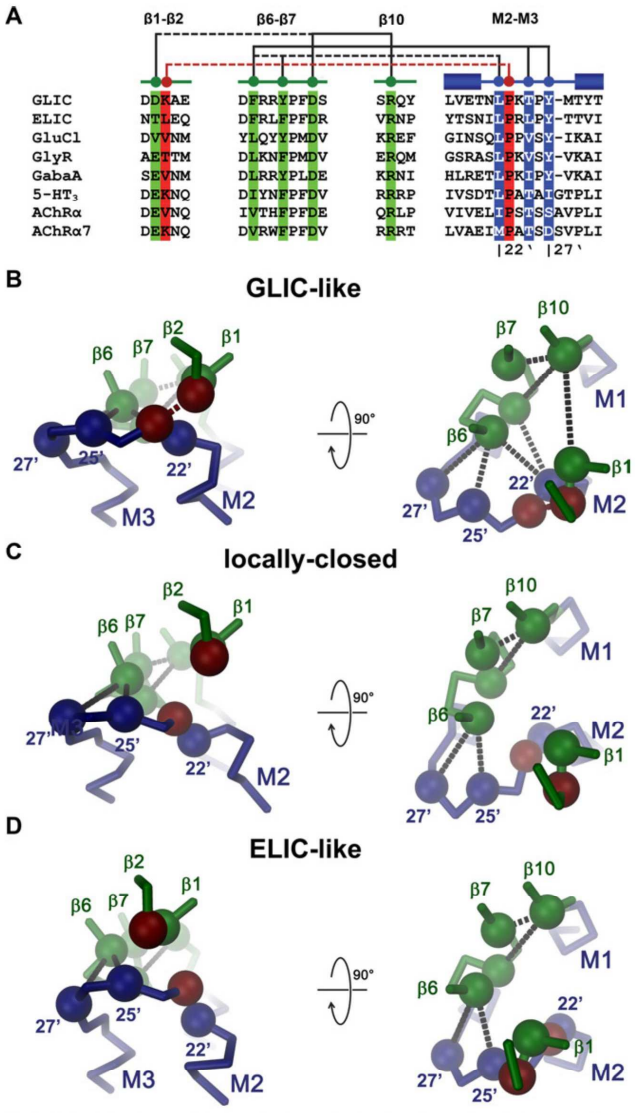

Fig 6. Role of the domain interface in channel activation. Interactions between residues at the domain interface in different channel conformations. (A) Sequence alignment of regions of the domain interface. Selected residues and their interactions are highlighted and schematically depicted above. Solid lines indicate interactions that are present in all conformations and dashed line interactions that are only formed in the presumably open GLIC-like conformation. Numbering below the sequences indicates the position of residues in the pore. Sequences are GLIC (UniProt: Q7NDN8), ELIC (GB: WP_013319743), GluCl (GB: AAA50785.1), GlyR (GB: NP_571477.1), $Gaba_A$ (GB: M82919), 5-HT3 (GB: NM_001099644.1), AChRα

(UniProt: P04756), AChRα7 (UniProt: P49582). Cα-trace of the interface of a single subunit of (B) GLIC in a presumably open conformation (GLIC-like), (C) GLIC at pH 7.0 (locally-closed), (D) ELIC (ELIC-like). The view is from within the membrane (left) and from the extracellular side (right). The pore domain is colored in blue and the extracellular domain in green. The positions of selected residues whose mutation exerts a strong effect on activation in ELIC and GLIC are shown as spheres. The residue at the tip of the β1-β2 turn and a conserved proline in the M2-M3 loop are colored in red. Selected interactions (as in A) are indicated by dashed lines.

doi:10.1371/journal.pbio.1002393.g006

observed for GluCl crystallized in the absence of ortho- and allosteric agonists, a conformation of the ligand-free protein in complex with a bound lipid [19], and for the GlyR bound to its competitive antagonist strychnine [12,21] (S9 Fig). This is remarkable in light of the controversy concerning the relationship of the ELIC structure to a resting conformation of the receptor [22,37,38,60]. The structure of the 5-HT_3 receptor is in between the two previously described states but closer to the GLIC-like conformation [18] (S9 Fig). Another distinct nonconducting conformation of the pore region was observed in a high pH crystal form of GLIC [20] and in several mutants of the same channel [33,34], including the structure of the mutant P246G determined in this study (S9 Fig). This third conformation has thus far only been observed in GLIC, a member of the family that is activated by protons, and it remains to be shown whether a similar conformation of the pore region can also be adopted by other family members. The fact that side chains that are truncated in nonactivating mutants point into a common core suggests that the mutation may have disrupted a critical interaction (Fig 2A and 2B and S3A Fig). These interactions appear to be most extended in the presumably open GLIC-like conformations (Fig 2A and Fig 6). In these cases, the interface between the extracellular domain and the pore region is tightly packed, residues from the M2-M3 loop are in close contact with residues of the β6-β7 loop, and in several structures a negatively charged residue in the β1-β2 turn interacts with a conserved arginine in the pre-M1 region and an equally conserved proline in the M2-M3 loop (Fig 6A and 6B, S3B and S3C Fig). This network is partially disrupted in the two nonconducting conformations, which might explain why several mutations in the interaction interface stabilize a closed state of the channel. In the locally-closed high pH structure of GLIC, the distance between the β1-β2 turn and the arginine in the pre-M1 region has increased and, due to a change of the conformation of the M2-M3 loop leading to a collapse of the pore-forming helix M2, the contact to the proline in the respective region is broken (Fig 6C, S3C Fig). This conformational change also causes an interruption of interactions between residues in the N-terminal part of the M2-M3 loop with the β6-β7 loop, whereas the interactions of the residues in the region preceding M3 appear less affected (Fig 6C). In the ELIC-like conformations, a similar pattern of interactions is observed, but in this case, the disruption of interdomain contacts is due to a concerted move of helices M2 and M3 while preserving the conformation of the M2-M3 loop (Fig 6D). The accompanying rearrangement of the β1-β2 turn of the extracellular domain weakens its interaction with the pre-M1 region and disrupts the contact to the proline in the M2-M3 loop. In both nonconducting conformations, the interactions with the C-terminal part of the M2-M3 loop with the β6-β7 linker remain intact, and the observed nonactivating phenotype of respective mutations (F116A and Y258A in ELIC and F115A and Y250A in GLIC) could thus originate from an interruption of the coupling between the extracellular domain and the pore region.

Despite the plethora of structural information, definitive assignments of observed conformations to functional states of the receptors and the resulting activation mechanisms are still controversial [22]. It is thus interesting to observe that, regardless of the difference of agonists, highly conserved and closely interacting residues at the domain interface of ELIC and GLIC exert similar effects on activation in both prokaryotic ion channels. Critical interactions involve

residues of the M2-M3 loop, the pre-M1 region and the β1-β2 turn that all contact the β6-β7 loop, whereas a direct interaction between the β1-β2 turn and the M2-M3 loop appears expendable. As in eukaryotic receptors, mutations at the interface predominantly affect the close to open equilibrium of the pore. Our results thus suggest that there is a common pathway for signal transduction in both proteins that, regardless of differences in the detailed energetic relationships between pro- and eukaryotic receptors, appears to be conserved within the entire family.

Materials and Methods

Expression Constructs

All expression constructs were cloned into vectors that were modified to be compatible with FX cloning [61]. For expression in *X. laevis* oocytes, WT and mutant open reading frames of ELIC and GLIC preceded by the signal sequence of the chicken α7 nAChR were cloned into a modified pTLN vector [62]. For surface expression analysis, the constructs contained an additional hemagglutinin-tag (HA-tag) attached to the N-terminus of the respective protein. For expression in human embryonic kidney 293 (HEK293) cells, the respective genes preceded by the signal sequence of the chicken α7 nAChR were cloned into a modified pcDNA3.1 vector (Invitrogen). For expression and purification in *E. coli*, the respective genes were cloned into a modified pET26b vector (Novagen) as constructs of the respective channels preceded by a fusion protein consisting of a pelB signal sequence, a His_{10}-tag, maltose-binding protein and a human rhinovirus (HRV) 3C protease cleavage site.

Two-Electrode Voltage Clamp Recording and Surface Expression Analysis in *Xenopus* Oocytes

X. laevis oocytes were obtained either from Ecocyte or from an in-house facility. Animal procedures and preparation of oocytes followed standard procedures and were in accordance with the Swiss Cantonal and Federal legislation relating to animal experimentation. Plasmid DNA containing the genes coding for the respective constructs for expression in *X. laevis* oocytes were linearized by MluI, and capped mRNA was transcribed with the mMessage mMachine kit (Ambion) and purified with the RNeasy kit (Qiagen). 10–200 ng of mRNA was injected into defolliculated *X. laevis* oocytes, which were subsequently incubated in Barth's solution (88 mM NaCl, 1 mM KCl, 1 mM $CaCl_2$, 0.33 mM $Ca(NO_3)_2$, 0.82 mM $MgSO_4$, 10 mM Na-Hepes (pH 7.4) and 50 μg / ml Gentamycin) and stored at 16°C. One to three days after injection, two-electrode voltage clamp measurements were performed at 20°C (OC-725B, Warner Instrument Corp.). For ELIC, maximal currents were recorded in a bath solution containing 10 mM Hepes (pH 7), 130 mM NaCl, 2 mM KCl, 0.5 mM $CaCl_2$ and either 5 mM or 25 mM Cysteamine. For GLIC, the maximal currents were recorded in a bath solution containing 10 mM Citrate (pH 4), 130 mM NaCl, 2 mM KCl, 1.8 mM $CaCl_2$ and 1 mM $MgCl_2$. Dose-response experiments were carried out at agonist concentrations indicated in the respective figures. Voltage was clamped at −40 mV, and data was filtered at 20 Hz unless stated otherwise. Surface expression in constructs containing an HA-tag was assayed after electrophysiological characterization as described [63]. For that purpose, the oocytes were placed in a 96-well plate (TPP) and incubated in ND96 solution (93.5 mM NaCl, 2 mM KCl, 1.8 mM $CaCl_2$, 2 mM $MgCl_2$ and 10 mM Hepes, pH 7.4) containing 1% BSA for at least 30 min. All steps were carried out at 4°C with the same buffer unless mentioned otherwise. Oocytes were subsequently transferred into buffer containing 1 μg/ml rat monoclonal anti-HA antibody (3F10, Roche) for 1 h, washed 3 times and incubated with buffer containing 0.16 μg/ml horseradish peroxidase (HRP) coupled to a

secondary antibody (HRP-conjugated goat anti-rat F(Ab)2 fragments, Jackson) for 30–60 min. The oocytes were washed 5 times with ND96 solution and subsequently transferred to a white 96-well plate (flat bottom, Nunclon Delta Surface). The solution was aspirated, 30 μl of Super Signal ELISA femto solutions 1 and 2 (Pierce) was added, and luminescence was quantitated with a Tecan infinite M1000 plate reader.

Patch Clamp Recording in *X*. oocytes

X. laevis oocytes were transferred to a hyperosmotic solution to manually remove the vitelline layer. Excised membrane patches were subsequently recorded in the outside-out configuration 3–5 d after injection of mRNA with an Axopatch 200B amplifier (Axon Instruments) at 20°C at −80 mV. Data was sampled at 20 kHz and filtered at 2 kHz and analyzed using Clampfit (Axon Instruments, Inc.). Bath solutions contained 10 mM HEPES, pH 7.0, 150 mM NaCl, 0.2 mM $CaCl_2$ and indicated concentrations of ligands. Electrodes had a resistance of 3–5 MΩ. Pipette solutions contained 150 mM NaCl, 10 mM EGTA, 5 mM $MgCl_2$ and 10 mM HEPES, pH 7.0. Bath electrodes were placed in 1 M KCl solution connected to the bath solution by Agar bridges. Freshly prepared agonist solutions were applied to the patch using a stepper motor (SF77B Perfusion fast step, Warner).

Patch Clamp Recording in HEK293 Cells

HEK293 cells (American Type Culture Collection-CRL-1573;LGC Promochem) were maintained at 37°C in a 95% air/5% CO_2 incubator in DMEM supplemented with 0.11 g/l sodium pyruvate, 10% (v/v) heat-inactivated fetal bovine serum, 100 U/ml penicillin G, 100 μg/ml streptomycin sulfate, and 2 mM L-glutamine (Invitrogen). Cells (passaged every 2 d, up to 30 times) were plated and transfected by calcium phosphate-DNA coprecipitation [64], with a total amount of DNA of 3 μg/dish (82% ELIC and 18% eGFP DNA, both subcloned in pcDNA3.1). Cells were bathed in an extracellular solution containing 150 mM KCl, 0.2 mM $CaCl_2$ and 10 mM HEPES, pH 7.4. Patch pipettes were pulled from thick-walled borosilicate glass (GC150F; Harvard Apparatus) and fire polished to a resistance of 8–12 MΩ. Intracellular solution contained 150 mM KCl, 0.5 mM $CaCl_2$, 5 mM EGTA and 10 mM HEPES, pH 7.4. Agonist-evoked currents were recorded at 20°C with an Axopatch 200B amplifier (Molecular Devices) from outside-out patches at −50 mV. No correction for junction potential was applied (calculated value 0.2 mV). Data was sampled at 10 kHz and filtered at 1 kHz and analyzed using Clampfit (Axon Instruments, Inc.). All concentration jumps were performed using a piezo stepper (Siskiyou) with an application tool made from theta tube glass (Hilgenberg; final tip diameter, 150 μm). Agonist solutions were freshly prepared before measurements.

Protein Expression and Purification

ELIC WT and point mutants were expressed and purified as described [9,13]. BL21-DE3 cells transformed with a pET26b vector carrying the respective expression constructs of ELIC were grown in M9 minimal medium containing 50 mg/l kanamycin at 37°C to an OD_{600} of 1.0 and subsequently cooled to 20°C. Expression was induced by addition of 0.2 mM IPTG and carried out overnight. BL21-DE3 cells transformed with a pET26b vector carrying the respective expression constructs of GLIC were grown at 37°C in TB medium containing 50 mg/l kanamycin to an OD_{600} of 1.6–1.8. Expression was induced by addition of 0.2 mM IPTG overnight at 20°C. All following steps were performed at 4°C. ELIC was extracted from isolated membranes in a buffer containing 1% n-Undecyl-β-D-Maltoside (UDM, Anatrace, Inc.) and further purified in buffers containing 0.145% UDM. GLIC was extracted from isolated membranes in a buffer containing 1% n-Dodecyl-β-D-Maltoside (DDM, Anatrace, Inc.) and further purified in

buffers containing 0.044% DDM. Both proteins were purified by Ni-NTA chromatography (Qiagen) and digested with HRV 3C protease to cleave the His_{10}-MBP fusion tag. His_{10}-MBP and 3C protease were subsequently removed from solution by binding to Ni-NTA resin and the flow-through was concentrated and subjected to gel-filtration on a Superdex 200 column (GE Healthcare). The protein peak corresponding to the ELIC pentamer was pooled, concentrated to 10 mg/ml and used for crystallization and ITC. The protein peak corresponding to the GLIC pentamer was pooled and concentrated to 10 mg/ml, and used for crystallization.

Crystallization and Structure Determination

Both proteins were crystallized in sitting drops at 4°C as described [9,13]. ELIC containing additional 0.5 mg/ml *E. coli* polar lipids (Avanti Polar Lipids, Inc.) was mixed in a 1:1 ratio with reservoir solution composed of 200 mM $(NH_4)_2SO_4$, 50 mM ADA, pH 6.5 and 10%–13% (w/v) PEG4000. GLIC containing additional 0.5 mg/ml *E. coli* polar lipids was in mixed in a 1:1 ratio with reservoir solution composed of 225 mM $(NH_4)_2SO_4$, 50 mM sodium acetate, pH 4.0 and 9%–12% (w/v) PEG 4000. The crystals were cryoprotected by transfer into solutions containing additional 30% ethylene glycol. All data sets were collected on frozen crystals on the X06SA beamline at the Swiss Light Source (SLS) of the Paul Scherrer Institute (PSI) on a PILATUS detector (Dectris). The data were indexed, integrated, and scaled with XDS [65] and further processed with CCP4 programs [66] (Tables 1 and 2). The structure of mutants was determined by molecular replacement in PHASER [67] using either the ELIC pentamer in a $P4_3$ crystal form (2YN6) or the GLIC pentamer (3EHZ) as search model. The models were rebuilt in Coot [68] and refined maintaining strong NCS restraints in PHENIX [69]. R and R_{free} were monitored throughout. R_{free} was calculated by selecting 5% of the reflection data in thin slices that were selected for the initial datasets of ELIC and GLIC and that were omitted in refinement. For low resolution data of the ELIC mutant T28D, refinement was restricted to rigid body refinement followed by few cycles of restrained positional and group b-factor refinement. The pore radii were calculated with HOLE [70].

ITC

Binding of the agonist propylamine and the antagonist acetylcholine to ELIC was measured by ITC with a MicroCal ITC200 system (GE Healthcare). The syringe was loaded with agonist solution containing between 30–37 mM propylamine or acetylcholine dissolved in measurement buffer (25 mM Hepes, pH 7.0, 150 mM NaCl and 0.9 mM UDM). The sample cell was loaded with 300 μl of purified ELIC in measurement buffer at a concentration between 80–110 μM. Agonist was applied by sequential injections of 2 μl aliquots followed by a 180 s equilibration period after each injection. The data was recorded at 4°C. For analysis, the heat released by each injection was integrated, and the background was subtracted with NITPIC [71]. The background-corrected data was analyzed by a fit to a single-site binding isotherm with the Origin ITC analysis package. ITC experiments were performed at least twice for each protein, with similar results.

Supporting Information

S1 Data. Numerical data used in preparation of Figs 2C, 2D, 3F, 3G, 3H, 3I, 4C, 4D, 5C, 5D, 5E, 5F, S2A, S2B, S6B, S6E, S6H, S6J, S8G and S9D.
(XLSX)

S1 Fig. View of the domain interface. Stereo view of the domain interface of ELIC (A) and GLIC (B). The view is from within the pore parallel to the membrane plane. The respective

proteins are displayed as Cα-trace, residues mutated in this study as sticks. Carbon atoms of different regions are shown in unique colors as indicated on the bottom. Selected secondary structure elements are labeled; apostrophes refer to adjacent subunit.
(TIF)

S2 Fig. Surface expression and agonist response of alanine mutants. Surface expression levels of alanine mutants of ELIC (A) and GLIC (B) determined by ELISA. Values are averages of 4–6 experiments. Background from empty oocytes was subtracted and signal was normalized to WT. Errors are SEM. The protein sequence is indicated above each chart with nonactivating mutations colored in red. The residue number of selected residues is indicated. Current response at high agonist concentration (ELIC: 25 mM cysteamine, GLIC: pH 4) of representative oocytes expressing the indicated mutants are shown above the respective chart for ELIC and below for GLIC. Currents were either recorded at −40 mV or scaled to the expected value at −40 mV assuming a linear macroscopic conductance. (See S1 Data for the raw data used to generate plots shown in panels A and B).
(TIF)

S3 Fig. Interactions at the domain interface. Important interactions at the domain interface in pLGICs of known structure. Top row shows nonconducting conformations, bottom row shows putative conducting conformations or related structures. Interface region of a single subunit is displayed as Cα trace with selected side chains shown as CPK models. (A) Interaction between residues that, upon mutation to alanine, prevent channel activation in ELIC and GLIC. The view is as in Fig 2A. (B) Interaction region between the β1-β2 turn, a conserved arginine at the end of β-10 and the β6-β7 loop. The view is as in Fig 4A. (C). Relationship between the residue at the tip of the β1-β2 turn and a conserved proline at the M2-M3 loop. The view is as in Fig 5A. A–C, figures were prepared with Protein Data Bank entries GLIC pH7 (4NPQ), ELIC (2VL0), GluCl (without agonist, 4TNV), GLYRs (strychnine complex, 3JAD), GLIC (3EHZ), $GABA_A$ (4COF), GluClgi (glutamate and ivermectin complex, 3RIF), GlyRgi (glycine and ivermectin complex, 3JAF), and 5-HT_3 (4PIR).
(TIF)

S4 Fig. Electron density of ELIC mutants. (A) Stereo view of the domain interface of the ELIC mutant F116A. $2F_o–F_c$ electron density (calculated at 3.5 Å and contoured at 1σ, cyan mesh) is shown superimposed on the refined structure. (B) Stereo view of the domain interface of the ELIC mutant Y258A. $2F_o–F_c$ electron density (calculated at 3.2 Å and contoured at 1σ, cyan mesh) is shown superimposed on the refined structure. (C) Structure of the ELIC mutant T28D. Left, Cα-trace of a subunit with $2F_o–F_c$ electron density (calculated at 4.5 Å and contoured at 1σ, blue mesh) superimposed. Center, view of the domain interface of the mutant T28D. A stick representation of the model and electron density are shown. Right, Cα-trace of part of the subunit of T28D surrounding the domain interface (grey) is superimposed on WT (orange). (D) Stereo view of the domain interface of the ELIC mutant P254G. $2F_o–F_c$ electron density (calculated at 3.3 Å and contoured at 1σ, cyan mesh) is shown superimposed on the refined structure. Residues forming a salt bridge that is absent in WT are labeled. A–D, sites of mutation are marked by an asterisk.
(TIF)

S5 Fig. ITC. Agonist and antagonist binding to (A) ELIC WT, (B), the ligand-binding site mutant R91A, the double mutants (C), R91A/F116A and (D), R91A/Y258A, and (E), the mutant T28D as determined by ITC. Top graphs show the uncorrected heat exchanged upon addition of the agonist propylamine (left) and the antagonist acetylcholine (right). Bottom graphs show the background (bg) from titrating propylamine (left) or acetylcholine (right) into

buffer solution not containing any protein. A fit of the integrated and corrected heat to a binding isotherm is shown in Fig 3F–3I. Experiments were repeated twice with similar results.
(TIF)

S6 Fig. Two-electrode voltage clamp electrophysiology. Current response of representative *X. laevis* oocytes expressing selected mutants of either ELIC or GLIC at different agonist concentrations. Currents were recorded at −40 mV unless specified otherwise. A bar indicates agonist application. Agonist concentrations (cysteamine in mM for ELIC and pH for GLIC) are shown above. (A) ELIC T28A (recorded at −60 mV), (B), ELIC T28D (recorded at −60 mV), (C), GLIC K32A (recorded at −80 mV), (D), ELIC L29A, (E), ELIC L29 deletion, (F), GLIC P246A, (G), ELIC P254A, (−80 mV), (H), GLIC P246G (−60 mV), (I), ELIC P254G, (−60 mV), (J), comparison of ELIC WT and P254G (both −60 mV). Surface expression of the respective mutants is shown on the right of panels B, E, H and J. Data show averages of at least five different oocytes and are normalized to WT. Background was subtracted. Errors are SEM. (See S1 Data for the raw data used to generate plots shown in panels B, E, H and J).
(TIF)

S7 Fig. X-ray structures of GLIC mutants of Pro246. (A) Stereo view of the domain interface of the GLIC mutant P246A. $2F_o–F_c$ electron density (calculated at 3.3 Å and contoured at 1σ, cyan mesh) is shown superimposed on the refined structure. (B) Cα-trace of residues at the domain interface of P246A (grey) superimposed on GLIC WT (green). (C) Stereo view of the domain interface of the GLIC mutant P246G. $2F_o–F_c$ electron density (calculated at 3.2 Å and contoured at 1σ, cyan mesh) is shown superimposed on the refined structure. A–C, an asterisk marks the site of mutation. (D) Superposition of Cα traces of the pore forming M2 helices of P246G (grey) and GLIC WT (green). (E) Transmembrane pore of GLIC WT (left) and P246G (right). Helices M2 are shown as sticks, the molecular surface in white. In D and E, the front subunits are omitted for clarity. (F) Region of P246G surrounding His234 (*), which was proposed to play a role in channel activation. Left, structure with $2F_o–F_c$ electron density superimposed. Right, superposition of the same regions of P246G (grey) and WT (green). A dashed line indicates the interaction between His234 (located on M2) and the backbone of helix M3 in WT.
(TIF)

S8 Fig. Kinetic analysis of patch clamp recordings. ELIC WT and mutants were expressed in HEK293 cells. Macroscopic currents recorded from representative excised patches in the outside-out configuration upon fast application and washout of 25 mM propylamine are shown. Application of agonist is indicated by a blue bar. Data was recorded at −50 mV. Time course of current activation and decay was fitted to a single exponential (red traces). Full traces are shown on the left, sections used for fitting in the center and on the right. (A) WT activation and deactivation. Traces in the center and on the right show a fit of the activation and deactivation time constants respectively. (B) WT, desensitization upon prolonged agonist application. Trace on the right shows a fit of the desensitization time constant. (C) P254G, (D), P254G/R255A, (E), R255A, activation and deactivation. Traces in the center and on the right show a fit of the activation and deactivation time constants. (F) R255A, desensitization upon prolonged agonist application. Trace on the right shows a fit of the desensitization time constant. (G) Table displaying the mean and SEM of time constants of 4–8 independent recordings. (See S1 Data for the raw data used to generate this table).
(TIF)

S9 Fig. Relationships between pLGICs of known structure. Superposition of subunits of different pLGICs of known structure. Proteins were assigned to one of three distinct groups: (A),

GLIC-like conformations, (B), ELIC-like conformations and (C), locally closed or collapsed pore conformations found in a structure of GLIC at pH 7 and in certain mutants of the same channel. A–C, panels show Cα traces of the pore domain and the domain interface from a single subunit of the respective channels. PDB entries are as in S3 Fig. Additional structures shown are GluCl (lipid complex, 4TNW), GlyRg (glycine complex, 3JAE) and GLIC Y250A (4LMK). Structural relationships of helices M2 and M3 within each group are schematically illustrated on the right, the pore axis is indicated by a dashed line. An asterisk in A indicates M2. (D) RMSD of the pore region calculated after least square superposition of equivalent Cα positions in helices M1, M2, and M3 in pentameric structures of different pLGICs. (See S1 Data for the raw data used to generate the plot shown in panel D).
(TIF)

Acknowledgments

We thank the staff of the X06SA beamline for support during data collection, E. Hänsenberger for preparation of *X. laevis* oocytes and members of the Dutzler lab for help in all stages of the project. Data collection was performed at the X06SA beamline at the SLS of the PSI.

Author Contributions

Conceived and designed the experiments: CB IZ SE RJCH RD. Performed the experiments: CB IZ SE RJCH. Analyzed the data: CB IZ SE RJCH RD. Wrote the paper: CB IZ SE RD.

References

1. Taly A, Corringer PJ, Guedin D, Lestage P, Changeux JP. Nicotinic receptors: allosteric transitions and therapeutic targets in the nervous system. Nat Rev Drug Discov. 2009; 8(9):733–50. PMID: 19721446. doi: 10.1038/nrd2927
2. Sine SM, Engel AG. Recent advances in Cys-loop receptor structure and function. Nature. 2006; 440 (7083):448–55. PMID: 16554804.
3. Karlin A. On the application of "a plausible model" of allosteric proteins to the receptor for acetylcholine. J Theor Biol. 1967; 16(2):306–20. PMID: 6048545.
4. Edelstein SJ, Changeux JP. Allosteric transitions of the acetylcholine receptor. Adv Protein Chem. 1998; 51:121–84. PMID: 9615170.
5. Auerbach A. Thinking in cycles: MWC is a good model for acetylcholine receptor-channels. J Physiol. 2012; 590(Pt 1):93–8. doi: 10.1113/jphysiol.2011.214684 PMID: 21807612.
6. Tasneem A, Iyer LM, Jakobsson E, Aravind L. Identification of the prokaryotic ligand-gated ion channels and their implications for the mechanisms and origins of animal Cys-loop ion channels. Genome Biol. 2005; 6(1):R4. PMID: 15642096.
7. Lester HA, Dibas MI, Dahan DS, Leite JF, Dougherty DA. Cys-loop receptors: new twists and turns. Trends Neurosci. 2004; 27(6):329–36. PMID: 15165737.
8. Bocquet N, Prado de Carvalho L, Cartaud J, Neyton J, Le Poupon C, Taly A, et al. A prokaryotic proton-gated ion channel from the nicotinic acetylcholine receptor family. Nature. 2007; 445(7123):116–9. PMID: 17167423.
9. Zimmermann I, Dutzler R. Ligand activation of the prokaryotic pentameric ligand-gated ion channel ELIC. PLoS Biol. 2011; 9(6):e1001101. Epub 2011/06/30. doi: 10.1371/journal.pbio.1001101 PMID: 21713033.
10. Unwin N. Refined structure of the nicotinic acetylcholine receptor at 4A resolution. J Mol Biol. 2005; 346 (4):967–89. PMID: 15701510.
11. Miyazawa A, Fujiyoshi Y, Unwin N. Structure and gating mechanism of the acetylcholine receptor pore. Nature. 2003; 423(6943):949–55. PMID: 12827192.
12. Du J, Lu W, Wu S, Cheng Y, Gouaux E. Glycine receptor mechanism elucidated by electron cryo-microscopy. Nature. 2015; 526(7572):224–9. doi: 10.1038/nature14853 PMID: 26344198.
13. Hilf RJ, Dutzler R. X-ray structure of a prokaryotic pentameric ligand-gated ion channel. Nature. 2008; 452(7185):375–9. PMID: 18322461. doi: 10.1038/nature06717

14. Hilf RJ, Dutzler R. Structure of a potentially open state of a proton-activated pentameric ligand-gated ion channel. Nature. 2009; 457(7225):115–8. PMID: 18987630. doi: 10.1038/nature07461

15. Bocquet N, Nury H, Baaden M, Le Poupon C, Changeux JP, Delarue M, et al. X-ray structure of a pentameric ligand-gated ion channel in an apparently open conformation. Nature. 2009; 457(7225):111–4. PMID: 18987633. doi: 10.1038/nature07462

16. Hibbs RE, Gouaux E. Principles of activation and permeation in an anion-selective Cys-loop receptor. Nature. 2011; 474(7349):54–60. PMID: 21572436. doi: 10.1038/nature10139

17. Miller PS, Aricescu AR. Crystal structure of a human GABAA receptor. Nature. 2014; 512(7514):270–5. doi: 10.1038/nature13293 PMID: 24909990.

18. Hassaine G, Deluz C, Grasso L, Wyss R, Tol MB, Hovius R, et al. X-ray structure of the mouse serotonin 5-HT3 receptor. Nature. 2014; 512(7514):276–81. doi: 10.1038/nature13552 PMID: 25119048.

19. Althoff T, Hibbs RE, Banerjee S, Gouaux E. X-ray structures of GluCl in apo states reveal a gating mechanism of Cys-loop receptors. Nature. 2014; 512(7514):333–7. doi: 10.1038/nature13669 PMID: 25143115.

20. Sauguet L, Shahsavar A, Poitevin F, Huon C, Menny A, Nemecz A, et al. Crystal structures of a pentameric ligand-gated ion channel provide a mechanism for activation. Proc Natl Acad Sci U S A. 2014; 111(3):966–71. doi: 10.1073/pnas.1314997111 PMID: 24367074.

21. Huang X, Chen H, Michelsen K, Schneider S, Shaffer PL. Crystal structure of human glycine receptor-alpha3 bound to antagonist strychnine. Nature. 2015; 526(7572):277–80. doi: 10.1038/nature14972 PMID: 26416729.

22. daCosta CJ, Baenziger JE. Gating of pentameric ligand-gated ion channels: structural insights and ambiguities. Structure. 2013; 21(8):1271–83. doi: 10.1016/j.str.2013.06.019 PMID: 23931140.

23. Nury H, Bocquet N, Le Poupon C, Raynal B, Haouz A, Corringer PJ, et al. Crystal Structure of the Extracellular Domain of a Bacterial Ligand-Gated Ion Channel. J Mol Biol. 2009. PMID: 19917292.

24. Dellisanti CD, Yao Y, Stroud JC, Wang ZZ, Chen L. Crystal structure of the extracellular domain of nAChR alpha1 bound to alpha-bungarotoxin at 1.94 A resolution. Nat Neurosci. 2007; 10(8):953–62. PMID: 17643119.

25. Bondarenko V, Tillman T, Xu Y, Tang P. NMR structure of the transmembrane domain of the n-acetylcholine receptor beta2 subunit. Biochim Biophys Acta. 2010; 1798(8):1608–14. doi: 10.1016/j.bbamem.2010.04.014 PMID: 20441771.

26. Sixma TK, Smit AB. Acetylcholine binding protein (AChBP): a secreted glial protein that provides a high-resolution model for the extracellular domain of pentameric ligand-gated ion channels. Annu Rev Biophys Biomol Struct. 2003; 32:311–34. PMID: 12695308.

27. Bouzat C, Gumilar F, Spitzmaul G, Wang HL, Rayes D, Hansen SB, et al. Coupling of agonist binding to channel gating in an ACh-binding protein linked to an ion channel. Nature. 2004; 430(7002):896–900. PMID: 15318223.

28. Hilf RJ, Dutzler R. A prokaryotic perspective on pentameric ligand-gated ion channel structure. Curr Opin Struct Biol. 2009; 19(4):418–24. PMID: 19646860. doi: 10.1016/j.sbi.2009.07.006

29. Marabelli A, Lape R, Sivilotti L. Mechanism of activation of the prokaryotic channel ELIC by propylamine: a single-channel study. J Gen Physiol. 2015; 145(1):23–45. doi: 10.1085/jgp.201411234 PMID: 25548135.

30. Zimmermann I, Marabelli A, Bertozzi C, Sivilotti LG, Dutzler R. Inhibition of the prokaryotic pentameric ligand-gated ion channel ELIC by divalent cations. PLoS Biol. 2012; 10(11):e1001429. doi: 10.1371/journal.pbio.1001429 PMID: 23185134.

31. Hilf RJ, Bertozzi C, Zimmermann I, Reiter A, Trauner D, Dutzler R. Structural basis of open channel block in a prokaryotic pentameric ligand-gated ion channel. Nat Struct Mol Biol. 2010; 17(11):1330–6. PMID: 21037567. doi: 10.1038/nsmb.1933

32. Pan J, Chen Q, Willenbring D, Yoshida K, Tillman T, Kashlan OB, et al. Structure of the pentameric ligand-gated ion channel ELIC cocrystallized with its competitive antagonist acetylcholine. Nat Commun. 2012; 3:714. Epub 2012/03/08. doi: 10.1038/ncomms1703 PMID: 22395605.

33. Prevost MS, Sauguet L, Nury H, Van Renterghem C, Huon C, Poitevin F, et al. A locally closed conformation of a bacterial pentameric proton-gated ion channel. Nat Struct Mol Biol. 2012; 19(6):642–9. doi: 10.1038/nsmb.2307 PMID: 22580559.

34. Gonzalez-Gutierrez G, Cuello LG, Nair SK, Grosman C. Gating of the proton-gated ion channel from Gloeobacter violaceus at pH 4 as revealed by X-ray crystallography. Proc Natl Acad Sci U S A. 2013; 110(46):18716–21. doi: 10.1073/pnas.1313156110 PMID: 24167270.

35. Wang HL, Cheng X, Sine SM. Intramembrane proton binding site linked to activation of bacterial pentameric ion channel. J Biol Chem. 2012; 287(9):6482–9. doi: 10.1074/jbc.M111.305839 PMID: 22084238.

36. Rienzo M, Lummis SC, Dougherty DA. Structural requirements in the transmembrane domain of GLIC revealed by incorporation of noncanonical histidine analogs. Chem Biol. 2014; 21(12):1700–6. doi: 10.1016/j.chembiol.2014.10.019 PMID: 25525989.

37. Gonzalez-Gutierrez G, Lukk T, Agarwal V, Papke D, Nair SK, Grosman C. Mutations that stabilize the open state of the Erwinia chrisanthemi ligand-gated ion channel fail to change the conformation of the pore domain in crystals. Proc Natl Acad Sci U S A. 2012. Epub 2012/04/05. doi: 10.1073/pnas.1119268109 PMID: 22474383.

38. Dellisanti CD, Ghosh B, Hanson SM, Raspanti JM, Grant VA, Diarra GM, et al. Site-directed spin labeling reveals pentameric ligand-gated ion channel gating motions. PLoS Biol. 2013; 11(11):e1001714. doi: 10.1371/journal.pbio.1001714 PMID: 24260024.

39. Purohit P, Gupta S, Jadey S, Auerbach A. Functional anatomy of an allosteric protein. Nat Commun. 2013; 4:2984. doi: 10.1038/ncomms3984 PMID: 24352193.

40. Bartos M, Corradi J, Bouzat C. Structural basis of activation of cys-loop receptors: the extracellular-transmembrane interface as a coupling region. Mol Neurobiol. 2009; 40(3):236–52. doi: 10.1007/s12035-009-8084-x PMID: 19859835.

41. Kash TL, Jenkins A, Kelley JC, Trudell JR, Harrison NL. Coupling of agonist binding to channel gating in the GABA(A) receptor. Nature. 2003; 421(6920):272–5. PMID: 12529644.

42. Shen XM, Ohno K, Tsujino A, Brengman JM, Gingold M, Sine SM, et al. Mutation causing severe myasthenia reveals functional asymmetry of AChR signature cystine loops in agonist binding and gating. J Clin Invest. 2003; 111(4):497–505. PMID: 12588888.

43. Chakrapani S, Bailey TD, Auerbach A. Gating dynamics of the acetylcholine receptor extracellular domain. J Gen Physiol. 2004; 123(4):341–56. doi: 10.1085/jgp.200309004 PMID: 15051806.

44. Campos-Caro A, Sala S, Ballesta JJ, Vicente-Agullo F, Criado M, Sala F. A single residue in the M2-M3 loop is a major determinant of coupling between binding and gating in neuronal nicotinic receptors. Proc Natl Acad Sci U S A. 1996; 93(12):6118–23. PMID: 8650229.

45. Lynch JW, Rajendra S, Pierce KD, Handford CA, Barry PH, Schofield PR. Identification of intracellular and extracellular domains mediating signal transduction in the inhibitory glycine receptor chloride channel. EMBO J. 1997; 16(1):110–20. doi: 10.1093/emboj/16.1.110 PMID: 9009272.

46. Grosman C, Salamone FN, Sine SM, Auerbach A. The extracellular linker of muscle acetylcholine receptor channels is a gating control element. J Gen Physiol. 2000; 116(3):327–40. PMID: 10962011.

47. Jha A, Cadugan DJ, Purohit P, Auerbach A. Acetylcholine receptor gating at extracellular transmembrane domain interface: the cys-loop and M2-M3 linker. J Gen Physiol. 2007; 130(6):547–58. PMID: 18040057.

48. Bafna PA, Purohit PG, Auerbach A. Gating at the mouth of the acetylcholine receptor channel: energetic consequences of mutations in the alphaM2-cap. PLoS One. 2008; 3(6):e2515. doi: 10.1371/journal.pone.0002515 PMID: 18575616.

49. Laha KT, Ghosh B, Czajkowski C. Macroscopic kinetics of pentameric ligand gated ion channels: comparisons between two prokaryotic channels and one eukaryotic channel. PLoS ONE. 2013; 8(11):e80322. doi: 10.1371/journal.pone.0080322 PMID: 24260369.

50. Lewis TM, Sivilotti LG, Colquhoun D, Gardiner RM, Schoepfer R, Rees M. Properties of human glycine receptors containing the hyperekplexia mutation alpha1(K276E), expressed in Xenopus oocytes. J Physiol. 1998; 507 (Pt 1):25–40. PMID: 9490812.

51. Bouzat C, Bartos M, Corradi J, Sine SM. The interface between extracellular and transmembrane domains of homomeric Cys-loop receptors governs open-channel lifetime and rate of desensitization. J Neurosci. 2008; 28(31):7808–19. doi: 10.1523/JNEUROSCI.0448-08.2008 PMID: 18667613.

52. Schofield CM, Trudell JR, Harrison NL. Alanine-scanning mutagenesis in the signature disulfide loop of the glycine receptor alpha 1 subunit: critical residues for activation and modulation. Biochemistry. 2004; 43(31):10058–63. PMID: 15287733.

53. Grutter T, de Carvalho LP, Dufresne V, Taly A, Edelstein SJ, Changeux JP. Molecular tuning of fast gating in pentameric ligand-gated ion channels. Proc Natl Acad Sci U S A. 2005; 102(50):18207–12. doi: 10.1073/pnas.0509024102 PMID: 16319224.

54. Lee WY, Free CR, Sine SM. Binding to gating transduction in nicotinic receptors: Cys-loop energetically couples to pre-M1 and M2-M3 regions. J Neurosci. 2009; 29(10):3189–99. doi: 10.1523/JNEUROSCI.6185-08.2009 PMID: 19279256.

55. Xiu X, Hanek AP, Wang J, Lester HA, Dougherty DA. A unified view of the role of electrostatic interactions in modulating the gating of Cys loop receptors. J Biol Chem. 2005; 280(50):41655–66. doi: 10.1074/jbc.M508635200 PMID: 16216879.

56. Price KL, Millen KS, Lummis SC. Transducing agonist binding to channel gating involves different interactions in 5-HT3 and GABAC receptors. J Biol Chem. 2007; 282(35):25623–30. doi: 10.1074/jbc.M702524200 PMID: 17606617.

57. Absalom NL, Lewis TM, Kaplan W, Pierce KD, Schofield PR. Role of charged residues in coupling ligand binding and channel activation in the extracellular domain of the glycine receptor. J Biol Chem. 2003; 278(50):50151–7. doi: 10.1074/jbc.M305357200 PMID: 14525990.

58. Purohit P, Auerbach A. Acetylcholine receptor gating at extracellular transmembrane domain interface: the "pre-M1" linker. J Gen Physiol. 2007; 130(6):559–68. PMID: 18040058.

59. Lee WY, Sine SM. Principal pathway coupling agonist binding to channel gating in nicotinic receptors. Nature. 2005; 438(7065):243–7. PMID: 16281039.

60. Velisetty P, Chalamalasetti SV, Chakrapani S. Structural basis for allosteric coupling at the membrane-protein interface in Gloeobacter violaceus ligand-gated ion channel (GLIC). J Biol Chem. 2014; 289 (5):3013–25. doi: 10.1074/jbc.M113.523050 PMID: 24338475.

61. Geertsma ER, Dutzler R. A versatile and efficient high-throughput cloning tool for structural biology. Biochemistry. 2011; 50(15):3272–8. doi: 10.1021/bi200178z PMID: 21410291.

62. Lorenz C, Pusch M, Jentsch TJ. Heteromultimeric CLC chloride channels with novel properties. Proc Natl Acad Sci U S A. 1996; 93(23):13362–6. PMID: 8917596.

63. Zerangue N, Schwappach B, Jan YN, Jan LY. A new ER trafficking signal regulates the subunit stoichiometry of plasma membrane K(ATP) channels. Neuron. 1999; 22(3):537–48. PMID: 10197533.

64. Groot-Kormelink PJ, Beato M, Finotti C, Harvey RJ, Sivilotti LG. Achieving optimal expression for single channel recording: a plasmid ratio approach to the expression of alpha 1 glycine receptors in HEK293 cells. J Neurosci Methods. 2002; 113(2):207–14. PMID: 11772442.

65. Kabsch W. Automatic Processing of Rotation Diffraction Data from Crystals of Initially Unknown Symmetry and Cell Constants. J Appl Cryst. 1993; 26(6):795–800.

66. CCP4. Collaborative Computational Project Nr. 4. The CCP4 Suite: Programs for X-ray crystallography. Acta Crystallogr D. 1994; 50:760–3. PMID: 15299374

67. McCoy RWG-K A. J., Adams P. D., Winn M. D., Storoni L.C. and Read R.J. Phaser crystallographic software. J Appl Cryst. 2007; 40:658–74

68. Emsley P, Lohkamp B, Scott WG, Cowtan K. Features and development of Coot. Acta Crystallogr D Biol Crystallogr. 2010; 66(Pt 4):486–501. PMID: 20383002. doi: 10.1107/S0907444910007493

69. Adams PD, Grosse-Kunstleve RW, Hung LW, Ioerger TR, McCoy AJ, Moriarty NW, et al. PHENIX: building new software for automated crystallographic structure determination. Acta Crystallogr D Biol Crystallogr. 2002; 58(Pt 11):1948–54. PMID: 12393927.

70. Smart OS, Neduvelil JG, Wang X, Wallace BA, Sansom MS. HOLE: a program for the analysis of the pore dimensions of ion channel structural models. J Mol Graph. 1996; 14(6):354–60, 76. PMID: 9195488.

71. Keller S, Vargas C, Zhao H, Piszczek G, Brautigam CA, Schuck P. High-precision isothermal titration calorimetry with automated peak-shape analysis. Anal Chem. 2012; 84(11):5066–73. doi: 10.1021/ac3007522 PMID: 22530732.

Curriculum Vitae

Name	Engeler
First Name	Sibylle
Date of Birth	19. Januar 1986
Place of Origin	Aadorf (TG)
Nationality	Swiss

Education

2000 – 2005	**Kantonsschule Romanshorn, Switzerland**
	Kantonale Matura
2005 – 2008	**University of Zurich, Switzerland**
	Bachelor of Science in Biochemistry (Biology Track)
2008 – 2009	**University of Zurich, Switzerland**
	Master of Science in Biochemistry (Biology Track)
	Master thesis at the Institute of Biochemistry in the group of Prof. Dr. Markus Grütter.
	Title of the Master thesis: The Caspase-8 Prodomain
2010	**University of Zurich, Switzerland**
	Scientific Assistant at the Institute of Biochemistry in the group of Prof. Dr. Markus Grütter, under supervision of Prof. Dr. Markus Seeger
2011 – 2016	**University of Zurich, Switzerland**
	PhD Student at the Institute of Biochemistry in the group of Prof. Dr. Raimund Dutzler
	Title of the PhD thesis: Structural and Functional Analysis of Procaryotic Pentameric Ligand-Gated Ion Channels

Publications

Design, construction, and characterization of a second-generation DARP in library with reduced hydrophobicity.
Seeger MA, Zbinden R, Flütsch A, Gutte PG, Engeler S, Roschitzki-Voser H, Grütter MG. Protein Science, Sept. 2013, 1239-57

Signal Transduction at the Domain Interface of Prokaryotic Pentameric Ligand-Gated Ion Channels.
Bertozzi C, Zimmermann I, Engeler S, Hilf RJ, Dutzler R, PLoS Biology, Mar. 2016

Bibliography

1. Pereda, A.E., *Electrical synapses and their functional interactions with chemical synapses.* Nat Rev Neurosci, 2014. **15**(4): p. 250-263.
2. Bennett, M.V.L., *Electrical synapses, a personal perspective (or history).* Brain Research Reviews, 2000. **32**(1): p. 16-28.
3. Bennett, M.V.L. and R.S. Zukin, *Electrical Coupling and Neuronal Synchronization in the Mammalian Brain.* Neuron, 2004. **41**(4): p. 495-511.
4. Goodenough, D.A. and D.L. Paul, *Gap Junctions.* Cold Spring Harbor Perspectives in Biology, 2009. **1**(1): p. a002576.
5. Li, Z. and S.K. Nair, *Quorum sensing: How bacteria can coordinate activity and synchronize their response to external signals?* Protein Science, 2012. **21**(10): p. 1403-1417.
6. Bandara, H.M.H.N., et al., *Microbial chemical signaling: a current perspective.* Critical Reviews in Microbiology, 2012. **38**(3): p. 217-249.
7. Sheng, M., B. Sabatini, and T.C. Südhof, *Synapses and Alzheimer's disease.* Cold Spring Harbor perspectives in biology, 2012. **4**(5): p. 10.1101/cshperspect.a005777 a005777.
8. Schofield, P.R., et al., *Sequence and functional expression of the GABAA receptor shows a ligand-gated receptor super-family.* Nature, 1987. **328**(6127): p. 221-227.
9. Sine, S.M. and A.G. Engel, *Recent advances in Cys-loop receptor structure and function.* Nature, 2006. **440**(7083): p. 448-455.
10. Hibbs, R.E. and E. Gouaux, *Principles of activation and permeation in an anion-selective Cys-loop receptor.* Nature, 2011. **474**(7349): p. 54-60.
11. Brejc, K., et al., *Crystal structure of an ACh-binding protein reveals the ligand-binding domain of nicotinic receptors.* Nature, 2001. **411**(6835): p. 269-276.
12. Changeux1, J.-P., *The Nicotinic Acetylcholine Receptor: The Founding Father of the Pentameric Ligand-gated Ion Channel Superfamily.* J Biol Chem, 2012.
13. Taly, A. and J.-P. Changeux, *Functional Organization and Conformational Dynamics of the Nicotinic Receptor.* Annals of the New York Academy of Sciences, 2008. **1132**(1): p. 42-52.
14. Hertling-Jaweed, S., et al., *Rapid preparation of the nicotinic acetylcholine receptor for crystallization in detergent solution.* FEBS Letters, 1988. **241**(1–2): p. 29-32.
15. Paas, Y., et al., *Electron microscopic evidence for nucleation and growth of 3D acetylcholine receptor microcrystals in structured lipid–detergent matrices.* Proceedings of the National Academy of Sciences of the United States of America, 2003. **100**(20): p. 11309-11314.
16. Padilla-Morales, L.F., et al., *Effects of Lipid-Analog Detergent Solubilization on the Functionality and Lipidic Cubic Phase Mobility of the Torpedo californica Nicotinic Acetylcholine Receptor.* The Journal of membrane biology, 2011. **243**(1-3): p. 47-58.
17. Cheng, H., et al., *Crystallization scale purification of [alpha]7 nicotinic acetylcholine receptor from mammalian cells using a BacMam expression system.* Acta Pharmacol Sin, 2015. **36**(8): p. 1013-1023.
18. Smit, A.B., et al., *A glia-derived acetylcholine-binding protein that modulates synaptic transmission.* Nature, 2001. **411**(6835): p. 261-268.
19. Hansen, S.B., et al., *Structures of Aplysia AChBP complexes with nicotinic agonists and antagonists reveal distinctive binding interfaces and conformations.* The EMBO Journal, 2005. **24**(20): p. 3635-3646.
20. Patrick H N Celie, I.E.K., Dmitry Y Mordvintsev, Ronald C Hogg, Pim van Nierop, René van Elk, Sarah E van Rossum-Fikkert, Maxim N Zhmak, Daniel Bertrand, Victor Tsetlin, Titia K Sixma & August B Smit, *Crystal structure of nicotinic acetylcholine receptor homolog AChBP in complex with an alpha-conotoxin PnIA variant.* Nature Structural & Molecular Biology 2005.
21. Dellisanti, C.D., et al., *Crystal structure of the extracellular domain of nAChR alpha1 bound to alpha-bungarotoxin at 1.94 A resolution.* Nat Neurosci, 2007. **10**(8): p. 953-62.

22. Billen, B., et al., *Molecular actions of smoking cessation drugs at α4β2 nicotinic receptors defined in crystal structures of a homologous binding protein.* Proceedings of the National Academy of Sciences of the United States of America, 2012. **109**(23): p. 9173-9178.
23. Unwin, N., *Refined structure of the nicotinic acetylcholine receptor at 4A resolution.* J Mol Biol, 2005. **346**(4): p. 967-89.
24. Tasneem, A., et al., *Identification of the prokaryotic ligand-gated ion channels and their implications for the mechanisms and origins of animal Cys-loop ion channels.* Genome Biol, 2005. **6**(1): p. R4.
25. Gonzalez-Gutierrez, G. and C. Grosman, *Bridging the gap between structural models of nicotinic-receptor superfamily ion channels and their corresponding functional states.* Journal of molecular biology, 2010. **403**(5): p. 693-705.
26. Hilf, R.J. and R. Dutzler, *Structure of a potentially open state of a proton-activated pentameric ligand-gated ion channel.* Nature, 2009. **457**(7225): p. 115-8.
27. Bocquet, N., et al., *X-ray structure of a pentameric ligand-gated ion channel in an apparently open conformation.* Nature, 2009. **457**(7225): p. 111-4.
28. Sauguet, L., et al., *Structural basis for ion permeation mechanism in pentameric ligand - gated ion channels.* The EMBO Journal, 2013. **32**(5): p. 728-741.
29. Velisetty, P. and S. Chakrapani, *Desensitization Mechanism in Prokaryotic Ligand-gated Ion Channel.* The Journal of Biological Chemistry, 2012. **287**(22): p. 18467-18477.
30. Parikh, R.B., M. Bali, and M.H. Akabas, *Structure of the M2 Transmembrane Segment of GLIC, a Prokaryotic Cys Loop Receptor Homologue from Gloeobacter violaceus, Probed by Substituted Cysteine Accessibility.* The Journal of Biological Chemistry, 2011. **286**(16): p. 14098-14109.
31. Nury, H., et al., *X-ray structures of general anaesthetics bound to a pentameric ligand-gated ion channel.* Nature, 2011. **469**(7330): p. 428-431.
32. Hilf, R.J. and R. Dutzler, *X-ray structure of a prokaryotic pentameric ligand-gated ion channel.* Nature, 2008. **452**(7185): p. 375-9.
33. Miller, P.S. and A.R. Aricescu, *Crystal structure of a human GABAA receptor.* Nature, 2014. **512**(7514): p. 270-5.
34. Hassaine, G., et al., *X-ray structure of the mouse serotonin 5-HT3 receptor.* Nature, 2014. **512**(7514): p. 276-81.
35. Prevost, M.S., et al., *A locally closed conformation of a bacterial pentameric proton-gated ion channel.* Nat Struct Mol Biol, 2012. **19**(6): p. 642-649.
36. Sauguet, L., et al., *Crystal structures of a pentameric ligand-gated ion channel provide a mechanism for activation.* Proc Natl Acad Sci U S A, 2014. **111**(3): p. 966-71.
37. Althoff, T., et al., *X-ray structures of GluCl in apo states reveal a gating mechanism of Cys-loop receptors.* Nature, 2014. **512**(7514): p. 333-7.
38. Du, J., et al., *Glycine receptor mechanism elucidated by electron cryo-microscopy.* Nature, 2015. **526**(7572): p. 224-229.
39. daCosta, C.J. and J.E. Baenziger, *Gating of pentameric ligand-gated ion channels: structural insights and ambiguities.* Structure, 2013. **21**(8): p. 1271-83.
40. Zimmermann, I. and R. Dutzler, *Ligand activation of the prokaryotic pentameric ligand-gated ion channel ELIC.* PLoS Biol, 2011. **9**(6): p. e1001101.
41. Bocquet, N., et al., *A prokaryotic proton-gated ion channel from the nicotinic acetylcholine receptor family.* Nature, 2007. **445**(7123): p. 116-9.
42. Lee, W.Y. and S.M. Sine, *Principal pathway coupling agonist binding to channel gating in nicotinic receptors.* Nature, 2005. **438**(7065): p. 243-7.
43. Lee, W.Y., C. Free, and S.M. Sine, *Binding to gating transduction in nicotinic receptors: Cys-loop energetically couples to pre-M1 and M2-M3 regions.* The Journal of neuroscience : the official journal of the Society for Neuroscience, 2009. **29**(10): p. 3189-3199.
44. Bouzat, C., et al., *Coupling of agonist binding to channel gating in an ACh-binding protein linked to an ion channel.* Nature, 2004. **430**(7002): p. 896-900.

45. Katz, B. and S. Thesleff, *A study of the `desensitization' produced by acetylcholine at the motor end-plate.* The Journal of Physiology, 1957. **138**(1): p. 63-80.
46. J, D.C. and B. Katz, *Interaction at end-plate receptors between different choline derivatives.* 1956.
47. Monod, J., J. Wyman, and J.-P. Changeux, *On the nature of allosteric transitions: A plausible model.* Journal of Molecular Biology, 1965. **12**(1): p. 88-118.
48. Ochoa EL, C.A., McNamee MG., *Desensitization of the nicotinic acetylcholine receptor: molecular mechanisms and effect of modulators.* Cell Mol Neurobiol., 1989.
49. Keramidas, A. and J. Lynch, *An outline of desensitization in pentameric ligand-gated ion channel receptors.* Cellular and Molecular Life Sciences, 2013. **70**(7): p. 1241-1253.
50. Corringer, P.-J., et al., *Critical Elements Determining Diversity in Agonist Binding and Desensitization of Neuronal Nicotinic Acetylcholine Receptors.* The Journal of Neuroscience, 1998. **18**(2): p. 648-657.
51. Kinde, Monica N., et al., *Conformational Changes Underlying Desensitization of the Pentameric Ligand-Gated Ion Channel ELIC.* Structure, 2015. **23**(6): p. 995-1004.
52. Hilf, R.J. and R. Dutzler, *A prokaryotic perspective on pentameric ligand-gated ion channel structure.* Curr Opin Struct Biol, 2009. **19**(4): p. 418-24.
53. Sennhauser, G., et al., *Drug Export Pathway of Multidrug Exporter AcrB Revealed by DARPin Inhibitors.* PLoS Biology, 2007. **5**(1): p. e7.
54. Seeger, M.A., et al., *Tuning the Drug Efflux Activity of an ABC Transporter in vivo by in vitro Selected DARPin Binders.* PLoS ONE, 2012. **7**(6): p. e37845.
55. Hino, T., et al., *G-protein-coupled receptor inactivation by an allosteric inverse-agonist antibody.* Nature, 2012. **482**(7384): p. 237-240.
56. Sennhauser, G. and M.G. Grütter, *Chaperone-Assisted Crystallography with DARPins.* Structure, 2008. **16**(10): p. 1443-1453.
57. Mittal, A., et al., *Asymmetry in the Homodimeric ABC Transporter MsbA Recognized by a DARPin.* The Journal of Biological Chemistry, 2012. **287**(24): p. 20395-20406.
58. Finlay WJ, A.J., *Natural and man-made V-gene repertoires for antibody discovery.* Front Immunology, 2012.
59. Foote, J. and G. Winter, *Antibody framework residues affecting the conformation of the hypervariable loops.* Journal of Molecular Biology, 1992. **224**(2): p. 487-499.
60. Abhinandan, K.R. and A.C.R. Martin, *Analysis and prediction of VH/VL packing in antibodies.* Protein Engineering Design and Selection, 2010. **23**(9): p. 689-697.
61. Alberts B, J.A., Lewis J, et al., *Molecular Biology of the Cell. B Cells and Antibodies.* 2002. **4th edition**.
62. De Genst, E., et al., *Antibody repertoire development in camelids.* Developmental & Comparative Immunology, 2006. **30**(1–2): p. 187-198.
63. Pardon E, L.T., Triest S, Rasmussen SG, Wohlkönig A, Ruf A, Muyldermans S, Hol WG, Kobilka BK, Steyaert J., *A general protocol for the generation of Nanobodies for structural biology.* Nat Protocols, 2014: p. 674-93.
64. Iwata, S., et al., *Structure at 2.8 A resolution of cytochrome c oxidase from Paracoccus denitrificans.* Nature, 1995. **376**(6542): p. 660-669.
65. Ostermeier, C., et al., *Structure at 2.7 Å resolution of the Paracoccus denitrificans two-subunit cytochrome c oxidase complexed with an antibody F(V) fragment.* Proceedings of the National Academy of Sciences of the United States of America, 1997. **94**(20): p. 10547-10553.
66. Zhou, Y., et al., *Chemistry of ion coordination and hydration revealed by a K+ channel-Fab complex at 2.0[thinsp][angst] resolution.* Nature, 2001. **414**(6859): p. 43-48.
67. Lange, C. and C. Hunte, *Crystal structure of the yeast cytochrome bc(1) complex with its bound substrate cytochrome c.* Proceedings of the National Academy of Sciences of the United States of America, 2002. **99**(5): p. 2800-2805.
68. Dutzler, R., E.B. Campbell, and R. MacKinnon, *Gating the Selectivity Filter in ClC Chloride Channels.* Science, 2003. **300**(5616): p. 108-112.

69. C. Hamers-Casterman, T.A., S. Muyldermans, G. Robinson, C. Hammers, E. Bajyana Songa, N. Bendahman & R. Hammers, *Naturally occurring antibodies devoid of light chains.* Nature, 1993: p. 446 - 448.
70. Greenberg, A.S., et al., *A new antigen receptor gene family that undergoes rearrangement and extensive somatic diversification in sharks.* Nature, 1995. **374**(6518): p. 168-173.
71. Nguyen, V., et al., *Heavy-chain antibodies in Camelidae; a case of evolutionary innovation.* Immunogenetics, 2002. **54**(1): p. 39-47.
72. De Genst E, S.K., Decanniere K, Conrath K, Loris R, Kinne J, Muyldermans S, Wyns L, *Molecular basis for the preferential cleft recognition by dromedary heavy-chain antibodies.* Proc Natl Acad Sci U S A, 2006: p. 4586-91.
73. Vincke C, M.S., *Introduction to heavy chain antibodies and derived Nanobodies.* Methods Mol Biol, 2012: p. 911-15.
74. Rasmussen, S.G.F., et al., *Structure of a nanobody-stabilized active state of the [bgr]2 adrenoceptor.* Nature, 2011. **469**(7329): p. 175-180.
75. Löw, C., et al., *Nanobody Mediated Crystallization of an Archeal Mechanosensitive Channel.* PLoS ONE, 2013. **8**(10): p. e77984.
76. Ehrnstorfer, I.A., et al., *Crystal structure of a SLC11 (NRAMP) transporter reveals the basis for transition-metal ion transport.* Nat Struct Mol Biol, 2014. **21**(11): p. 990-996.
77. Geertsma, E.R., et al., *Structure of a prokaryotic fumarate transporter reveals the architecture of the SLC26 family.* Nat Struct Mol Biol, 2015. **advance online publication**.
78. Binz, H.K., et al., *High-affinity binders selected from designed ankyrin repeat protein libraries.* Nat Biotech, 2004. **22**(5): p. 575-582.
79. Lambert S, Y.H., Prchal JT, Lawler J, Ruff P, Speicher D, Cheung MC, Kan YW, Palek J., *cDNA sequence for human erythrocyte ankyrin.* Proc Natl Acad Sci U S A, 1990.
80. Bork, P., *Hundreds of ankyrin-like repeats in functionally diverse proteins: Mobile modules that cross phyla horizontally?* Proteins: Structure, Function, and Bioinformatics, 1993. **17**(4): p. 363-374.
81. Huber, T., et al., *In vitro selection and characterization of DARPins and Fab fragments for the co-crystallization of membrane proteins: The Na+-citrate symporter CitS as an example.* Journal of Structural Biology, 2007. **159**(2): p. 206-221.
82. Milovnik, P., et al., *Selection and characterization of DARPins specific for the neurotensin receptor 1.* Protein Engineering, Design and Selection, 2009. **22**(6): p. 357-366.
83. Guzman L-M, D.B., M. J. Carson, and J Beckwith, *Tight regulation, modulation, and high-level expression by vectors containing the arabinose PBAD promoter.* JOURNAL OF BACTERIOLOGY, 1995. **177**: p. 4121–4130
84. GP, S., *Filamentous fusion phage: novel expression vectors that display cloned antigens on the virion surface.* Science, 1985: p. 1315-7.
85. Vieira, J. and J. Messing, *[1] Production of single-stranded plasmid DNA*, in *Methods in Enzymology*. 1987, Academic Press. p. 3-11.
86. Smolarek D., B.O., Czerwinski M., *Variable fragments of heavy chain antibodies (VHHs): a new magic bullet molecule of medicine?* Postepy Hig Med Dosw, 2012.
87. Lowman HB1, B.S., Simpson N, Wells JA., *Selecting high-affinity binding proteins by monovalent phage display*., in *Biochemistry*. 1991. p. 10832-8.
88. Garrard LJ1, Y.M., O'Connell MP, Kelley RF, Henner DJ., *Fab assembly and enrichment in a monovalent phage display system.* Biotechnology, 1991: p. 1373-7.
89. Kristensen, P. and G. Winter, *Proteolytic selection for protein folding using filamentous bacteriophages.* Folding and Design, 1998. **3**(5): p. 321-328.
90. Demartis, S., et al., *A strategy for the isolation of catalytic activities from repertoires of enzymes displayed on phage1.* Journal of Molecular Biology, 1999. **286**(2): p. 617-633.

91. Bird RE, H.K., Jacobson JW, Johnson S, Kaufman BM, Lee SM, Lee T, Pope SH, Riordan GS, Whitlow M., *Single-chain antigen-binding proteins.* Science, 1988: p. 423-6.
92. Kim DJ, C.J., Ryu YS, Rhim JH, Kim CW, Suh Y, Chung HK., *Production and characterisation of a recombinant scFv reactive with human gastrointestinal carcinomas.* Br J Cancer, 2002: p. 405-13.
93. Bedzyk WD, W.K., Denzin LK, Johnson LS, Hardman KD, Pantoliano MW, Asel ED, Voss EW Jr., *Immunological and structural characterization of a high affinity anti-fluorescein single-chain antibody.* J Biol Chem, 1990: p. 18615-20.
94. Pantoliano MW, B.R., Johnson S, Asel ED, Dodd SW, Wood JF, Hardman KD., *Conformational stability, folding, and ligand-binding affinity of single-chain Fv immunoglobulin fragments expressed in Escherichia coli.* Biochemistry, 1991: p. 10117-25.
95. Silacci, M., et al., *Design, construction, and characterization of a large synthetic human antibody phage display library.* PROTEOMICS, 2005. **5**(9): p. 2340-2350.
96. Griffiths, A.D., et al., *Isolation of high affinity human antibodies directly from large synthetic repertoires.* The EMBO Journal, 1994. **13**(14): p. 3245-3260.
97. Hoogenboom HR, G.A., Johnson KS, Chiswell DJ, Hudson P, Winter G., *Multi-subunit proteins on the surface of filamentous phage: methodologies for displaying antibody (Fab) heavy and light chains.* Nucleic Acdis Res, 1991: p. 4133-7.
98. Stefan Ewert, T.H., Annemarie Honegger, Andreas Plückthun, *Biophysical Properties of Human Antibody Variable Domains.* Journal of Molecular Biology. **325**(13): p. 531–553.
99. Majka J, S.C., *Analysis of protein-DNA interactions using surface plasmon resonance.* Adv Biochem Eng Biotechnol, 2007: p. 13-36.
100. Teh HF, P.W., Su X, Thomsen JS, *Characterization of protein--DNA interactions using surface plasmon resonance spectroscopy with various assay schemes.* Biochemistry, 2007: p. 27-35.
101. Gutiérrez-Gallego, R., et al., *Surface plasmon resonance immuno assays – A perspective.* Growth Hormone & IGF Research, 2009. **19**(4): p. 388-398.
102. *SPRpages.nl.*
103. Marquart, J.A., *Surface Plasmon Resonance and Biomolecular Interaction Analysis, Theorie and Practice.*
104. Kikuchi Y, U.S., Nanami M, Yoshimura Y, Iida S, Fukushima N, Tsuchiya M., *Determination of concentration and binding affinity of antibody fragments by use of surface plasmon resonance.* J Biosci Bioeng, 2005: p. 311-7.
105. Luginbühl B, K.Z., Jones RM, Fletterick RJ, Prusiner SB, Cohen FE, Williamson RA, Burton DR, Plückthun A, *Directed evolution of an anti-prion protein scFv fragment to an affinity of 1 pM and its structural interpretation.* J Mol Biol, 2006: p. 75-97.
106. Prochazka, L., *Master Thesis.* 2010.
107. Bai, X.-c., et al., *An atomic structure of human [ggr]-secretase.* Nature, 2015. **525**(7568): p. 212-217.
108. Batchelor, A.H., et al., *The Structure of GABPα/β: An ETS Domain- Ankyrin Repeat Heterodimer Bound to DNA.* Science, 1998. **279**(5353): p. 1037-1041.
109. Binz HK, S.M., Forrer P, Amstutz P, Plückthun A, *Designing repeat proteins: well-expressed, soluble and stable proteins from combinatorial libraries of consensus ankyrin repeat proteins.* J Mol Biol, 2003: p. 489-503.
110. Merz, T., et al., *Stabilizing Ionic Interactions in a Full-consensus Ankyrin Repeat Protein.* Journal of Molecular Biology, 2008. **376**(1): p. 232-240.
111. Seeger, M.A., et al., *Design, construction, and characterization of a second-generation DARPin library with reduced hydrophobicity.* Protein Science, 2013. **22**(9): p. 1239-1257.
112. Zahnd C, A.P., Plückthun A, *Ribosome display: selecting and evolving proteins in vitro that specifically bind to a target.* Nat Methods, 2007: p. 269-79.

113. Hanes J, P.A., *In vitro selection and evolution of functional proteins by using ribosome display.* Proc Natl Acad Sci U S A, 1997. **94**: p. 4937-42.
114. Amstutz, P., et al., *In vitro display technologies: novel developments and applications.* Current Opinion in Biotechnology, 2001. **12**(4): p. 400-405.
115. Sinz, A., *Chemical cross-linking and mass spectrometry for mapping three-dimensional structures of proteins and protein complexes.* Journal of Mass Spectrometry, 2003. **38**(12): p. 1225-1237.
116. Brauchle M, H.S., Caussinus E, Lenard A, Ochoa-Espinosa A, Scholz O, Sprecher SG, Plückthun A, Affolter M, *Protein interference applications in cellular and developmental biology using DARPins that recognize GFP and mCherry.* Biol Open, 2014: p. 1252-61.
117. Toporkiewicz M, M.J., Matusewicz L, Czogalla A, Sikorski AF, *Toward a magic or imaginary bullet? Ligands for drug targeting to cancer cells: principles, hopes, and challenges.* Int J Nanomedicine, 2015: p. 1399-414.
118. Schofield, C.M., J.R. Trudell, and N.L. Harrison, *Alanine-scanning mutagenesis in the signature disulfide loop of the glycine receptor alpha 1 subunit: critical residues for activation and modulation.* Biochemistry, 2004. **43**(31): p. 10058-63.
119. Purohit, P. and A. Auerbach, *Acetylcholine receptor gating at extracellular transmembrane domain interface: the "pre-M1" linker.* J Gen Physiol, 2007. **130**(6): p. 559-68.
120. Chakrapani, S., T.D. Bailey, and A. Auerbach, *Gating dynamics of the acetylcholine receptor extracellular domain.* J Gen Physiol, 2004. **123**(4): p. 341-56.
121. Jean-Pierre Changeux, M.K., and Chen-Yuan Lee, *Use of a Snake Venom Toxin to Characterize the Cholinergic Receptor Protein.* PNAS, 1970. **67**(3): p. 1241–1247.
122. Kim, J., et al., *Subnanometre-resolution electron cryomicroscopy structure of a heterodimeric ABC exporter.* Nature, 2015. **517**(7534): p. 396-400.
123. Gao, F., et al., *Agonist-mediated Conformational Changes in Acetylcholine-binding Protein Revealed by Simulation and Intrinsic Tryptophan Fluorescence.* Journal of Biological Chemistry, 2005. **280**(9): p. 8443-8451.
124. Bouzat, C., et al., *Coupling of agonist binding to channel gating in an ACh-binding protein linked to an ion channel.* Nature, 2004. **430**(7002): p. 896-900.
125. Campos-Caro, A., et al., *A single residue in the M2-M3 loop is a major determinant of coupling between binding and gating in neuronal nicotinic receptors.* Proc Natl Acad Sci U S A, 1996. **93**(12): p. 6118-23.
126. Xiu, X., et al., *A unified view of the role of electrostatic interactions in modulating the gating of Cys loop receptors.* J Biol Chem, 2005. **280**(50): p. 41655-66.
127. Kerry L. Price , K.S.M.a.S.C.R.L., A, *Transducing Agonist Binding to Channel Gating Involves Different Interactions in 5-HT3 and GABAC Receptors.* The Journal of Biological Chemistry, 2007.
128. Nathan L. Absalom, T.M.L., Warren Kaplan, Kerrie D. Pierce, and Peter R. Schofield *Role of Charged Residues in Coupling Ligand Binding and Channel Activation in the Extracellular Domain of the Glycine Receptor* Journal of Biological Chemistry, 2003. **278**: p. 50151-50157.
129. Purohit, P. and A. Auerbach, *Acetylcholine Receptor Gating at Extracellular Transmembrane Domain Interface: the “Pre-M1” Linker.* The Journal of General Physiology, 2007. **130**(6): p. 559-568.
130. Huang, X., et al., *Crystal structure of human glycine receptor-[agr]3 bound to antagonist strychnine.* Nature, 2015. **526**(7572): p. 277-280.
131. Zerangue, N., et al., *A new ER trafficking signal regulates the subunit stoichiometry of plasma membrane K(ATP) channels.* Neuron, 1999. **22**(3): p. 537-48.